Electronic Supplementary Information

Unexpected Solvent Effect on the Binding of Positively-Charged Macrocycles to Neutral Aromatic Hydrocarbons

Yu-Mei Wang,[a,b] Huan Yao,[b] Mao Quan,[b] Hongxin Chai,[b] Liu-Pan Yang,[b] Ying-Ming Pan*[a] and Wei Jiang*[b]

[a] *State Key Laboratory for* Chemistry *and Molecular Engineering of Medicinal Resources, School of Chemistry and Pharmaceutical Sciences of Guangxi Normal University, Guilin 541004, China.*
[b] *Shenzhen Grubbs Institute and Department of Chemistry, Southern University of Science and Technology, Shenzhen,* 518055*, China *E-mail: jiangw@sustech.edu.cn*

Table of Contents

1. General Method

All the reagents involved in this research were commercially available and used without further purification unless otherwise noted. Solvents were either employed as purchased or dried prior to use by standard laboratory procedures. Thin-layer chromatography (TLC) was carried out on 0.25 mm Yantai silica gel plates (60F-254). Column chromatography was performed on silica gel 60 (Tsingdao 40 – 63 nm, 200 – 300 mesh). ^{1}H, ^{13}C, $^{1}H,^{1}H$-COSY, and $^{1}H,^{1}H$-ROESY NMR spectra were recorded on Bruker Avance-400, 500 spectrometers. All chemical shifts are reported in ppm with residual solvents as the internal standards. The following abbreviations were used for signal multiplicities: s, singlet; d, doublet; t triplet; m, multiplet. Electrospray-ionization time-of-flight high-resolution mass spectrometry (ESI-HRMS) experiments were conducted on an applied Q EXACTIVE mass spectrometry system. Compound **3** were synthesized according to the literature procedures.[1]

Quantum chemistry calculations were performed using Gaussian 09 package.[2] The structure of the host-guest complex between **9** and **1b** was optimized by employing density functional theory (DFT) with dispersion corrected method (wB97XD)[3] in combination with 6-31G* basis set including the solvent effects for CH_2Cl_2 using the SMD solution model.[4] Minima were characterized by the absence of imaginary frequencies.

2 .Synthetic Procedures

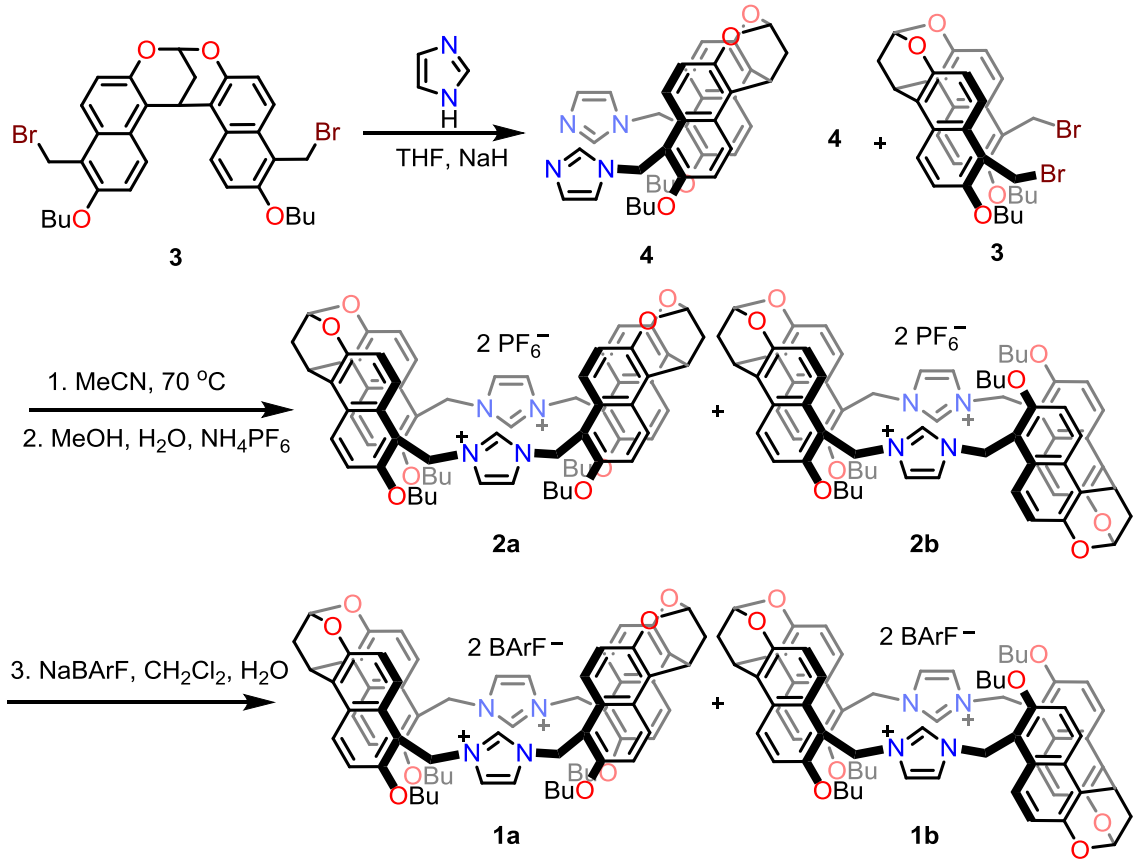

Compound C4

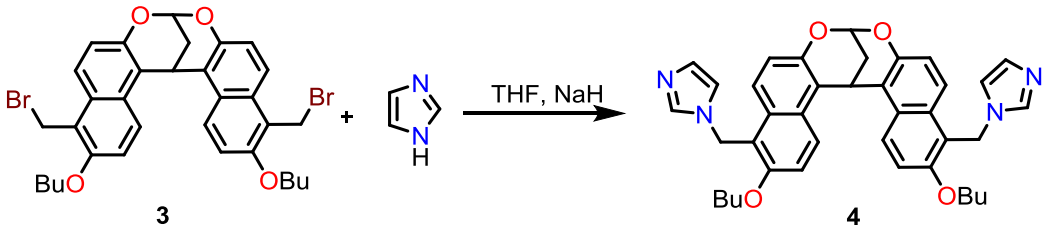

To the solution of imidazole (0.26 g, 3.82 mmol) in dry THF (100 mL) was added NaH (0.18 g, 7.64 mmol) at 0 °C and the resulting mixture was stirred for 30 min at 0 °C. **3** (0.5 g, 0.764 mmol) was then added. After stirring for additional 4 h at room temperature, the mixture was filtered. The filtrate was rotavapped under vacuum to remove the solvent. The solid was washed with diethyl ether to afford **4** (0.44 g, 92%). m.p.=225 °C. ^{1}H NMR (500 MHz, CD_3CN, 298 K) δ [ppm] = 8.68 (d, *J* = 9.4 Hz, 2H), 7.81 (d, *J* = 9.3 Hz, 2H), 7.51 – 7.46 (m, 4H), 7.16 (d, *J* = 9.2 Hz, 2H), 6.88 (s, 2H), 6.75 (s, 2H), 6.27 – 6.25 (m, 1H), 5.53 – 5.42 (m, 5H), 4.15 (m, 4H), 2.47 – 2.43 (m, 2H), 1.83 – 1.75 (m,

4H), 1.49 (m, 7.4 Hz, 4H), 0.96 (t, J = 7.4 Hz, 6H). ^{13}C NMR (126 MHz, CD_3CN, 298 K) δ [ppm] = 153.92, 149.01, 137.43, 129.19, 128.66, 126.73, 126.07, 122.99, 120.09, 119.97, 119.32, 114.83, 92.03, 69.23, 40.68, 31.68, 19.42, 13.52. ESI-HRMS: m/z calcd for $[M+2H]^{2+}$ $C_{39}H_{42}N_4O_4^{2+}$, 315.3128; found 315.3118 (error = - 3.2 ppm).

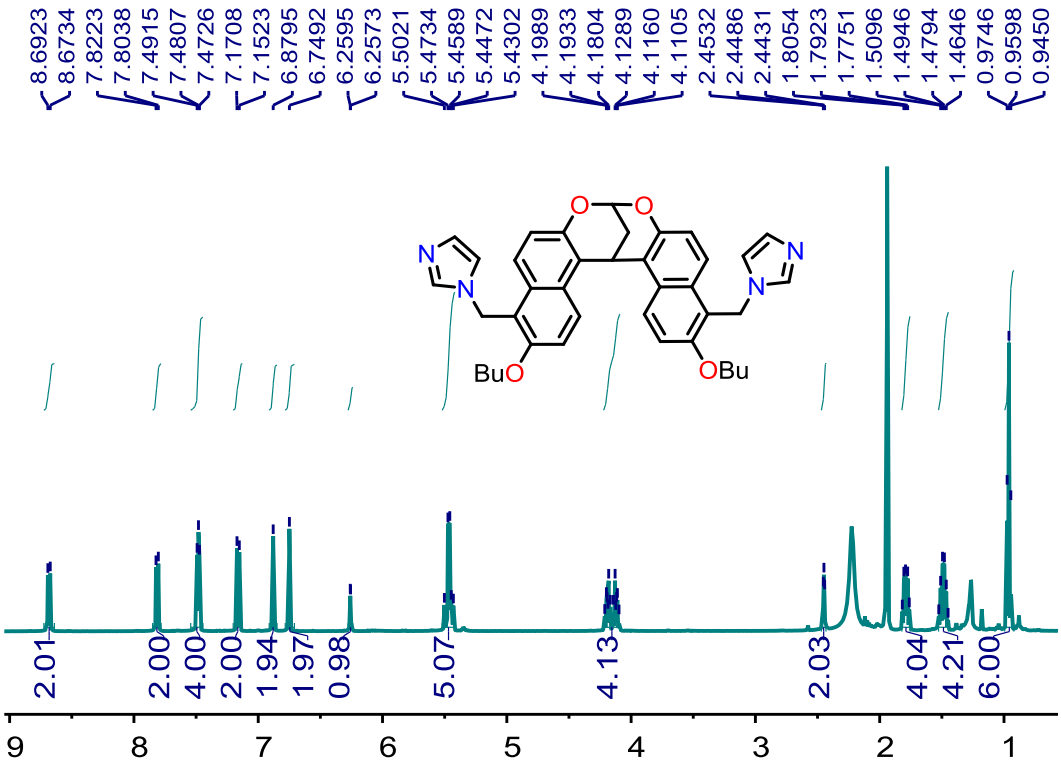

^{1}H NMR spectrum (500 MHz, CD_3CN, 298 K) of Compound **4**

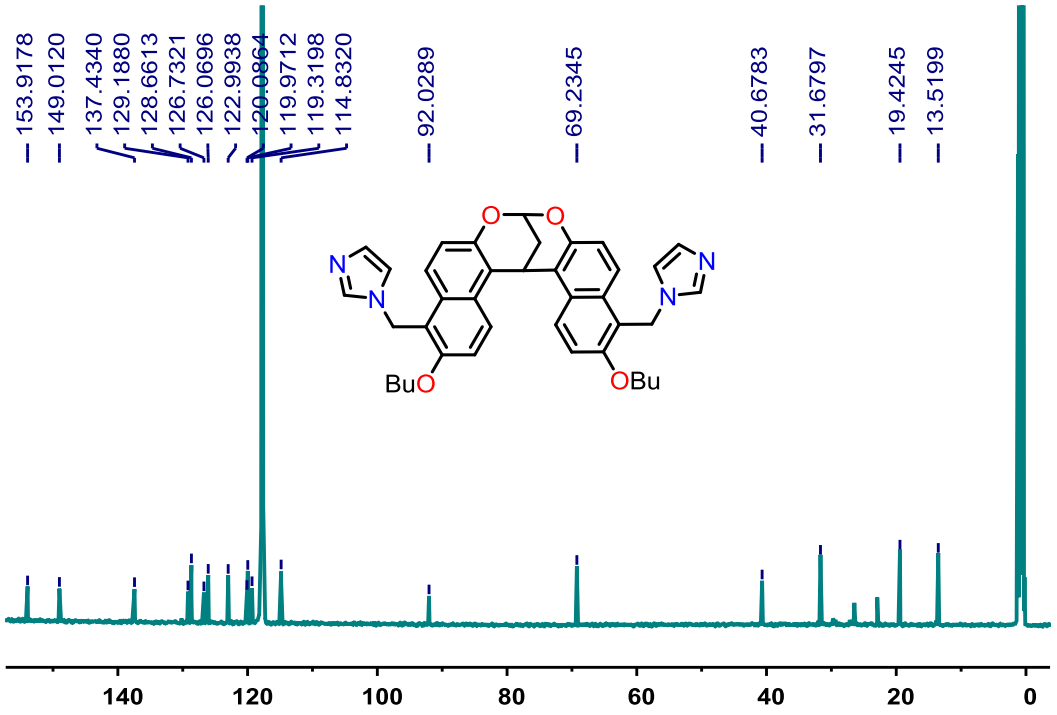

^{13}C NMR spectrum (126 MHz, CD_3CN, 298 K) of Compound **4**

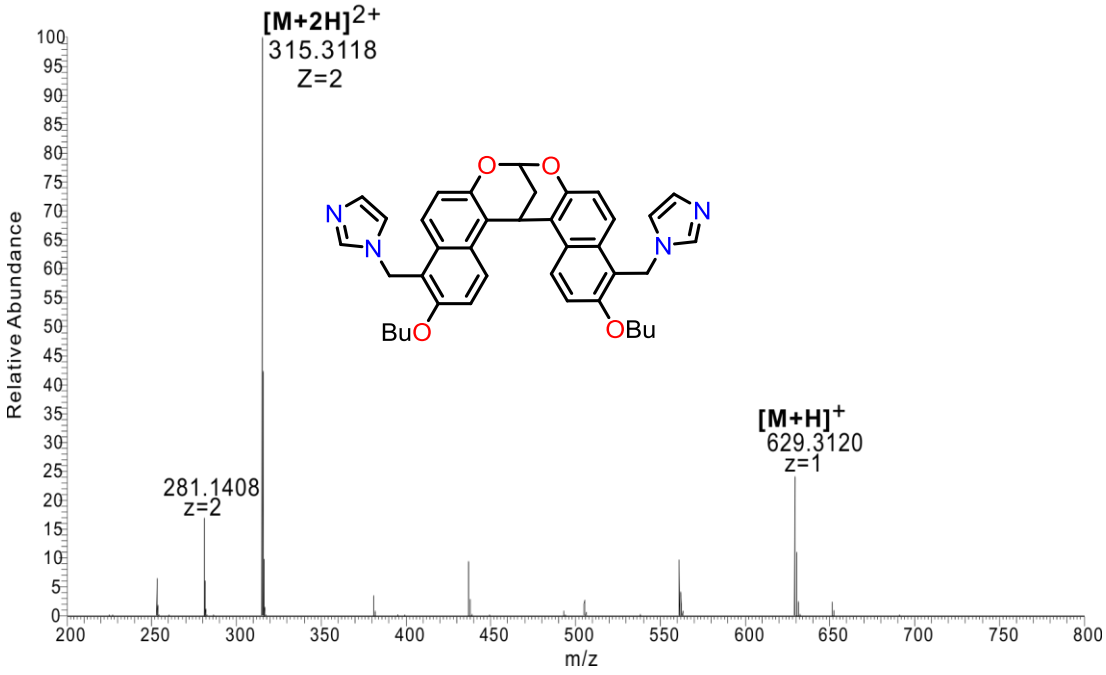

ESI-HRMS mass spectrum of compound **4**

Naphthotube 2a and 2b

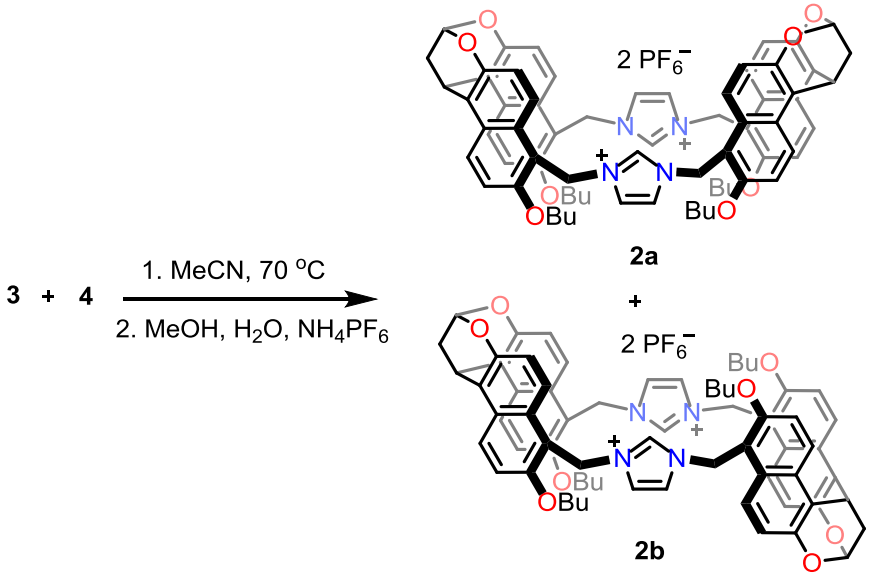

400 mL MeCN was added into a 1000-mL three-neck flask charged with a magnetic stirring bar. The flask was then evacuated and refilled with Ar (using a gas balloon). The solutions of **3** (1.4 g, 2.14 mmol, in 60 mL MeCN) and **4** (1.35 g, 2.14 mmol, in 60 mL MeCN) were added dropwise during 10 h by using two separate syringes to the flask *via* a double-channel syringe pump. The reaction mixture was stirred for another 24 h at 70 °C. After removing most of the solvent in vacuum, 100 ml of methanol and 10 ml of the aqueous solution of NH_4PF_6(1.6 g, 4.28 mmol) were added to the mixture which was stirred for another 2 h. The suspension is filtered. Collecting the filter cake was collected and washed repeatedly with acetone to afford **2b** (1.0 g, 33%) as a white solid. The solvent in the filtrate was removed undergo vacuum, and the residue was washed repeatedly with a small amount of acetone and ethyl acetate to afford **2a** (0.42 g, 14%) as a white solid.

2a: m.p. >320 °C. ^{1}H NMR (500 MHz, CD_3CN, 298 K) δ [ppm] = 9.19 (s, 1H), 8.70 (d, *J* = 9.4 Hz, 2H), 7.65 (d, *J* = 9.1 Hz, 2H), 7.48 (d, *J* = 9.4 Hz, 2H), 7.23 (d, *J* = 9.1 Hz, 2H), 6.61 (s, 2H), 6.30 (s, 1H), 5.79 (d, *J* = 14.9 Hz, 2H), 5.58 (d, *J* = 14.9 Hz, 2H), 5.40 (s, 1H), 4.19 (m, 4H), 2.41 (s, 2H), 1.80 (m, 4H), 1.49 (m, 4H), 0.95 (t, *J* = 7.3 Hz, 6H). ^{13}C NMR (126 MHz, CD_3CN, 298 K) δ [ppm] = 154.77, 149.48, 136.37, 129.35, 128.02, 127.26, 122.81, 120.70, 115.05, 114.70, 92.30, 69.87, 44.36, 32.05, 26.56, 23.06, 19.93,

14.06. ESI-HRMS: m/z calcd for $[M-2PF_6^-]^{2+}$ $C_{72}H_{74}N_4O_8^{2+}$, 561.2748; found 561.2746 (error = - 0.4 ppm).

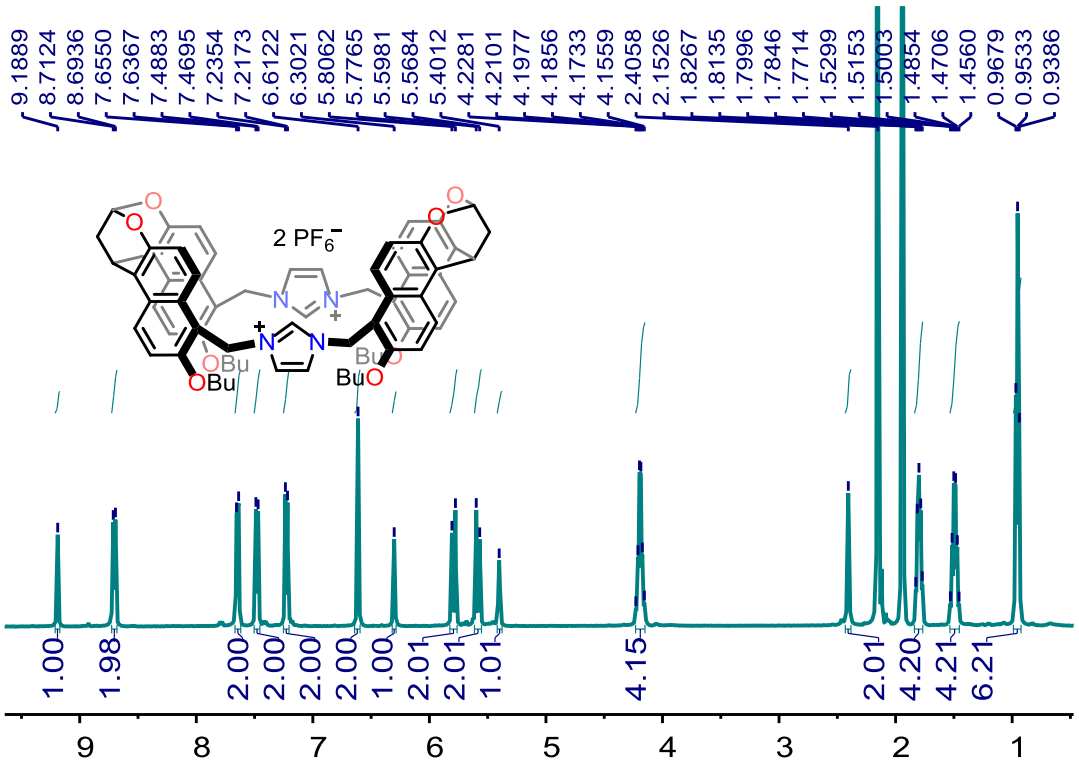

^{1}H NMR spectrum (500 MHz, CD_3CN, 298 K) of Naphthotube **2a**

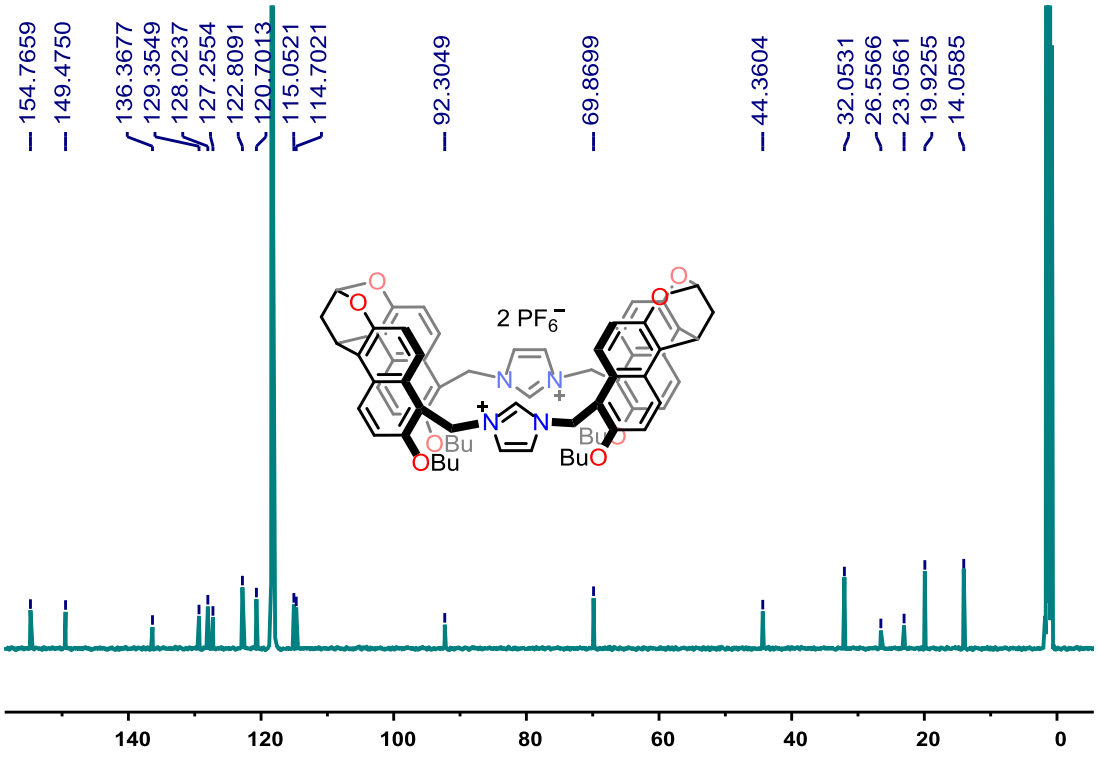

^{13}C NMR spectrum (126 MHz, CD_3CN, 298 K) of Naphthotube **2a**

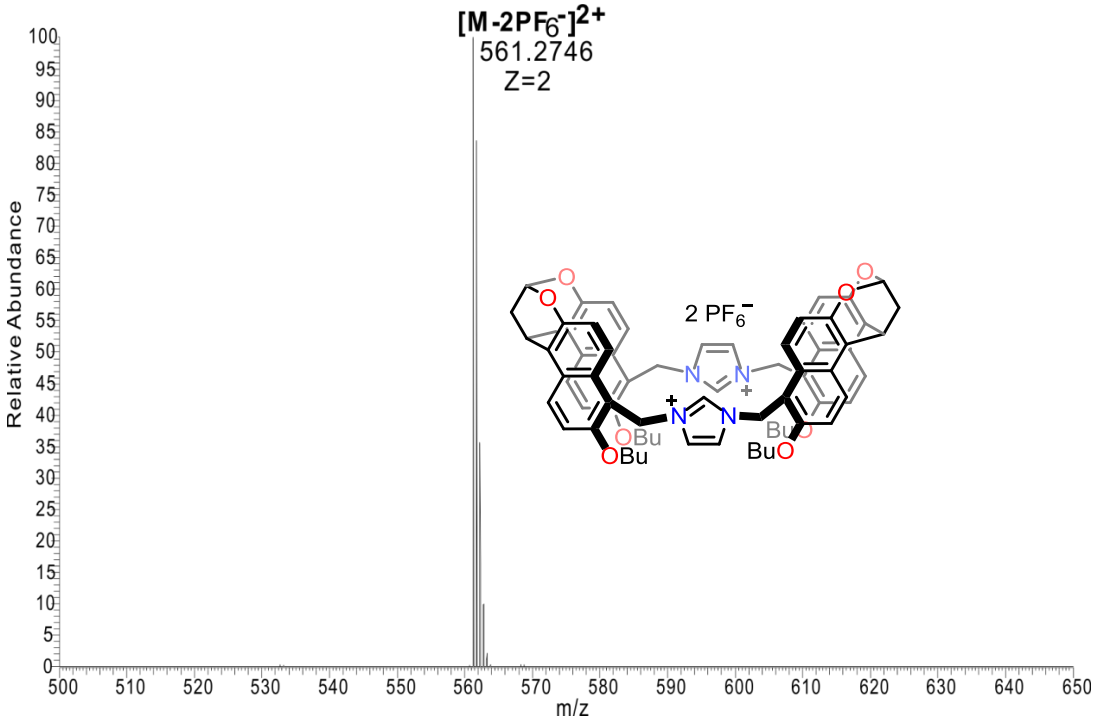

ESI-HRMS mass spectrum of Naphthotube **2a**

2b: m.p. >320 °C. ^{1}H NMR (500 MHz, CD_3CN, 298 K) δ [ppm] = 8.99 (s, 1H), 8.71 (d, J = 9.5 Hz, 2H), 7.80 (d, J = 9.3 Hz, 2H), 7.41 (d, J = 9.5 Hz, 2H), 7.18 (d, J = 9.2 Hz, 2H), 6.59 (d, J = 1.5 Hz, 2H), 6.28 (s, 1H), 5.73 – 5.60 (m, 4H), 5.45 (s, 1H), 4.16 (m, 4H), 2.46 (s, 2H), 1.80 (m, 4H), 1.49 (m, 4H), 0.96 (t, J = 7.4 Hz, 6H). ^{13}C NMR (126 MHz, CD_3CN, 298 K) δ [ppm] = 155.04, 149.64, 136.74, 129.36, 127.95, 127.19, 122.77, 122.48, 120.96, 120.70, 114.96, 114.88, 92.35, 69.74, 44.28, 32.04, 26.49, 23.12, 19.90, 14.10. ESI-HRMS: m/z calcd for $[M-2PF_6^-]^{2+}$ $C_{72}H_{74}N_4O_8^{2+}$, 561.2748; found 561.2746 (error = - 0.4 ppm).

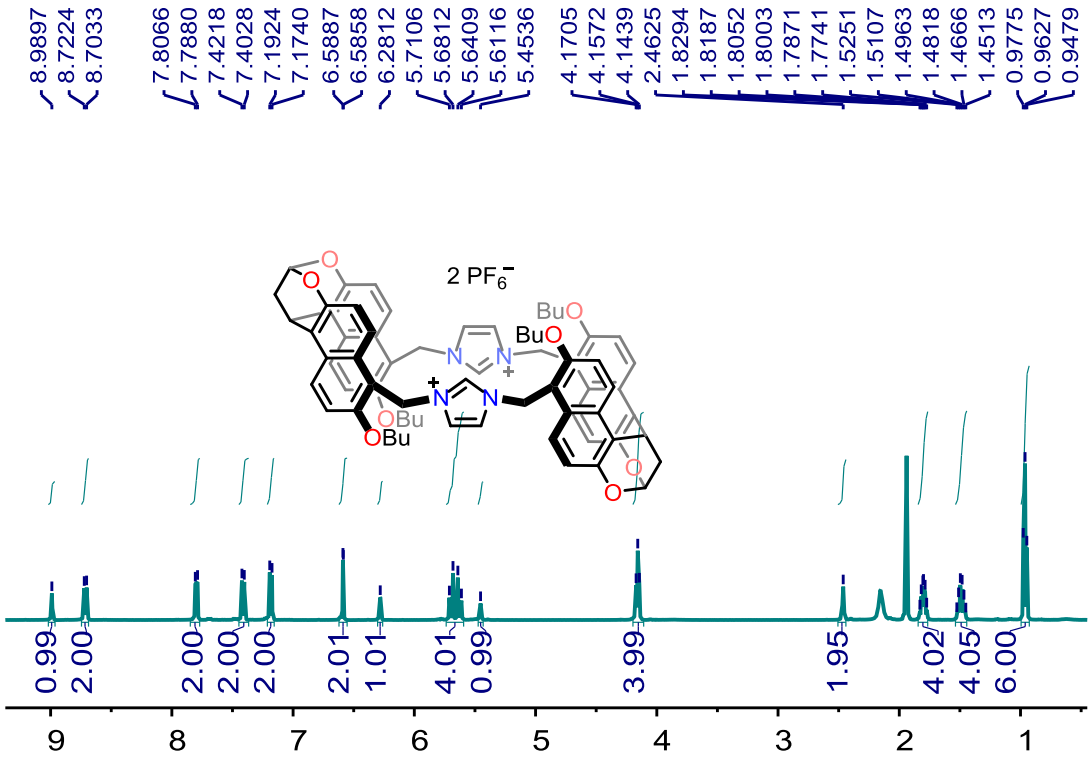

^{1}H NMR spectrum (500 MHz, CD_3CN, 298 K) of Naphthotube **2b**

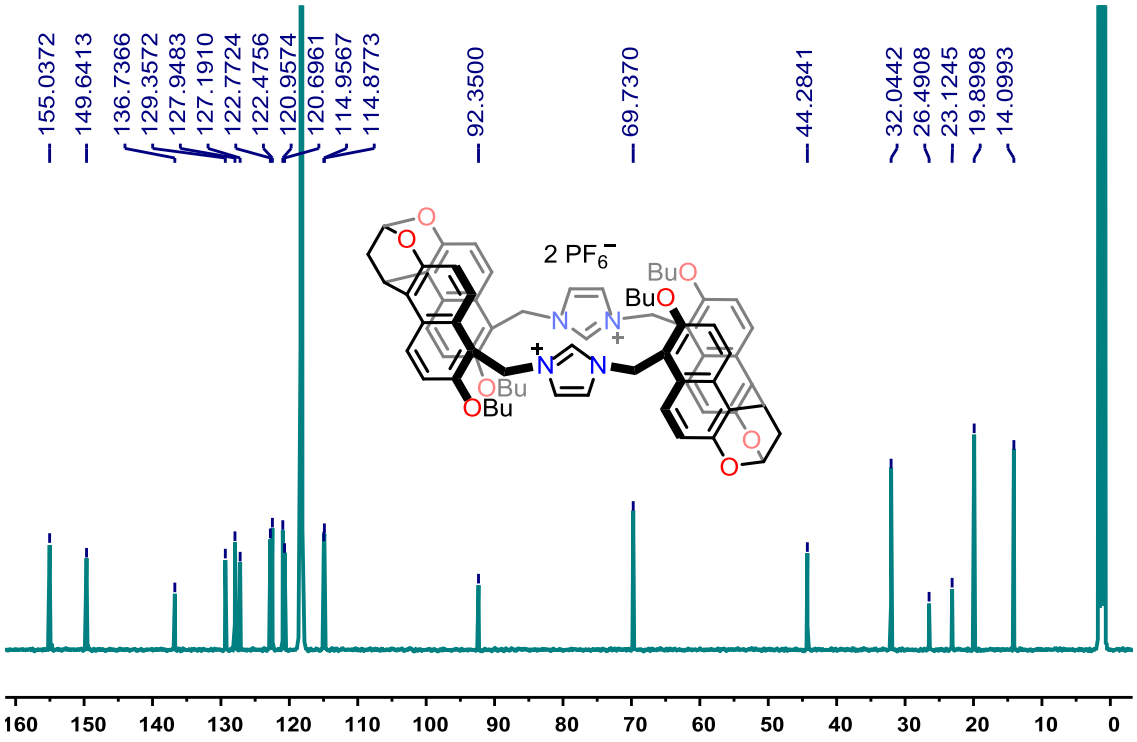

^{13}C NMR spectrum (126 MHz, CD_3CN, 298 K) of Naphthotube **2b**

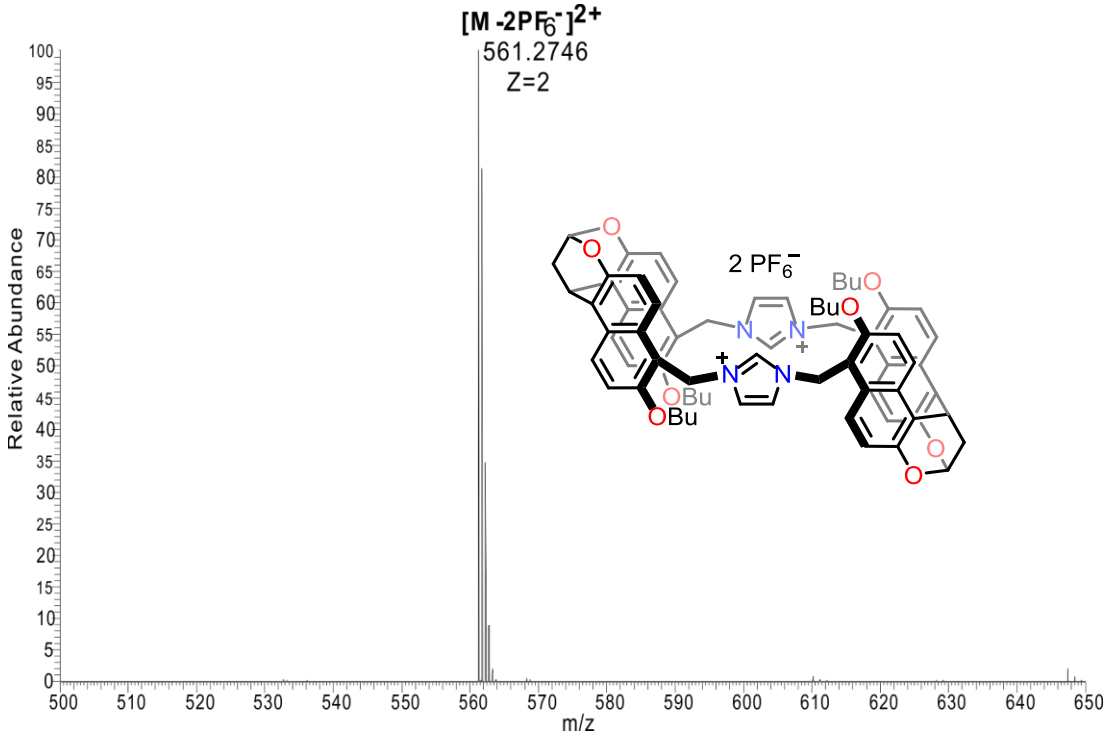

ESI-HRMS mass spectrum of Naphthotube **2b**

Naphthotube 1a and 1b

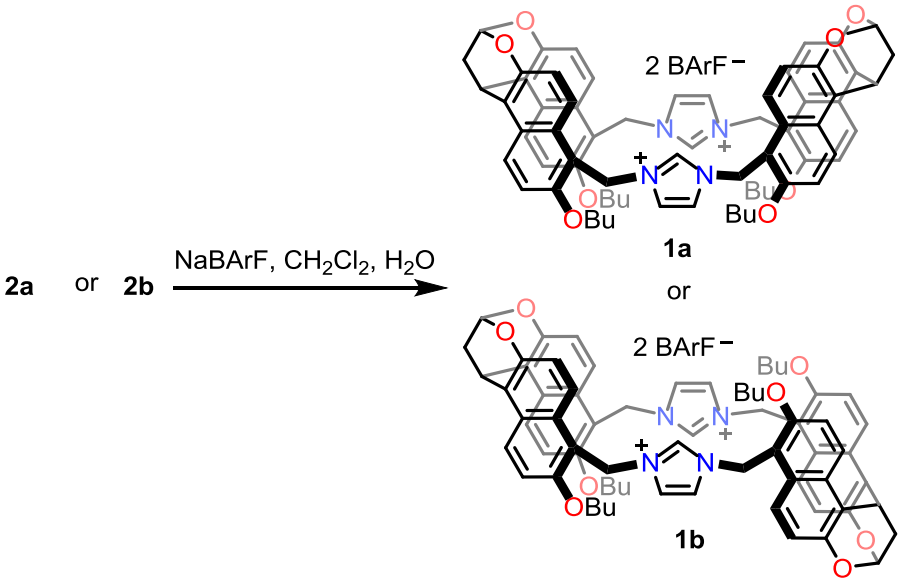

To the solution of **2a** or **2b** (300 mg, 0.21 mmol) in CH_2Cl_2 (100 mL) and H_2O (100 mL) was added NaBArF (558 mg, 0.63 mmol) at room temperature. The resulting mixture was stirred for 2 h, and was then extracted with CH_2Cl_2. The combined organic layers (CH_2Cl_2) were washed with saturated solution of $NaHCO_3$. After removing solvent under vacuum, the residue was washed with diethyl ether to afford **1a** or **1b** (600 mg, 99%).

1a: m.p. =130 °C. ^{1}H NMR (500 MHz, CD_3CN, 298 K) δ [ppm] = 9.15 (s, 1H), 8.70 (d, *J* = 9.5 Hz, 2H), 7.69 (s, 12H), 7.64 (d, *J* = 9.2 Hz, 2H), 7.47 (d, *J* = 9.5 Hz, 2H), 7.23 (d, *J* = 9.2 Hz, 2H), 6.60 (s, 2H), 6.30 (s, 1H), 5.68 (m, 4H), 5.40 (s, 1H), 4.19 (t, *J* = 6.3 Hz, 4H), 2.40 (s, 2H), 1.79 (m, 4H), 1.49 (m, 4H), 0.95 (t, *J* = 7.4 Hz, 6H). ^{13}C NMR (126 MHz, CD_3CN, 298 K) δ [ppm] = 162.20, 161.81, 161.41, 161.01, 153.85, 148.57, 135.40, 134.66, 129.33, 129.31, 129.28, 129.26, 129.08, 129.06, 129.03, 129.01, 128.83, 128.80, 128.78, 128.76, 128.57, 128.55, 128.53, 128.51, 128.44, 127.71, 127.11, 126.34, 125.55, 123.39, 121.87, 121.85, 121.22, 119.79, 119.76, 114.11, 113.76, 91.39, 68.94, 43.45, 31.12, 25.63, 22.14, 18.99, 13.10. ESI-HRMS: m/z calcd for $[M\text{-}2BArF^-]^{2+}$ $C_{72}H_{74}N_4O_8^{2+}$, 561.2748; found 561.2747(error = - 0.2 ppm).

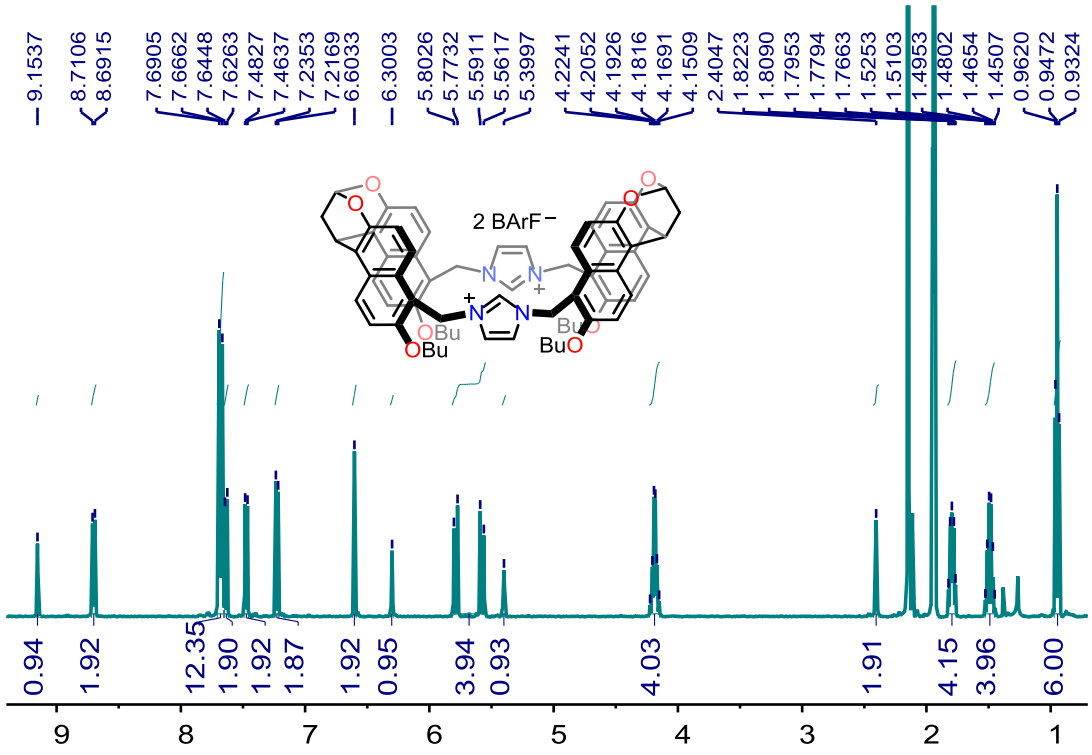

^{1}H NMR spectrum (500 MHz, CD_3CN, 298 K) of Naphthotube **1a**

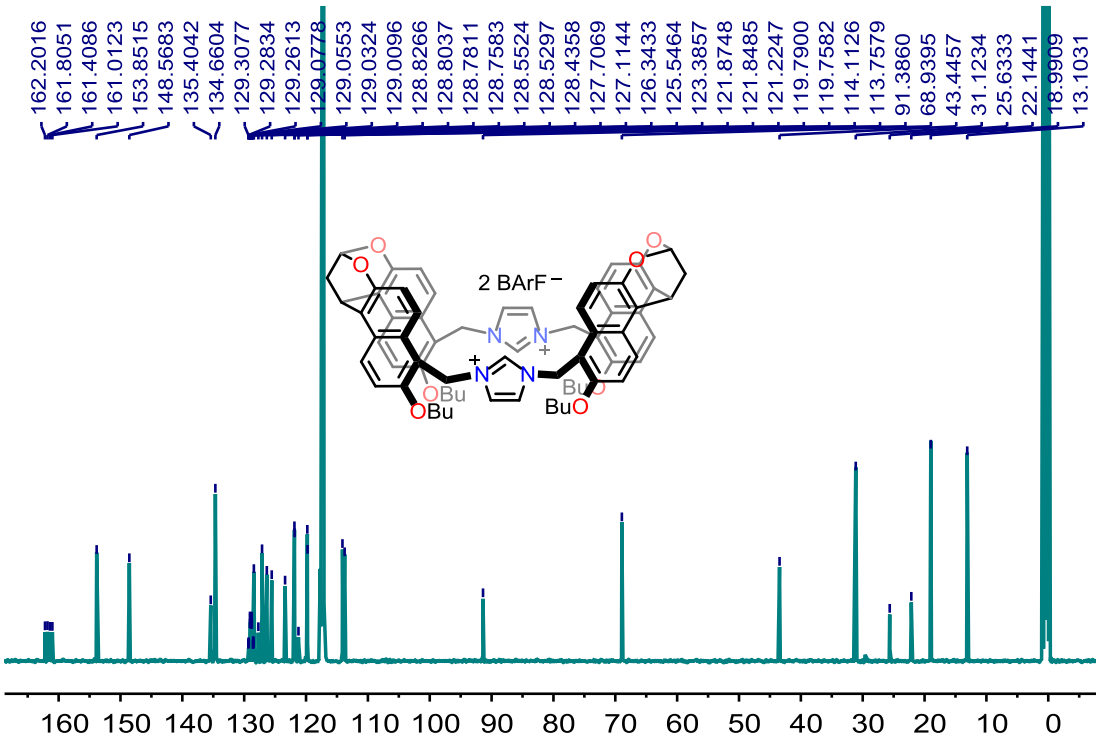

^{13}C NMR spectrum (126 MHz, CD_3CN, 298 K) of Naphthotube **1a**

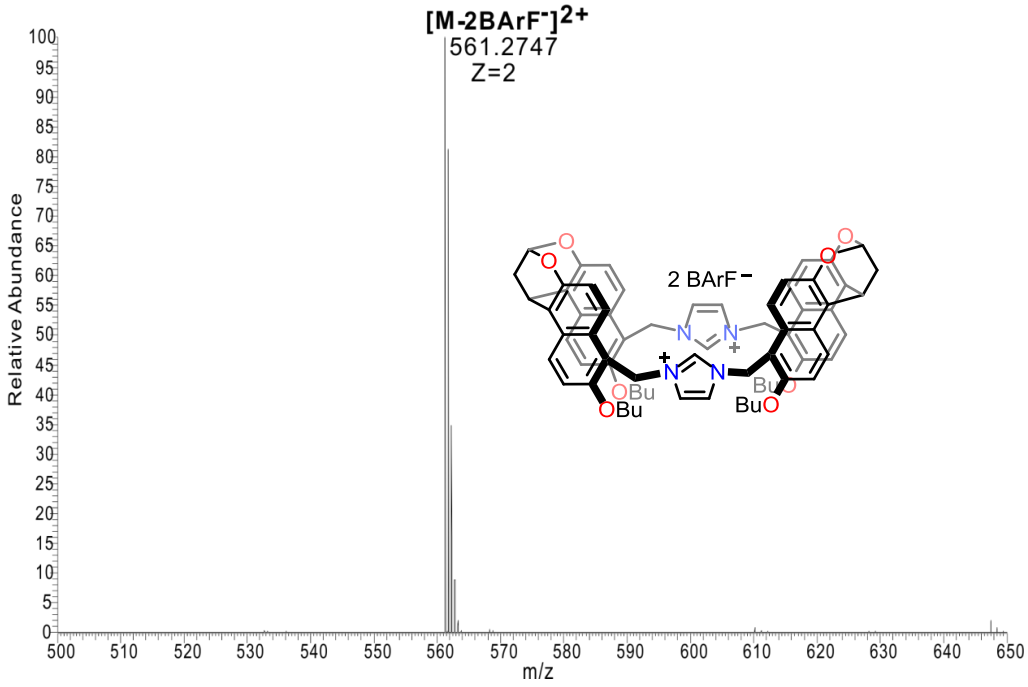

ESI-HRMS mass spectrum of Naphthotube **1a**

1b: m.p. =189 °C. ^{1}H NMR (500 MHz, CD_3CN,298 K) δ [ppm] = 8.94 (s, 1H), 8.74 (d, *J* = 9.5 Hz, 2H), 7.81 (d, *J* = 9.3 Hz, 2H), 7.71 (d, *J* = 12.0 Hz, 12H), 7.43 (d, *J* = 9.5 Hz, 2H), 7.21 (d, *J* = 9.2 Hz, 2H), 6.61 (s, 2H), 6.31 (s, 1H), 5.79 – 5.57 (m, 4H), 5.48 (s, 1H), 4.18 (t, *J* = 6.6 Hz, 4H), 2.49 (s, 2H), 1.90 – 1.77 (m, 4H), 1.62 – 1.40 (m, 4H), 0.99 (t, *J* = 7.4 Hz, 6H). ^{13}C NMR (126 MHz, CD_3CN, 298 K) δ [ppm] = 162.20, 161.80, 161.41, 161.01, 154.12, 148.73, 135.74, 134.66, 129.33, 129.31, 129.28, 129.26, 129.08, 129.05, 129.03, 129.01, 128.83, 128.80, 128.78, 128.76, 128.57, 128.55, 128.53, 128.51, 128.43, 127.71, 127.04, 126.28, 125.55, 123.38, 121.82, 121.57, 121.22, 120.05, 119.78, 114.01, 113.93, 91.43, 68.81, 43.37, 31.13, 25.56, 22.21, 18.97, 13.16. ESI-HRMS: m/z calcd for $[M\text{-}2BArF^-]^{2+}$ $C_{72}H_{74}N_4O_8^{2+}$, 561.2746; found 561.2746(error = - 0.2 ppm).

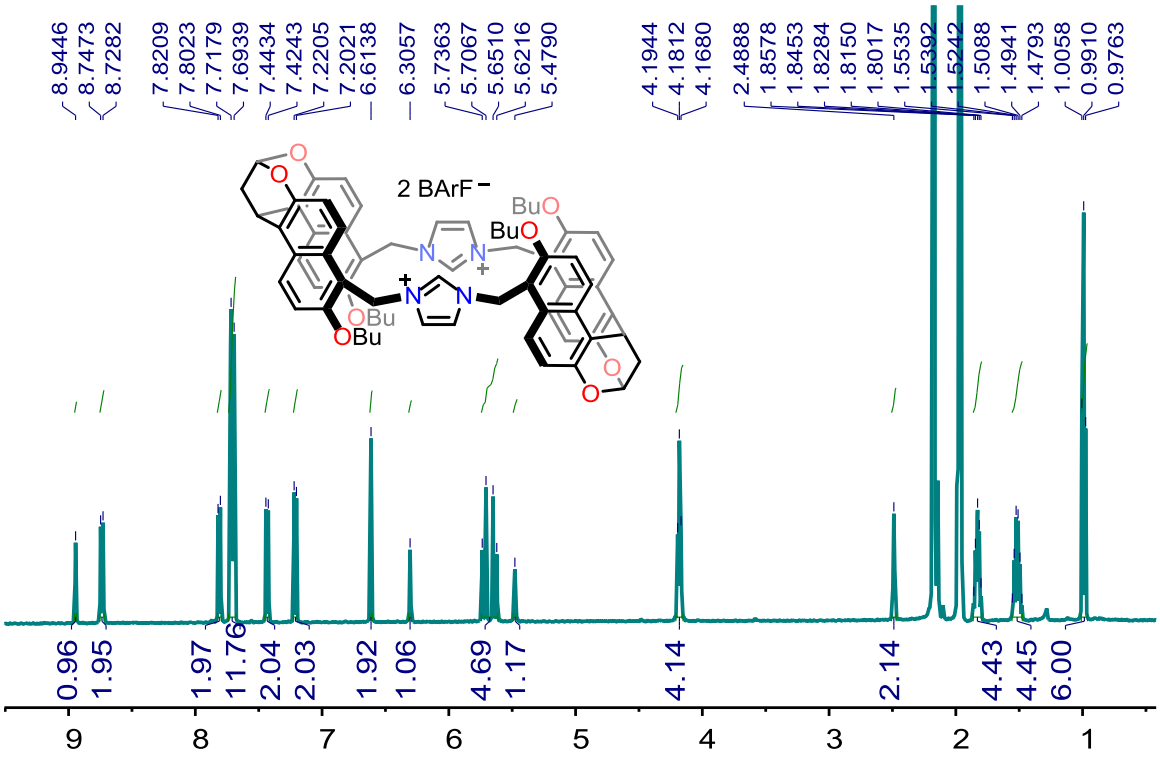

^{1}H NMR spectrum (500 MHz, CD_3CN, 298 K) of Naphthotube **1b**

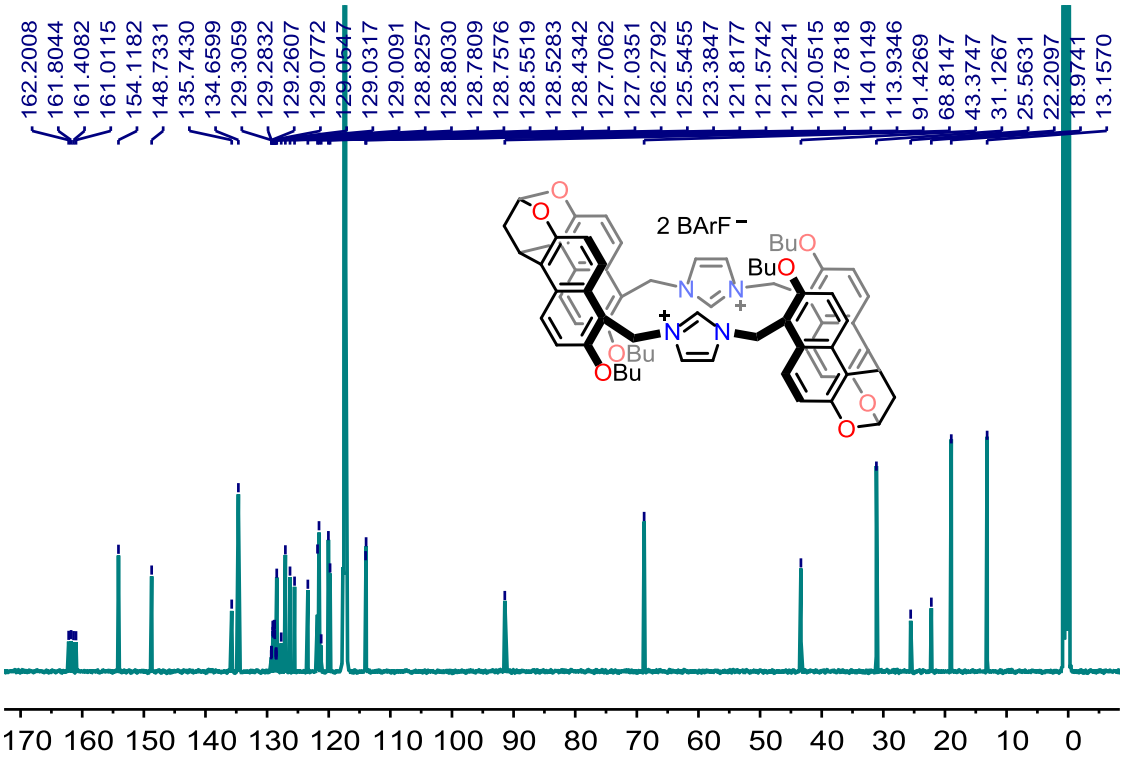

^{13}C NMR spectrum (126 MHz, CD_3CN, 298 K) of Naphthotube **1b**

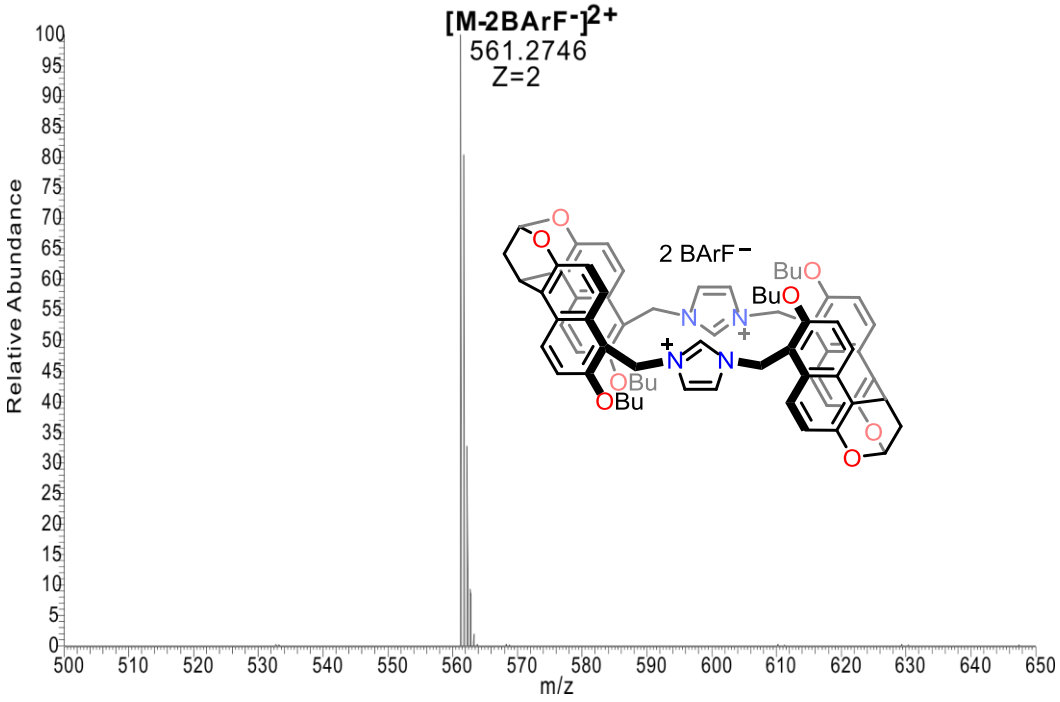

ESI-HRMS mass spectrum of Naphthotube **1b**

3. 2D NMR of Naphthotubes 1a, 1b, and 2b

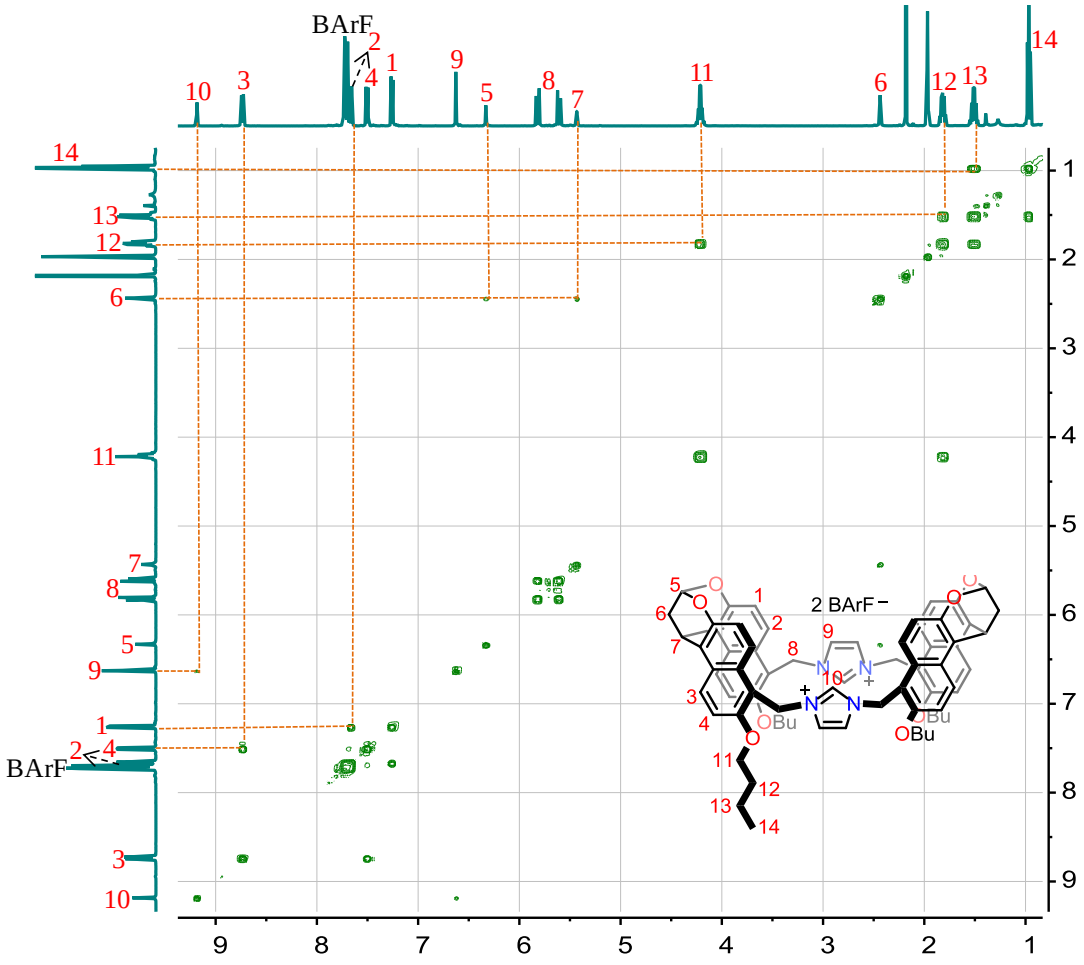

Fig. S1 ^{1}H,^{1}H-COSY NMR spectrum (500 MHz, CD_3CN, 298 K) of **1a**

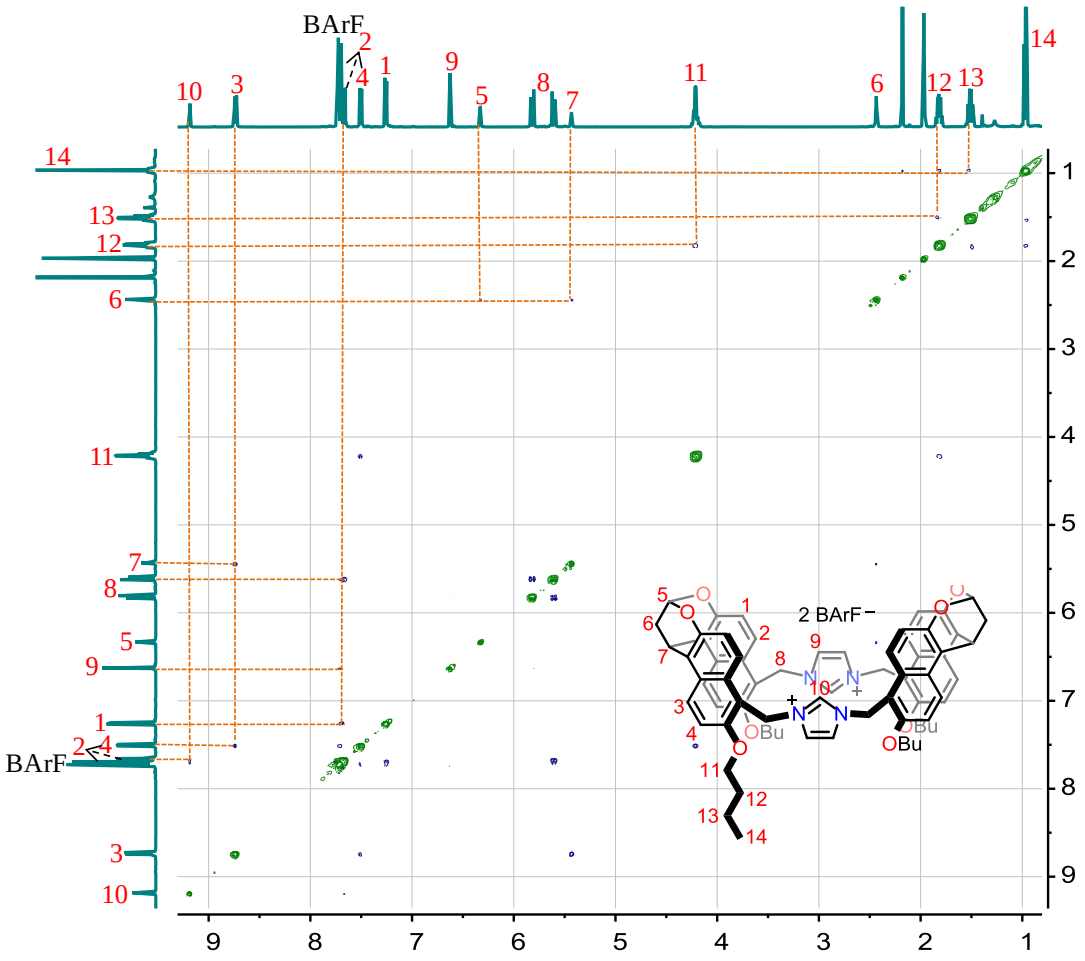

Fig. S2 ^{1}H,^{1}H-ROESY NMR spectrum (500 MHz, CD_3CN, 298 K) of **1a.** The absolute configurations (syn or anti) cannot be assigned based on ROESY NMR spectrum, but were assigned from X-ray single crystal structure.

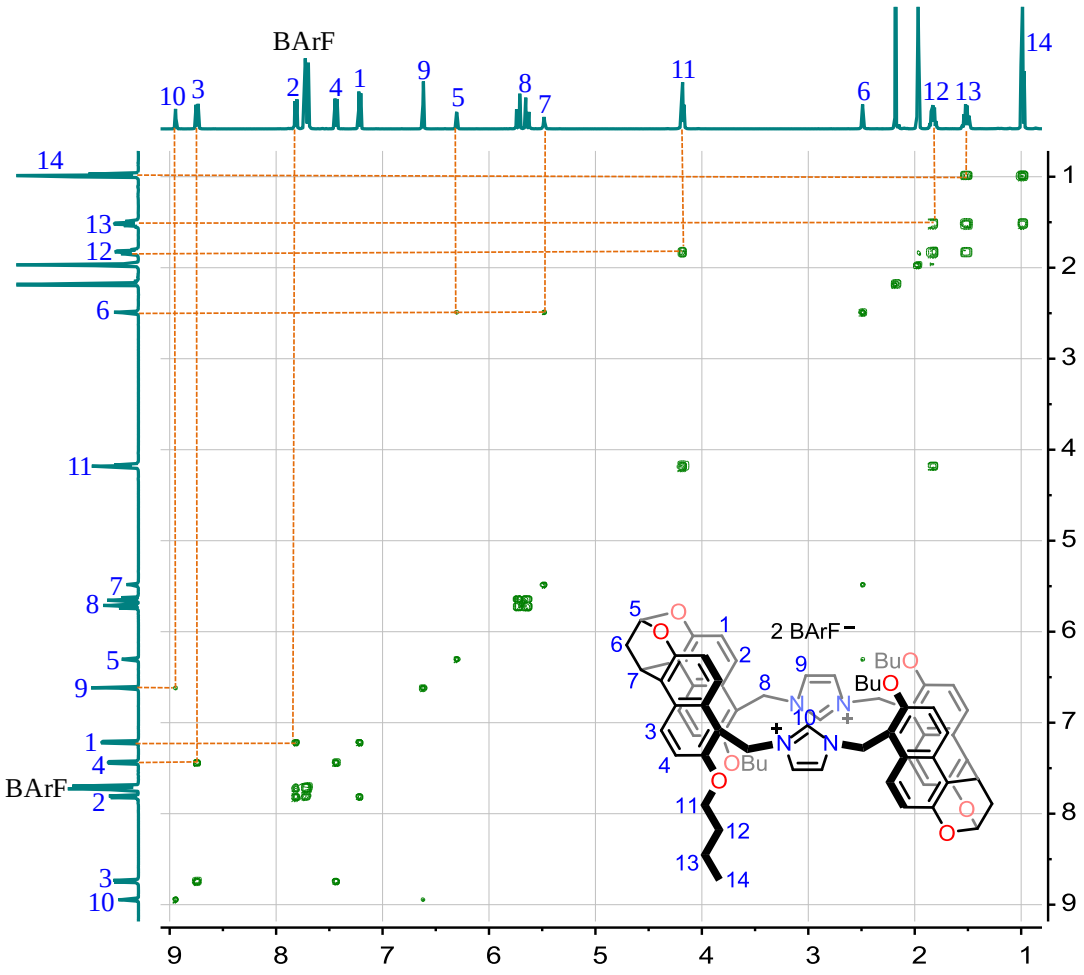

Fig. S3 ^{1}H,^{1}H-COSY NMR spectrum (500 MHz, CD_3CN, 298 K) of Naphthotube **1b**

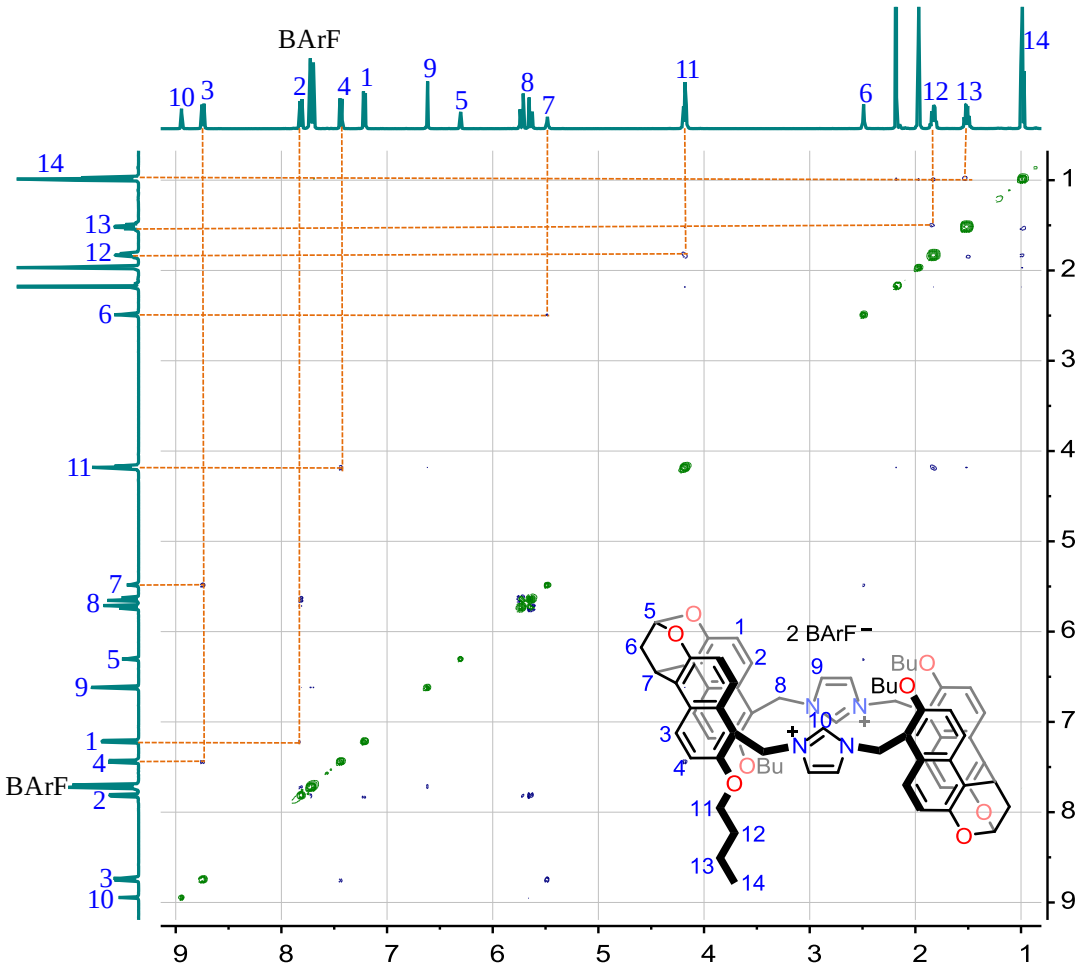

Fig. S4 ^{1}H,^{1}H-ROESY NMR spectrum (500 MHz, CD_3CN, 298 K) of **1b**. The absolute configurations (syn or anti) cannot be assigned based on ROESY NMR spectrum, but were assigned from X-ray single crystal structure.

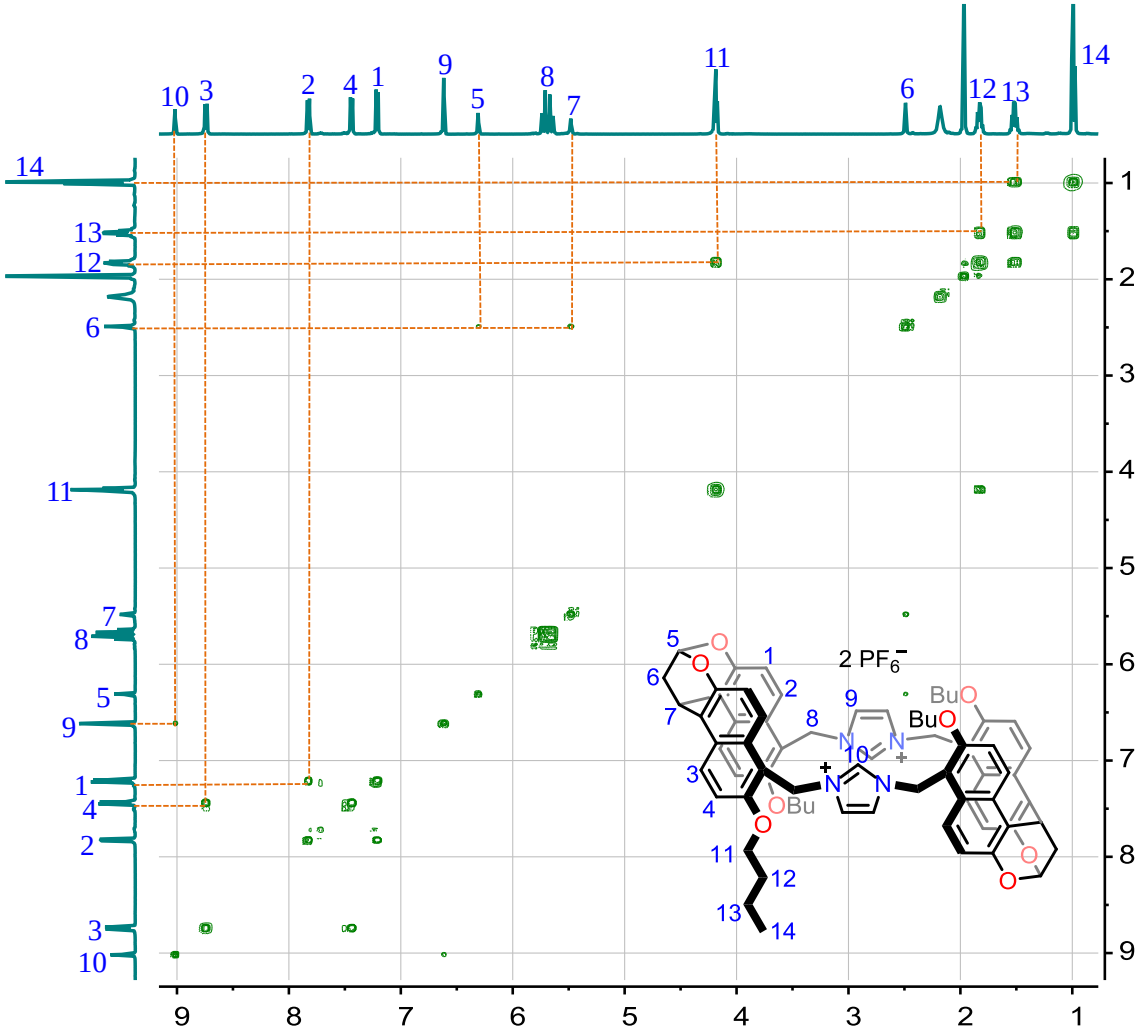

Fig. S5 ^{1}H,^{1}H-COSY NMR spectrum (500 MHz, CD_3CN, 298 K) of Naphthotube **2b**

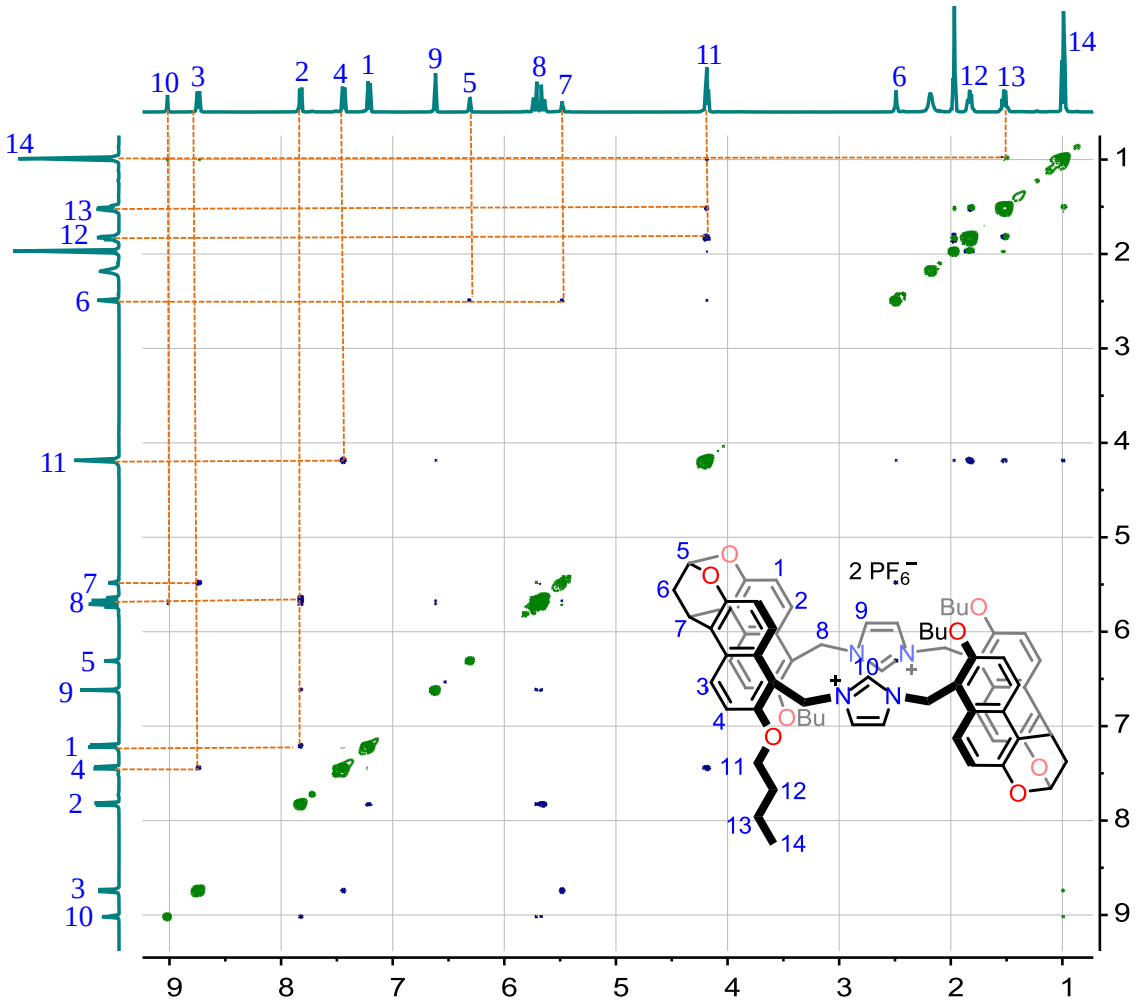

Fig. S6 ^{1}H,^{1}H-ROESY NMR spectrum (500 MHz, CD_3CN, 298 K) of **2b.** The absolute configurations (syn or anti) cannot be assigned based on ROESY NMR spectrum, but were assigned from X-ray single crystal structure.

4. NMR Spectra of Host-Guest Complexes

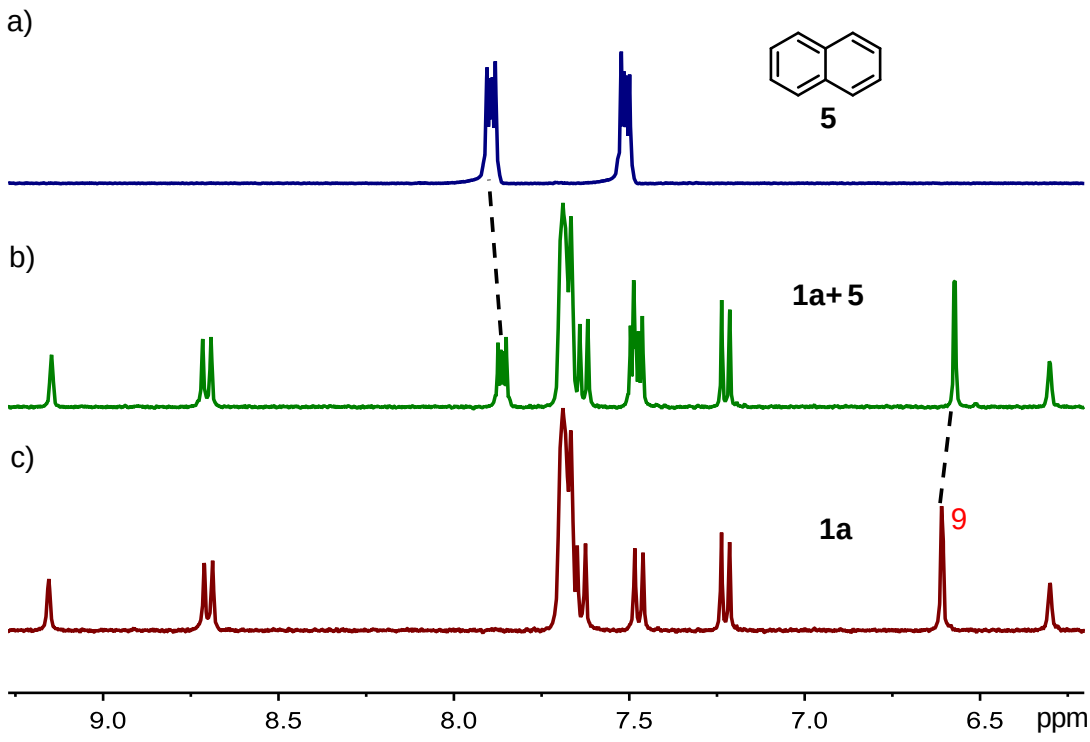

Fig. S7 ^{1}H NMR spectra (400 MHz, CD_3CN, 298 K) of (a) guest **5**, (c) **1a** and (b) its equimolar mixture. The proton of the guest experiences the upfield shift, the proton 9 of the host experiences the upfield shift, suggesting that the complexation between **1a** and guest **5**.

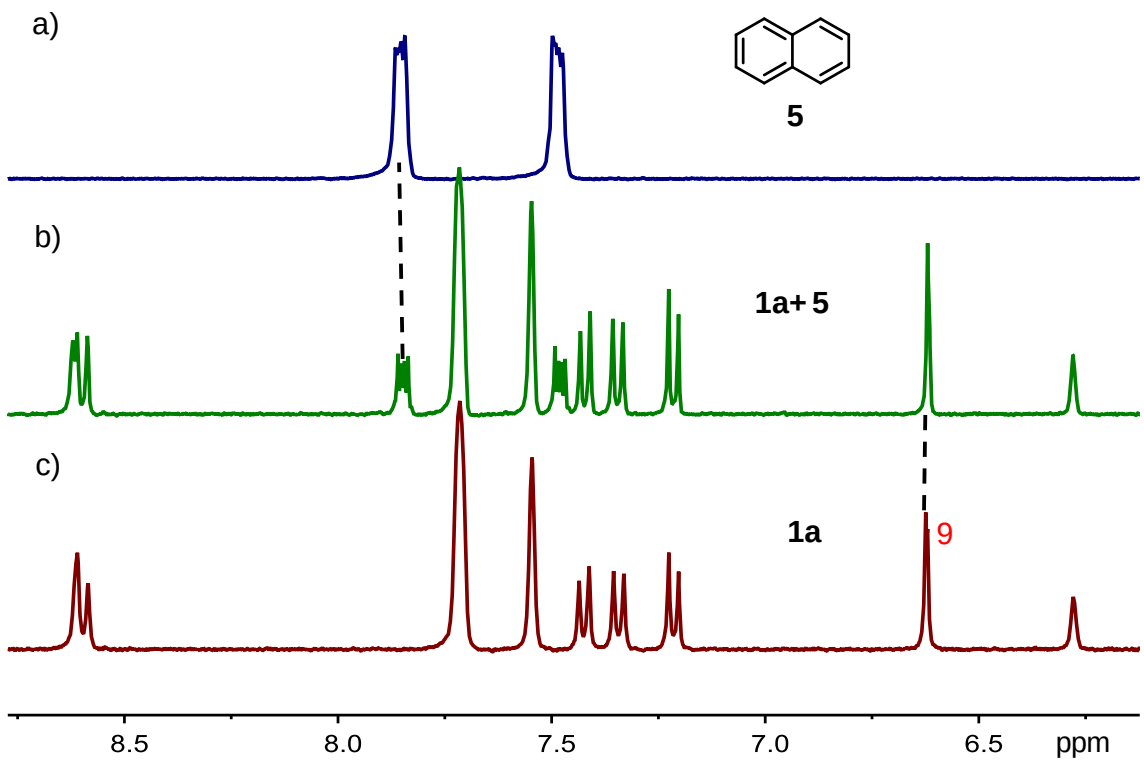

Fig. S8 ^{1}H NMR spectra (400 MHz, CD_2Cl_2, 298 K) of (a) guest **5**, (c) **1a** and (b) its equimolar mixture. The proton of the guest experiences the upfield shift, the proton 9 of the host experiences the upfield shift, suggesting that the complexation between **1a** and guest **5**.

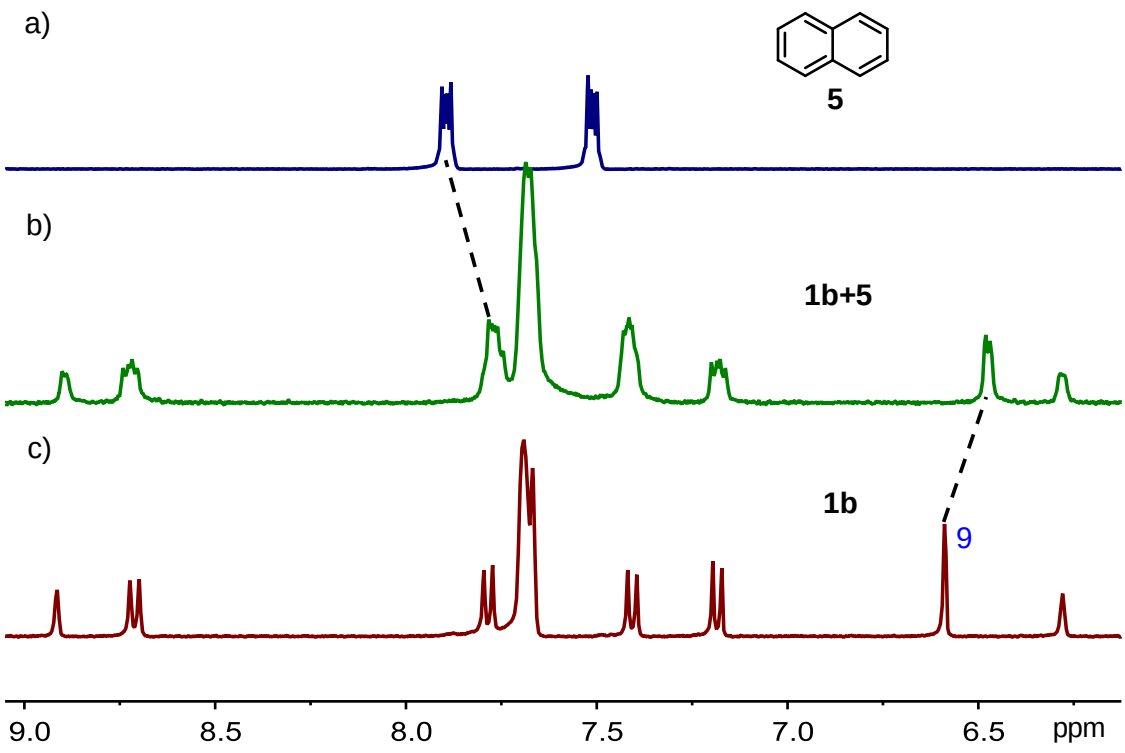

Fig. S9 ^{1}H NMR spectra (400 MHz, CD_3CN, 298 K) of (a) guest **5**, (c) **1b** and (b) its equimolar mixture. The proton of the guest experiences the upfield shift, the proton 9 of the host experiences the upfield shift, suggesting that the complexation between **1b** and guest **5**.

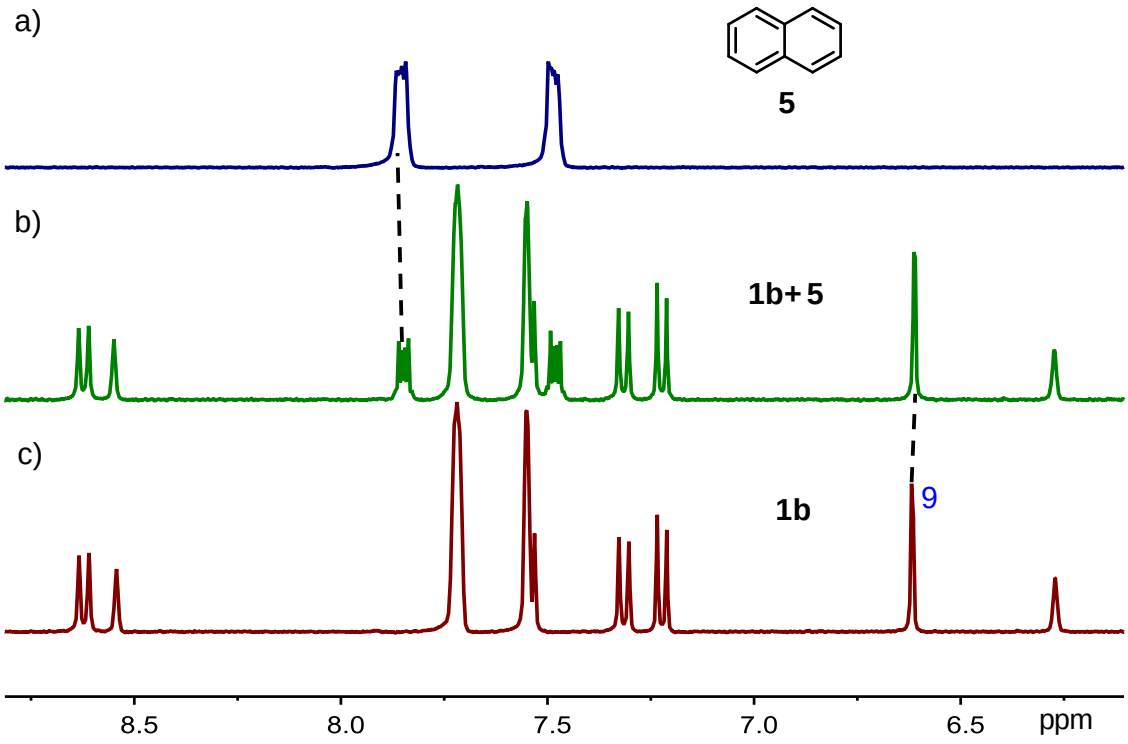

Fig. S10 ^{1}H NMR spectra (400 MHz, CD_2Cl_2, 298 K) of (a) guest **5**, (c) **1b** and (b) its equimolar mixture. The proton of the guest experiences the upfield shift, the proton 9 of the host experiences the upfield shift, suggesting that the complexation between **1b** and guest **5**.

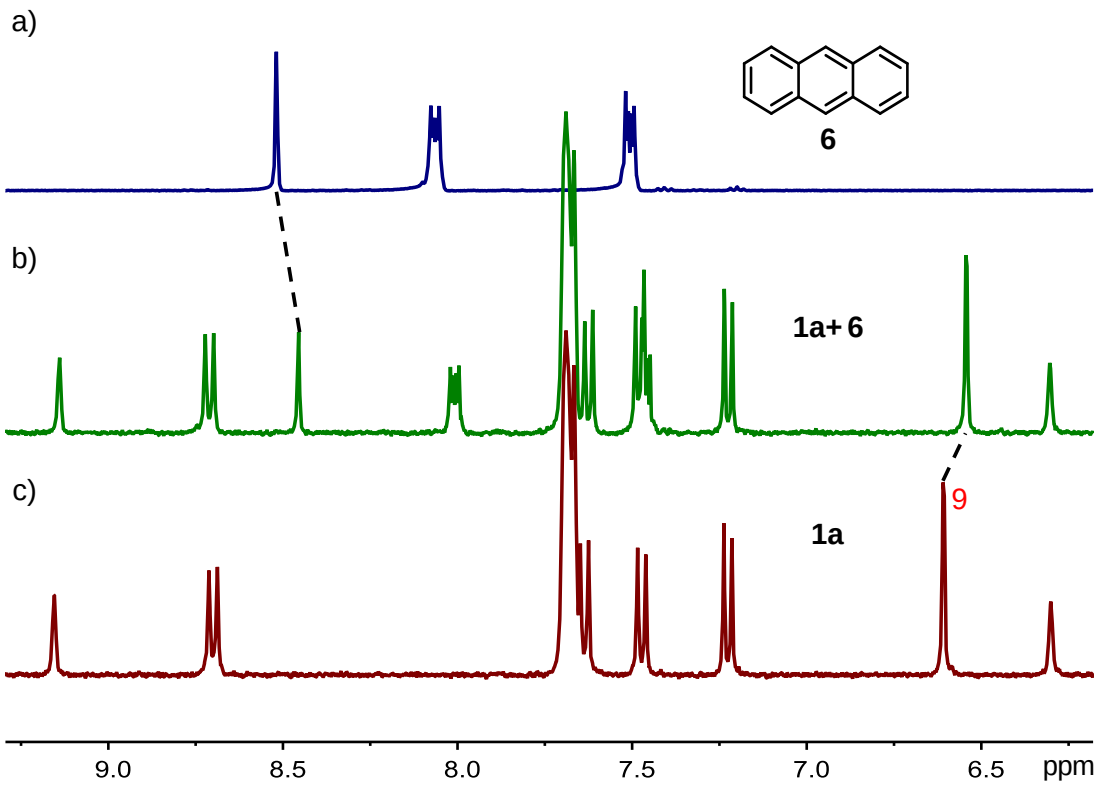

Fig. S11 ^{1}H NMR spectra (400 MHz, CD_3CN, 298 K) of (a) guest **6**, (c) **1a** and (b) its equimolar mixture. The proton of the guest experiences the upfield shift, the proton 9 of the host experiences the upfield shift, suggesting that the complexation between **1a** and guest **6**.

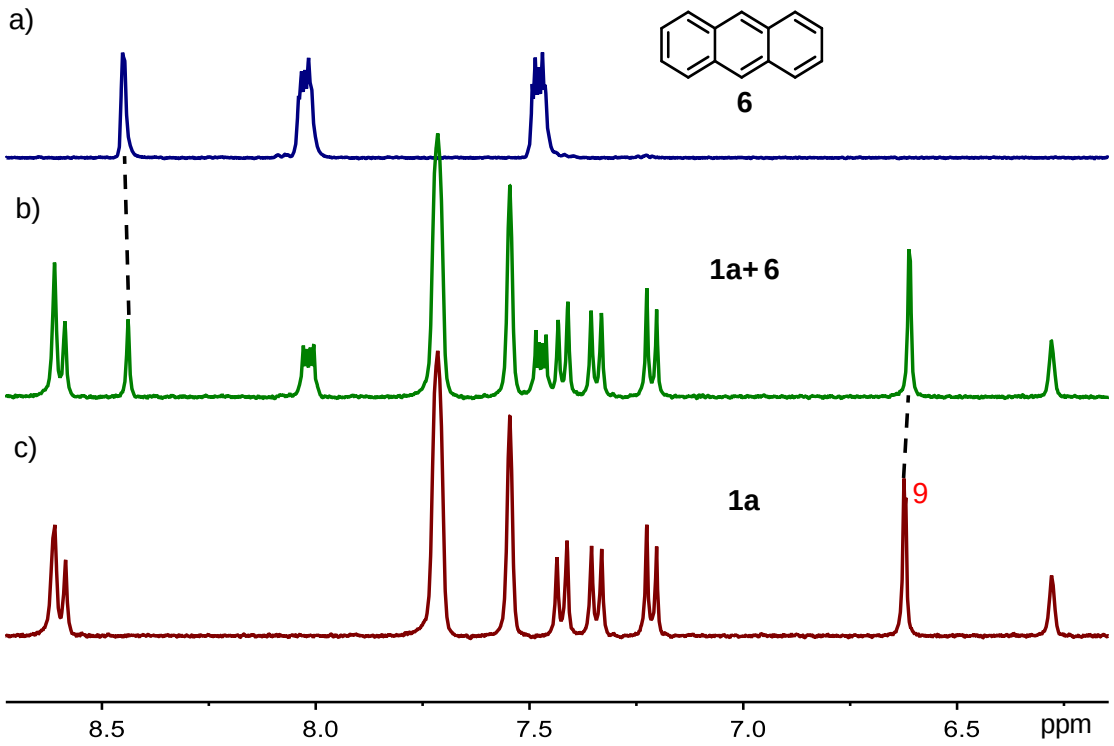

Fig. S12 ^{1}H NMR spectra (400 MHz, CD_2Cl_2, 298 K) of (a) guest **6**, (c) **1a** and (b) its equimolar mixture. The proton of the guest experiences the upfield shift, the proton 9 of the host experiences the upfield shift, suggesting that the complexation between **1a** and guest **6**.

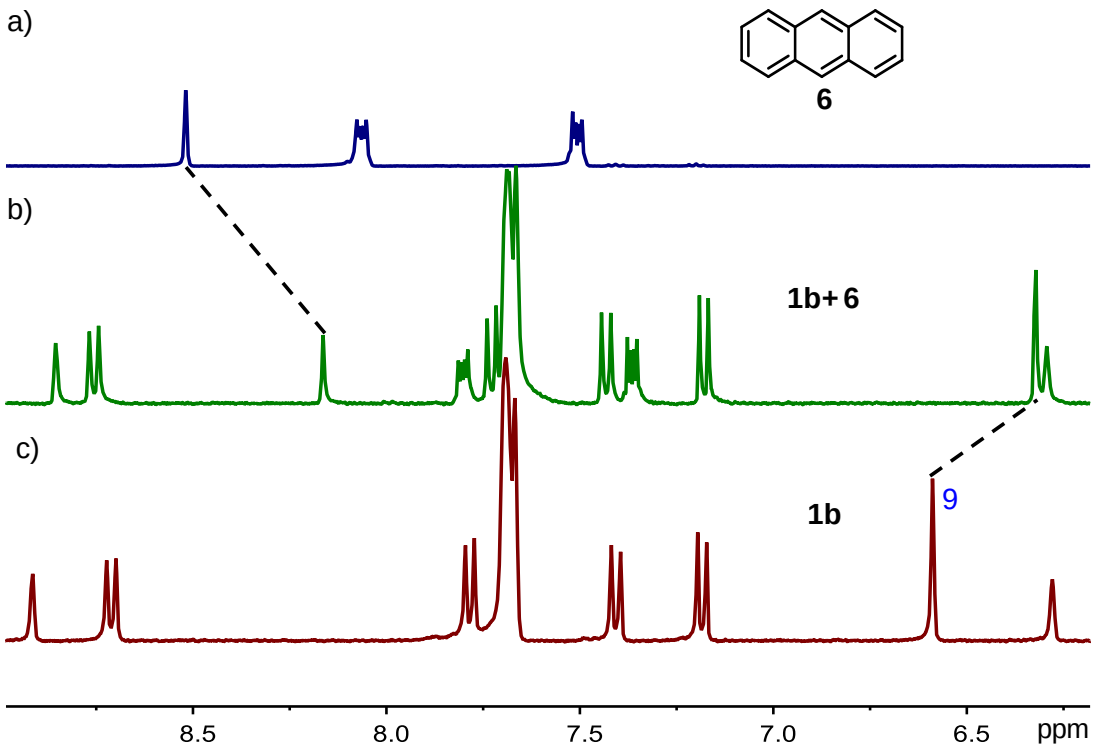

Fig. S13 ^{1}H NMR spectra (400 MHz, CD_3CN, 298 K) of (a) guest **6**, (c) **1b** and (b) its equimolar mixture. The proton of the guest experiences the upfield shift, the proton 9 of the host experiences the upfield shift, suggesting that the complexation between **1b** and guest **6**.

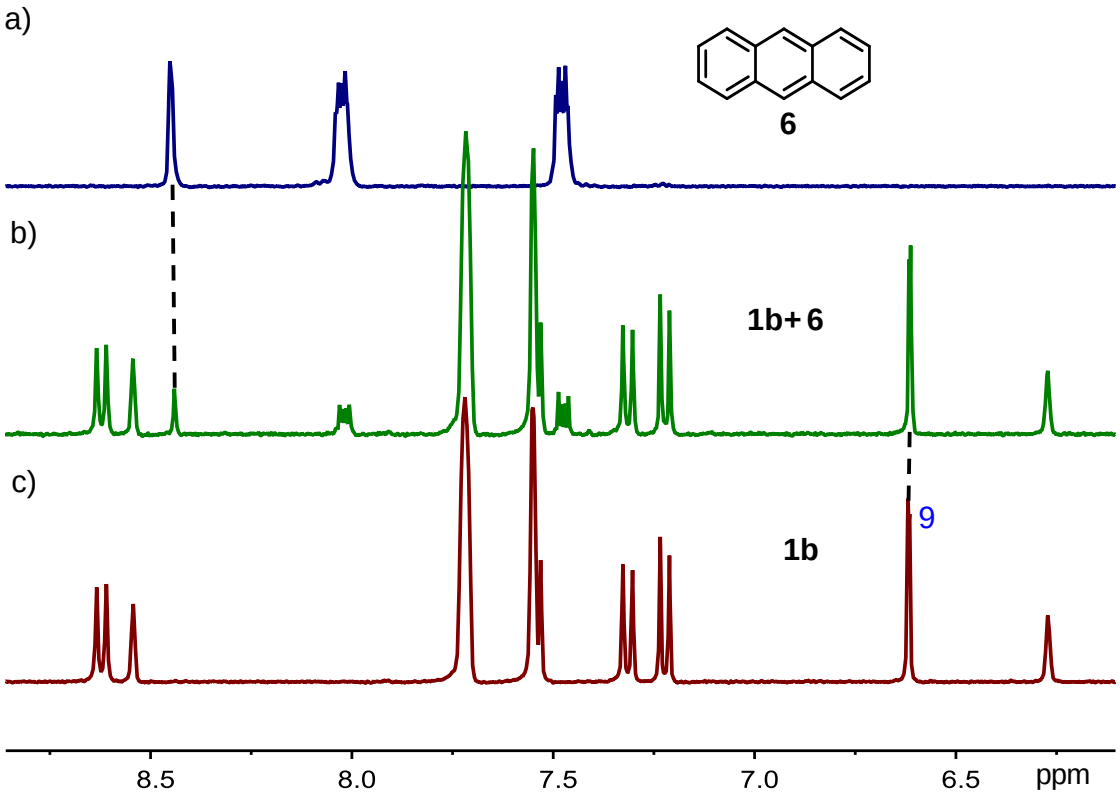

Fig. S14 ^{1}H NMR spectra (400 MHz, CD_2Cl_2, 298 K) of (a) guest **6**, (c) **1b** and (b) its equimolar mixture. The proton of the guest experiences the upfield shift, the proton 9 of the host experiences the upfield shift, suggesting that the complexation between **1b** and guest **6**.

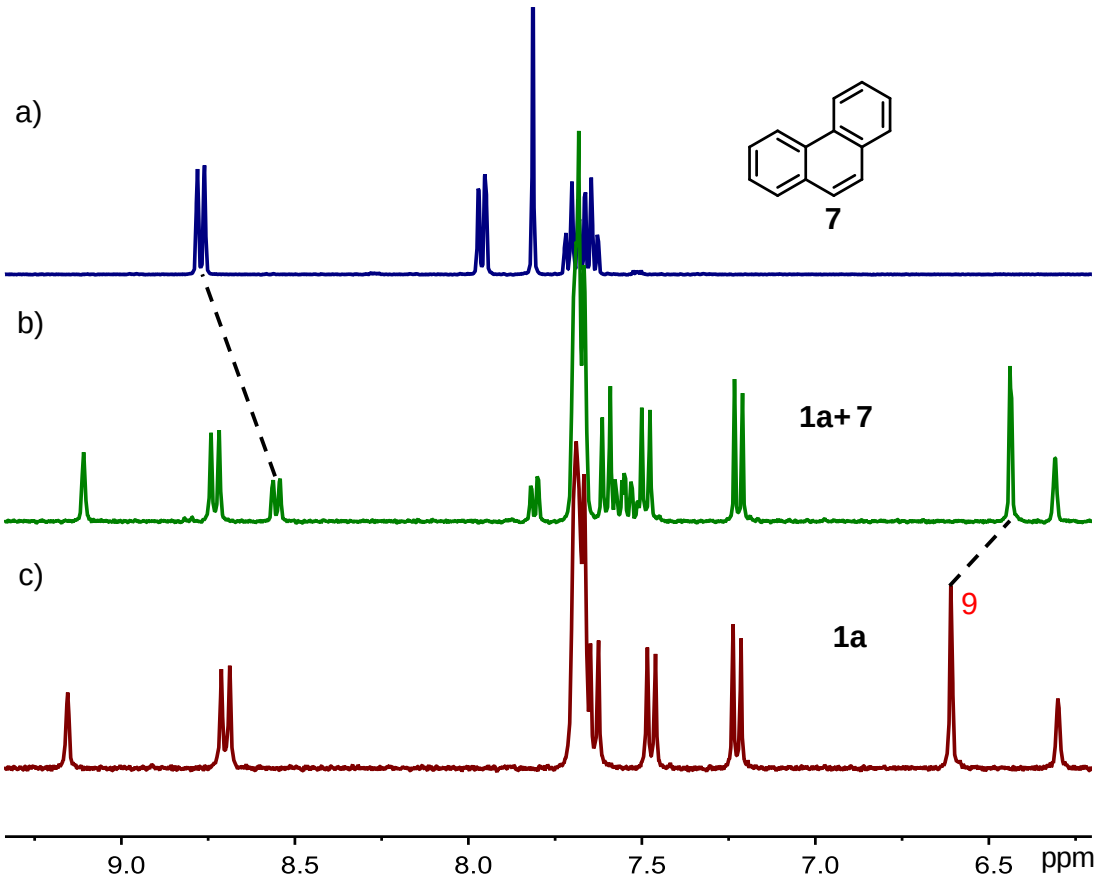

Fig. S15 ^{1}H NMR spectra (400 MHz, CD_3CN, 298 K) of (a) guest **7**, (c) **1a** and (b) its equimolar mixture. The proton of the guest experiences the upfield shift, the proton 9 of the host experiences the upfield shift, suggesting that the complexation between **1a** and guest **7**.

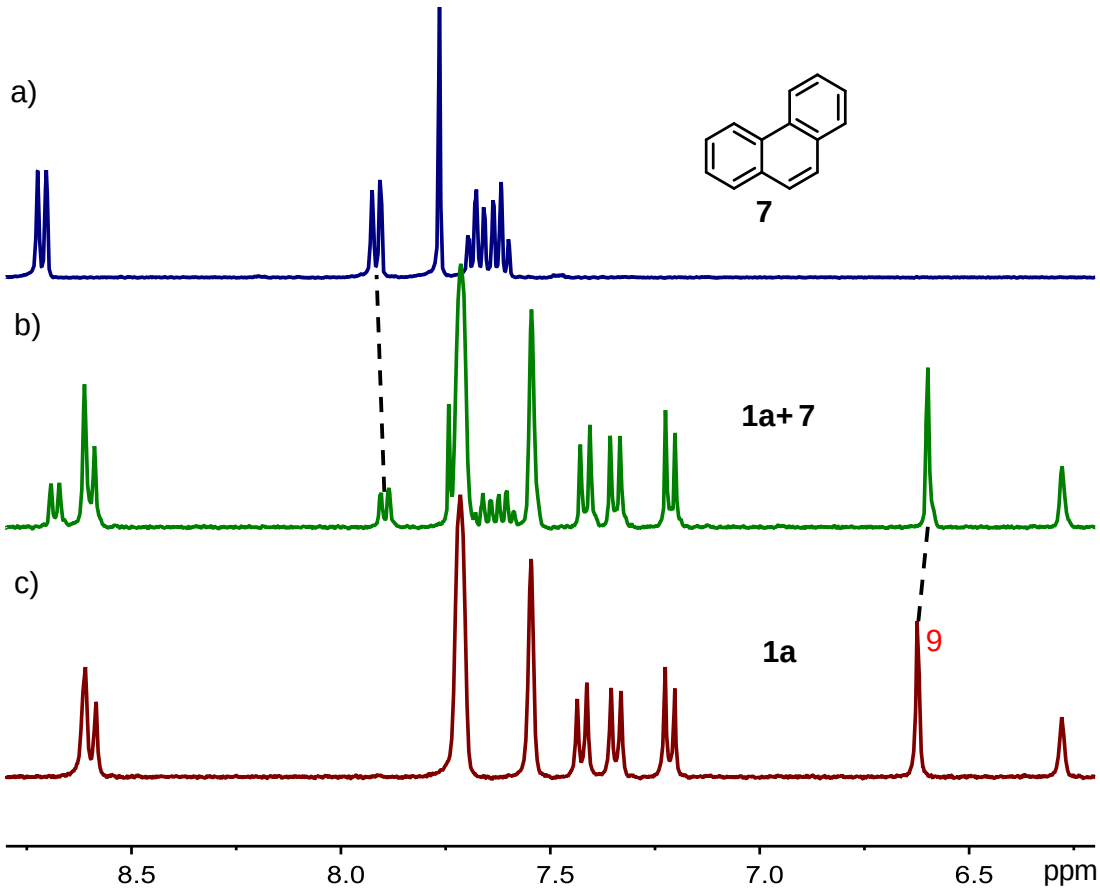

Fig. S16 ^{1}H NMR spectra (400 MHz, CD_2Cl_2, 298 K) of (a) guest **7**, (c) **1a** and (b) its equimolar mixture. The proton of the guest experiences the upfield shift, the proton 9 of the host experiences the upfield shift, suggesting that the complexation between **1a** and guest **7**.

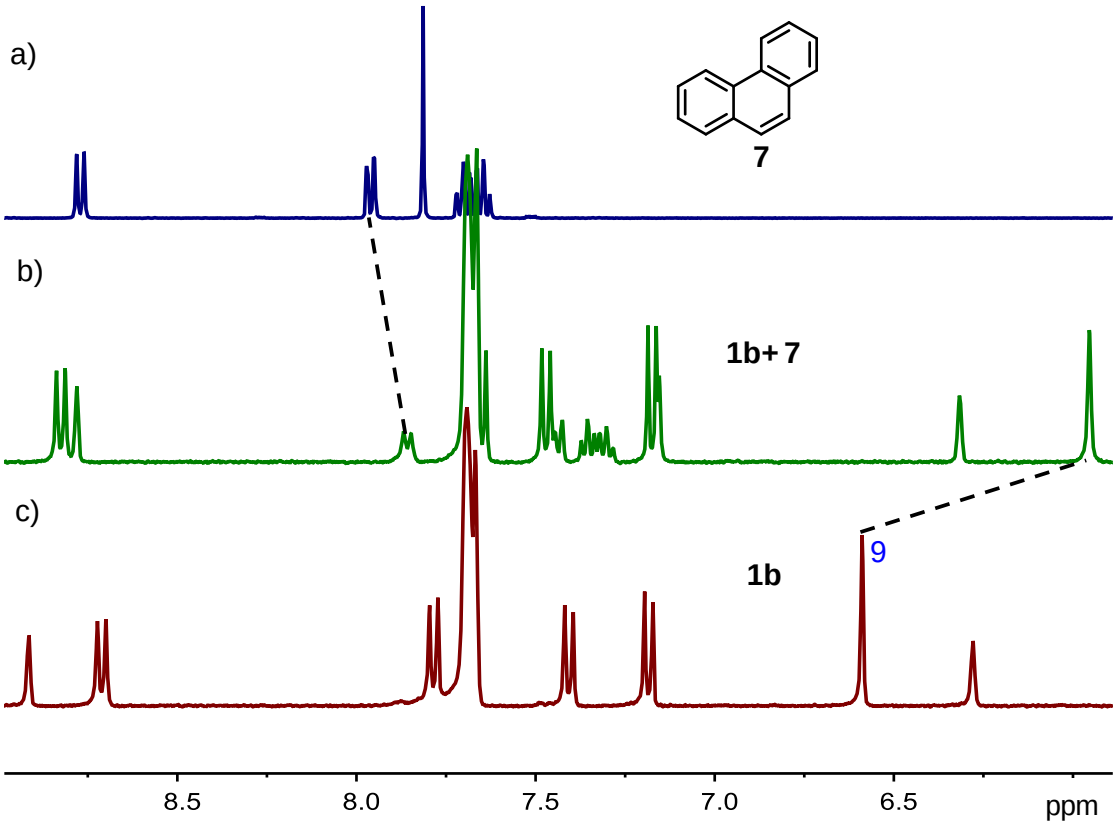

Fig. S17 ^{1}H NMR spectra (400 MHz, CD_3CN, 298 K) of (a) guest **7**, (c) **1b** and (b) its equimolar mixture. The proton of the guest experiences the upfield shift, the proton 9 of the host experiences the upfield shift, suggesting that the complexation between **1b** and guest **7**.

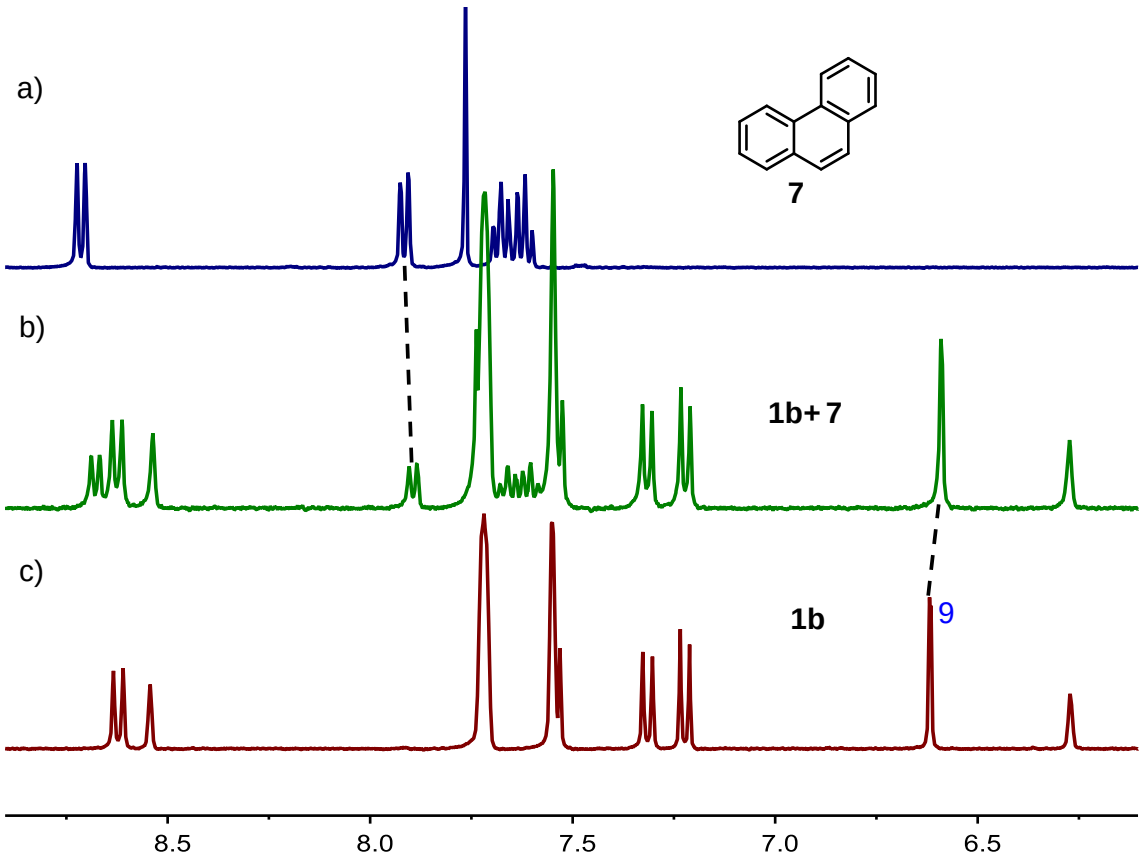

Fig. S18 ^{1}H NMR spectra (400 MHz, CD_2Cl_2, 298 K) of (a) guest **7**, (c) **1b** and (b) its equimolar mixture. The proton of the guest experiences the upfield shift, the proton 9 of the host experiences the upfield shift, suggesting that the complexation between **1b** and guest **7**.

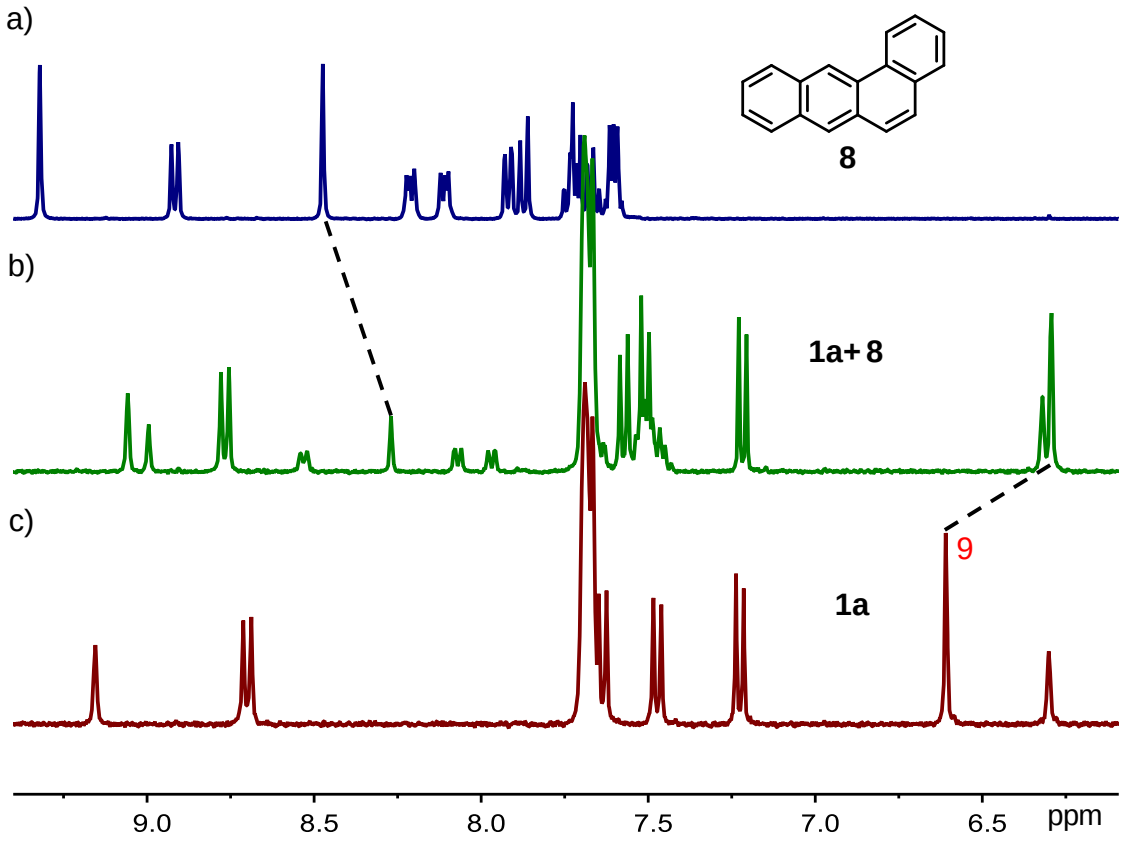

Fig. S19 ^{1}H NMR spectra (400 MHz, CD_3CN, 298 K) of (a) guest **8**, (c) **1a** and (b) its equimolar mixture. The proton of the guest experiences the upfield shift, the proton 9 of the host experiences the upfield shift, suggesting that the complexation between **1a** and guest **8**.

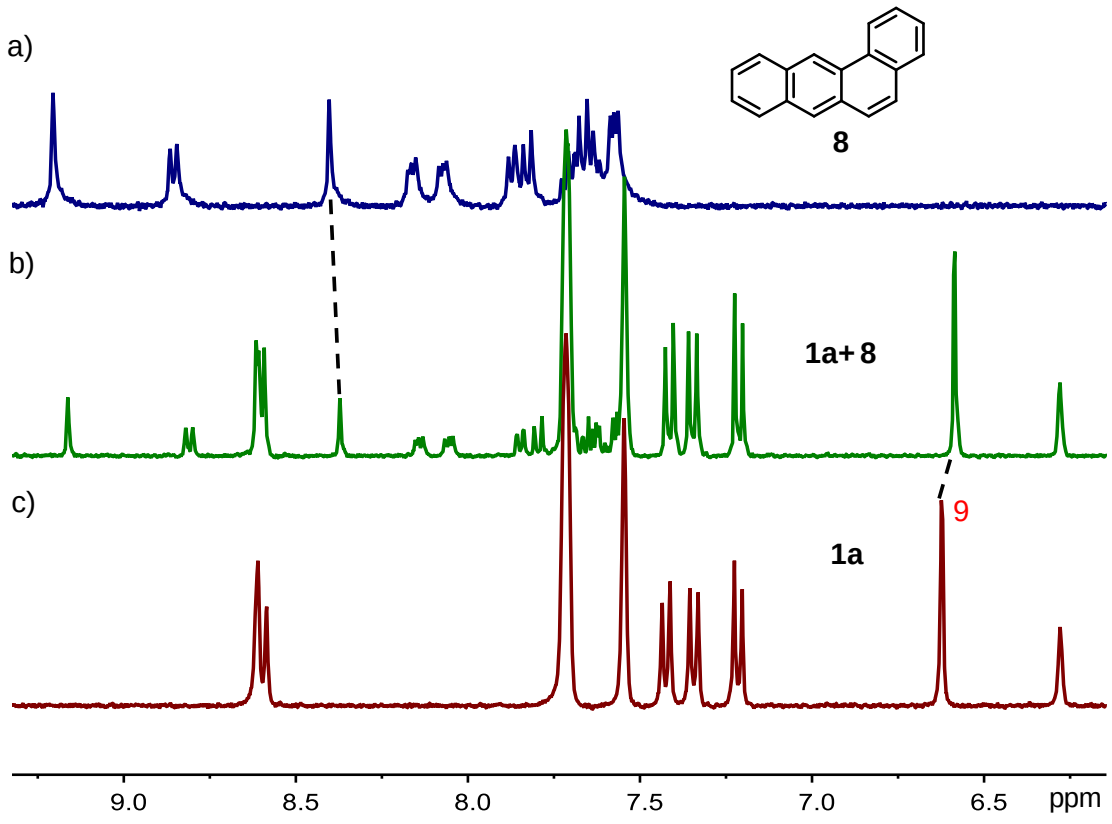

Fig. S20 ^{1}H NMR spectra (400 MHz, CD_2Cl_2, 298 K) of (a) guest **8**, (c) **1a** and (b) its equimolar mixture. The proton of the guest experiences the upfield shift, the proton 9 of the host experiences the upfield shift, suggesting that the complexation between **1a** and guest **8**.

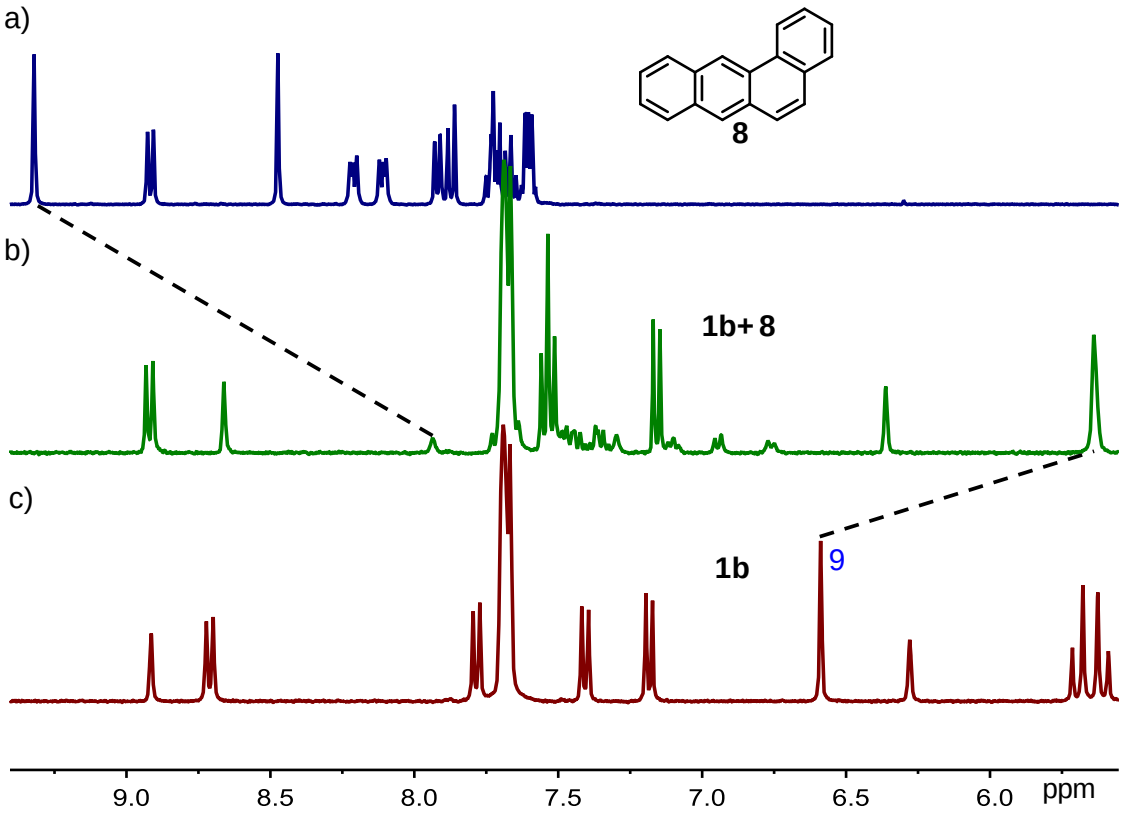

Fig. S21 ^{1}H NMR spectra (400 MHz, CD_3CN, 298 K) of (a) guest **8**, (c) **1b** and (b) its equimolar mixture. The proton of the guest experiences the upfield shift, the proton 9 of the host experiences the upfield shift, suggesting that the complexation between **1b** and guest **8**.

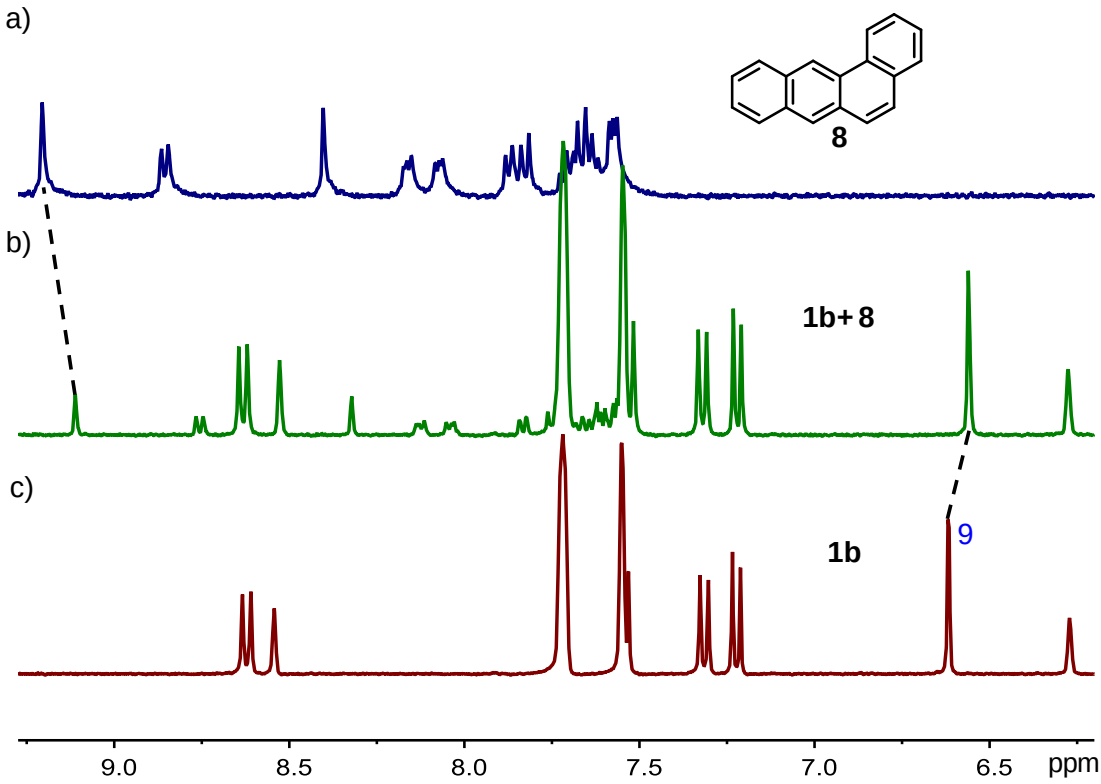

Fig. S22 ^{1}H NMR spectra (400 MHz, CD_2Cl_2, 298 K) of (a) guest **8**, (c) **1b** and (b) its equimolar mixture. The proton of the guest experiences the upfield shift, the proton 9 of the host experiences the upfield shift, suggesting that the complexation between **1b** and guest **8**.

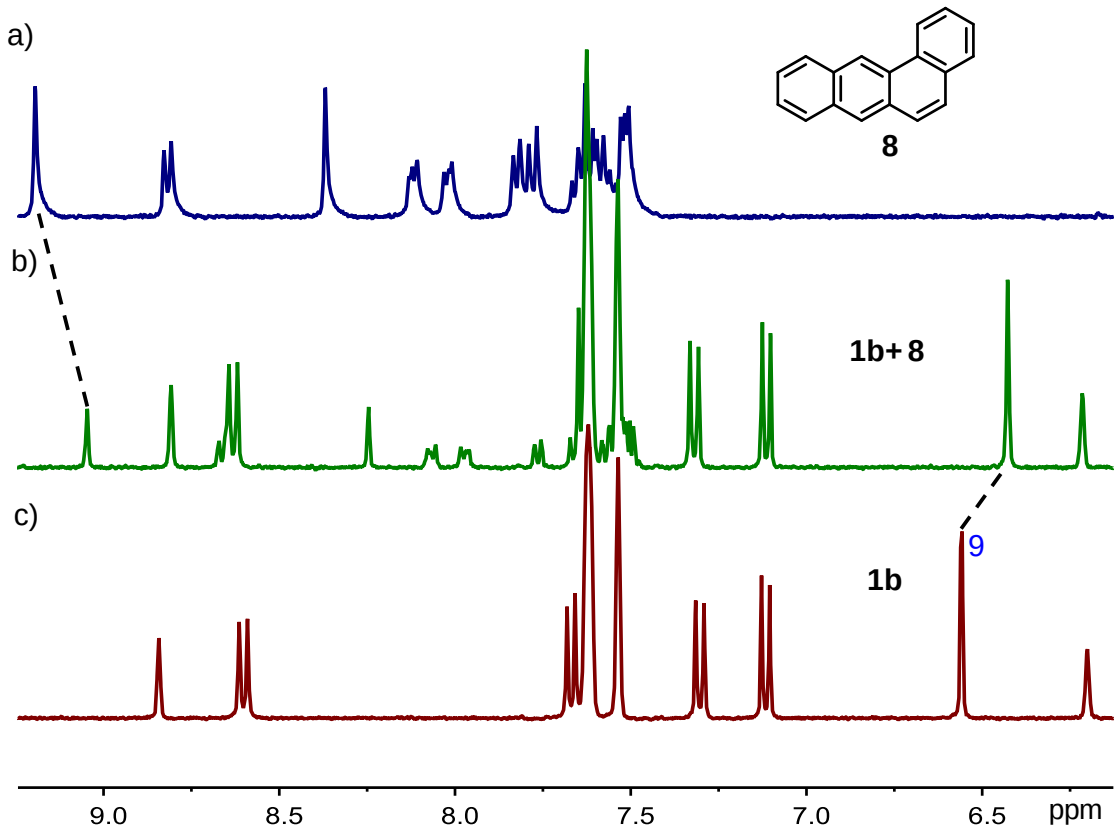

Fig. S23 ^{1}H NMR spectra (400 MHz, CD_3CN:CD_2Cl_2= 1:1, 298 K) of (a) guest **8**, (c) **1b** and (b) its equimolar mixture. The proton of the guest experiences the upfield shift, the proton 9 of the host experiences the upfield shift, suggesting that the complexation between **1b** and guest **8**.

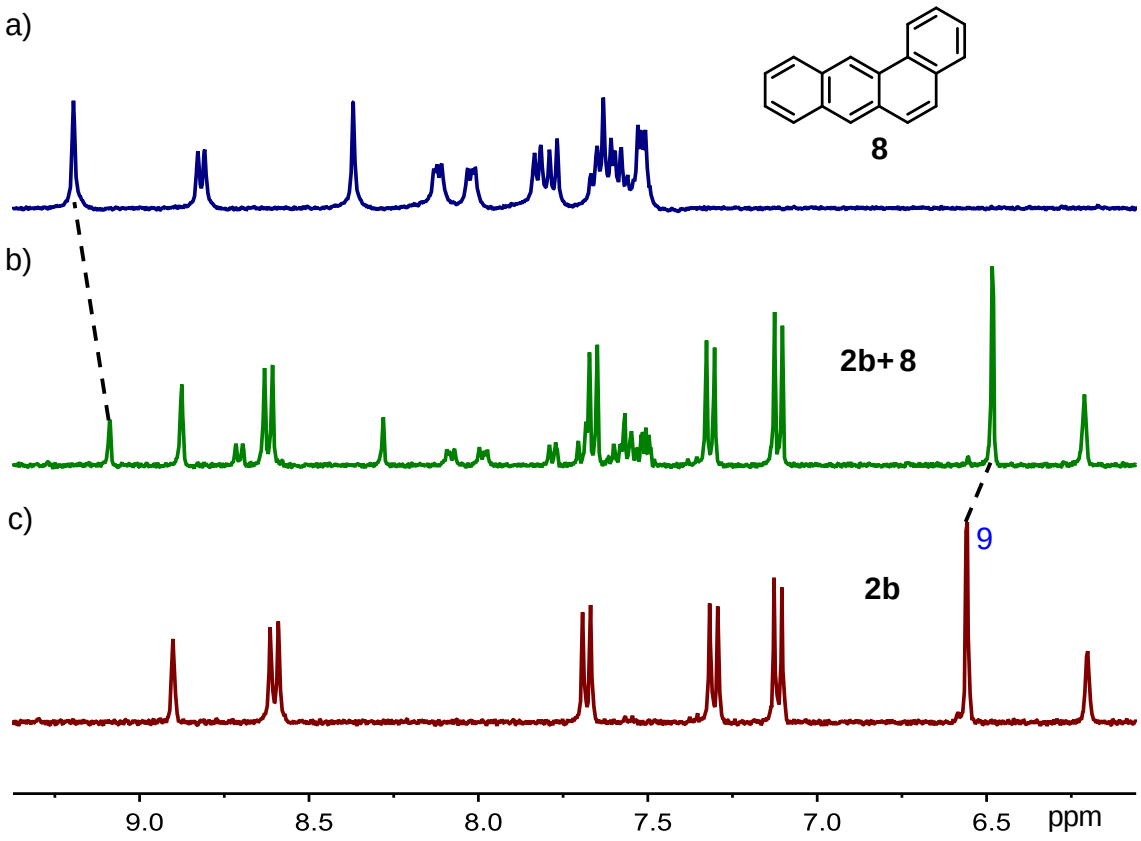

Fig. S24 ^{1}H NMR spectra (400 MHz, CD_3CN:CD_2Cl_2= 1:1, 298 K) of (a) guest **8**, (c) **2b** and (b) its equimolar mixture. The proton of the guest experiences the upfield shift, the proton 9 of the host experiences the upfield shift, suggesting that the complexation between **2b** and guest **8**.

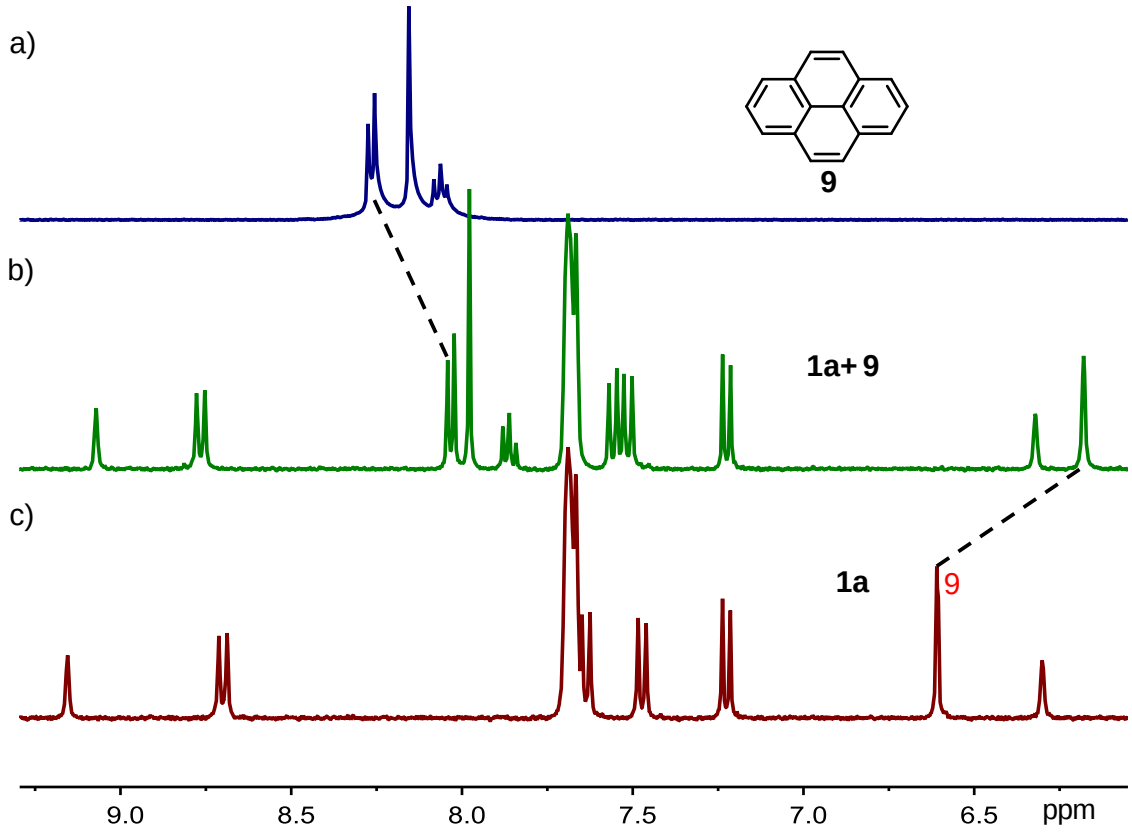

Fig. S25 ^{1}H NMR spectra (400 MHz, CD_3CN, 298 K) of (a) guest **9**, (c) **1a** and (b) its equimolar mixture. The proton of the guest experiences the upfield shift, the proton 9 of the host experiences the upfield shift, suggesting that the complexation between **1a** and guest **9**.

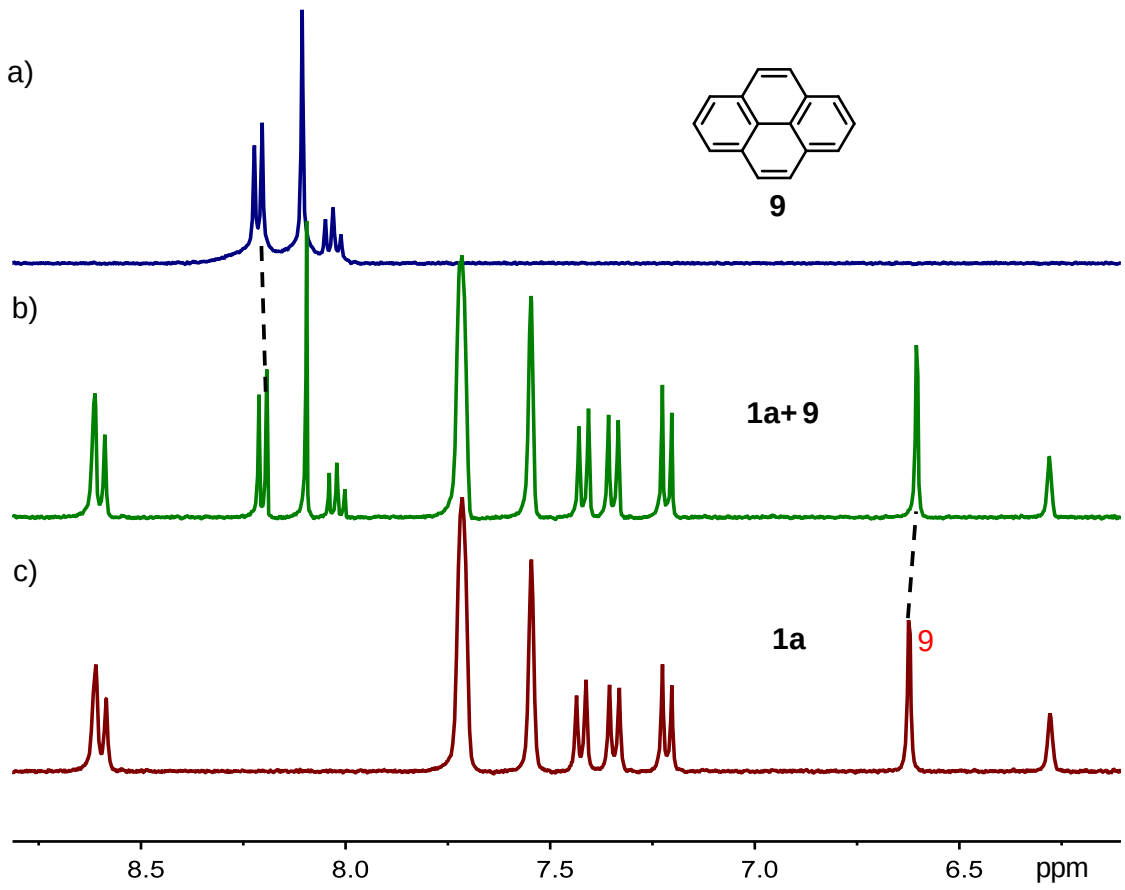

Fig. S26 ^{1}H NMR spectra (400 MHz, CD_2Cl_2, 298 K) of (a) guest **9**, (c) **1a** and (b) its equimolar mixture. The proton of the guest experiences the upfield shift, the proton 9 of the host experiences the upfield shift, suggesting that the complexation between **1a** and guest **9**.

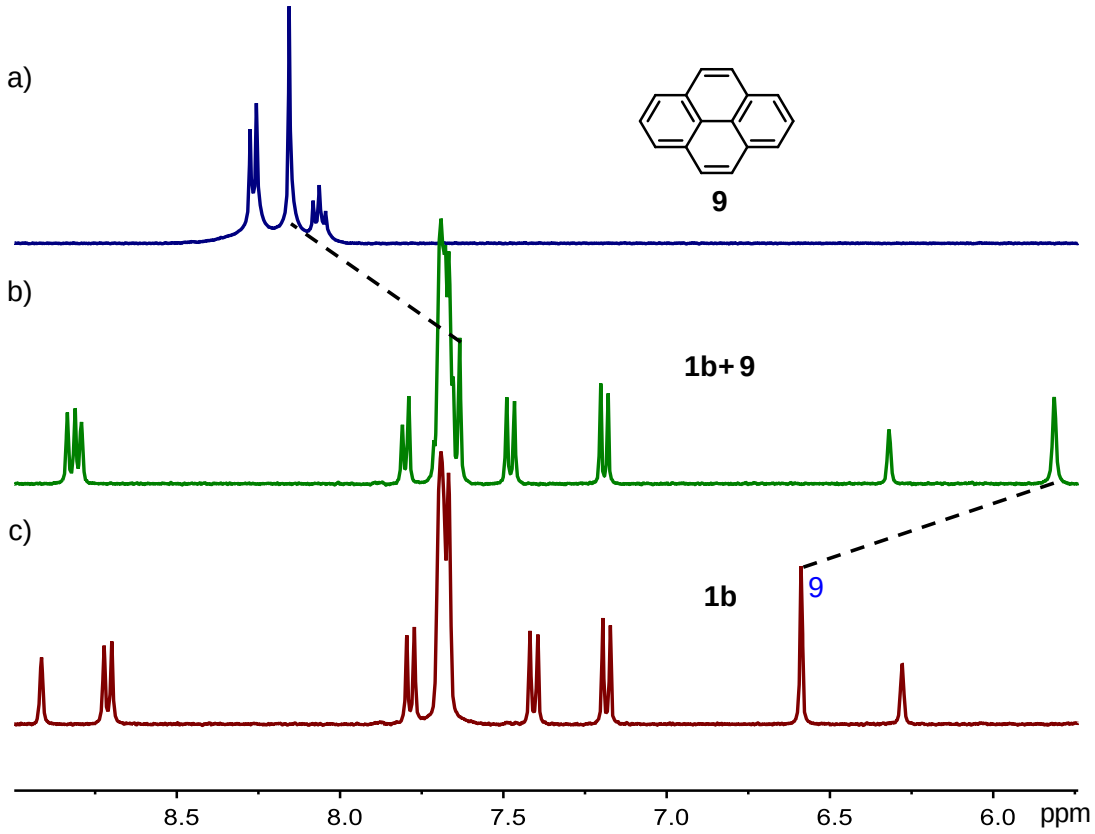

Fig. S27 ^{1}H NMR spectra (400 MHz, CD_3CN, 298 K) of (a) guest **9**, (c) **1b** and (b) its equimolar mixture. The proton of the guest experiences the upfield shift, the proton 9 of the host experiences the upfield shift, suggesting that the complexation between **1b** and guest **9**.

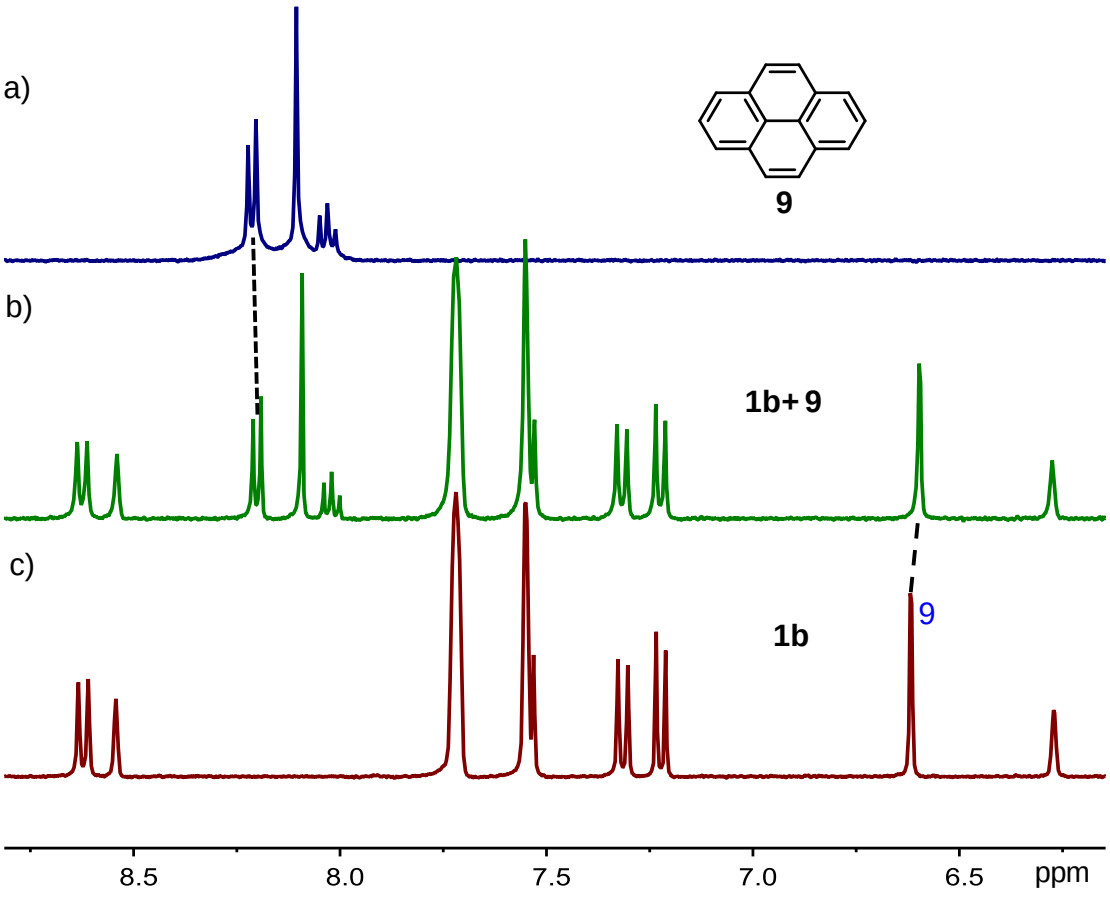

Fig. S28 ^{1}H NMR spectra (400 MHz, CD_2Cl_2, 298 K) of (a) guest **9**, (c) **1b** and (b) its equimolar mixture. The proton of the guest experiences the upfield shift, the proton 9 of the host experiences the upfield shift, suggesting that the complexation between **1b** and guest **9**.

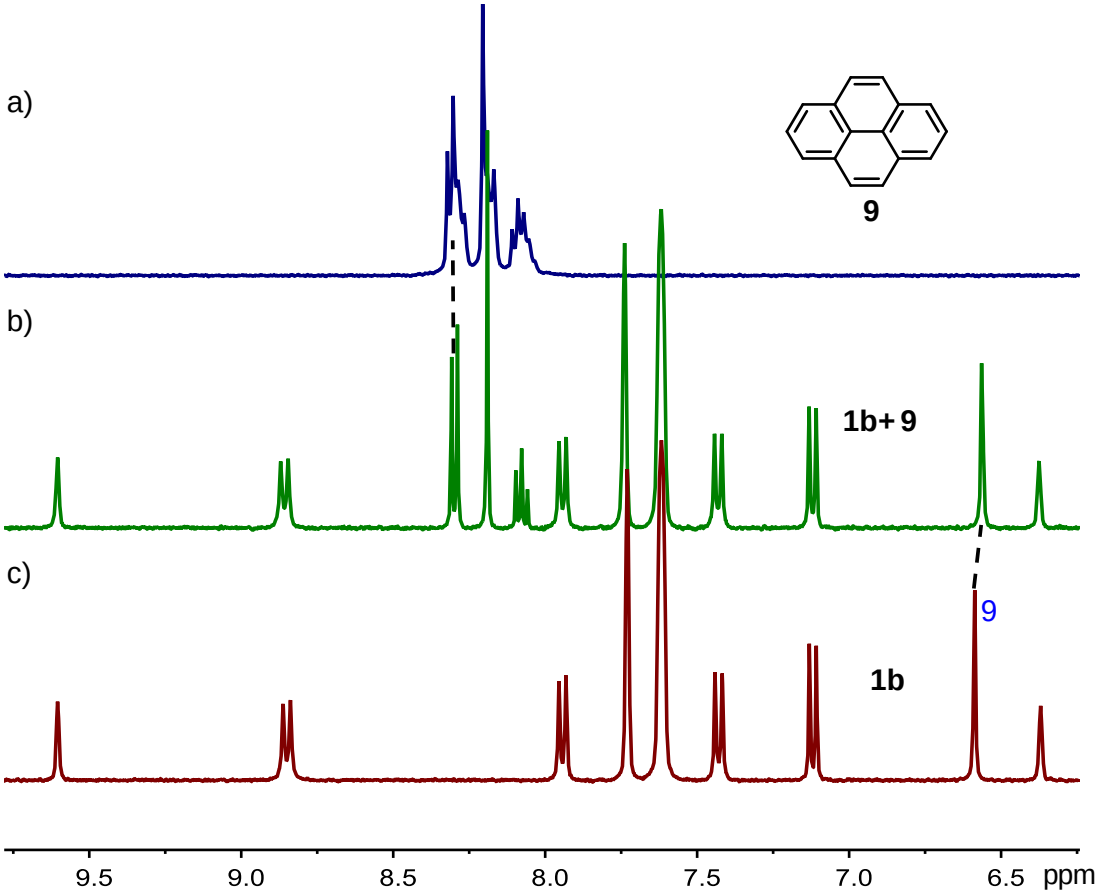

Fig. S29 ^{1}H NMR spectra (400 MHz, DMSO-d_6, 298 K) of (a) guest **9**, (c) **1b** and (b) its equimolar mixture. The proton of the guest experiences the upfield shift, the proton 9 of the host experiences the upfield shift, suggesting that the complexation between **1b** and guest **9**.

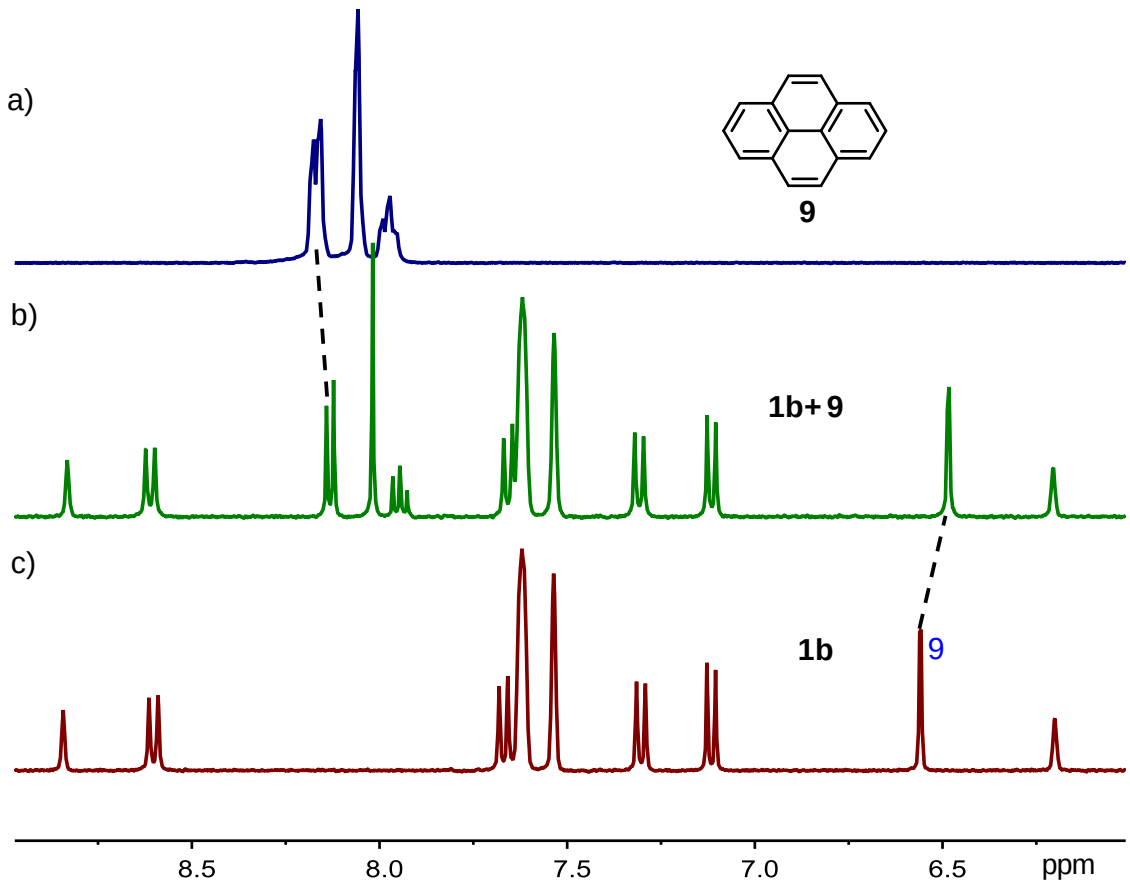

Fig. S30 ^{1}H NMR spectra (400 MHz, CD_3CN:CD_2Cl_2= 1:1, 298 K) of (a) guest **9**, (c) **1b** and (b) its equimolar mixture. The proton of the guest experiences the upfield shift, the proton 9 of the host experiences the upfield shift, suggesting that the complexation between **1b** and guest **9**.

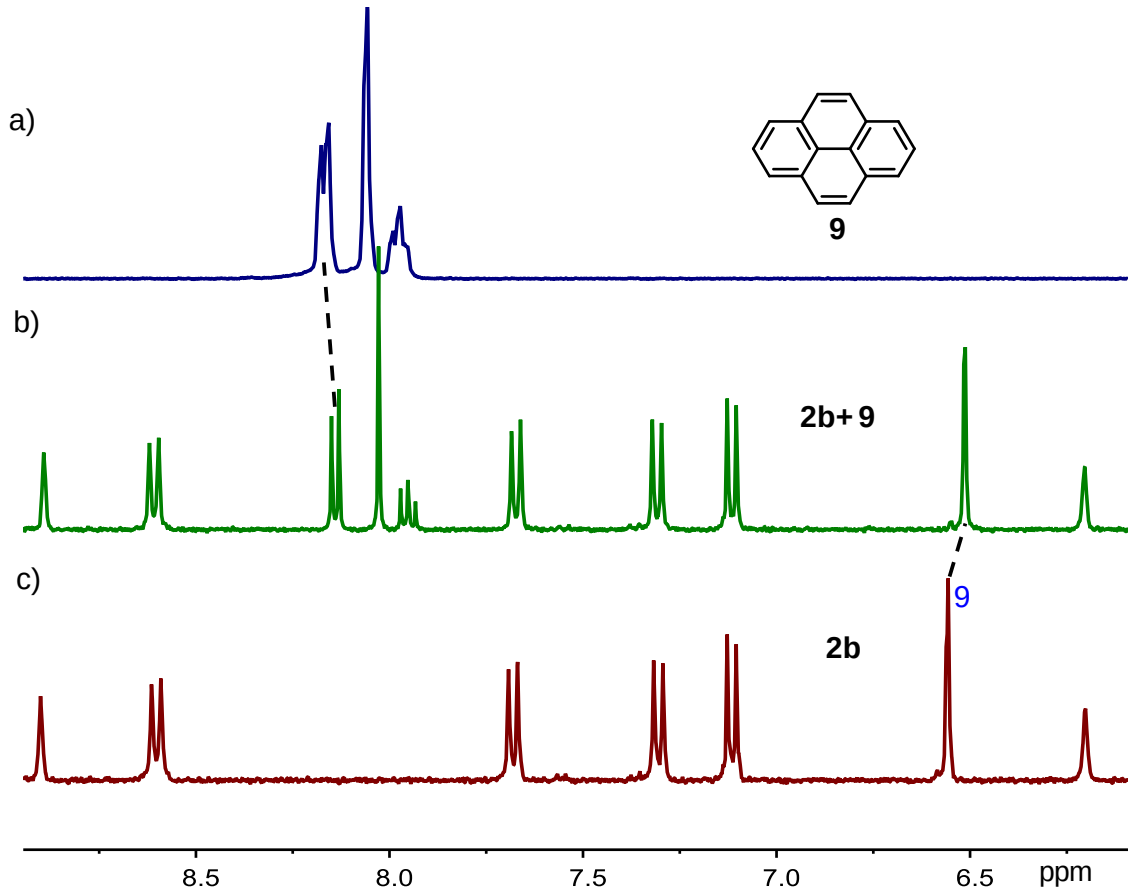

Fig. S31 ^{1}H NMR spectra (400 MHz, CD_3CN:CD_2Cl_2= 1:1, 298 K) of (a) guest **9**, (c) **2b** and (b) its equimolar mixture. The proton of the guest experiences the upfield shift, the proton 9 of the host experiences the upfield shift, suggesting that the complexation between **2b** and guest **9**.

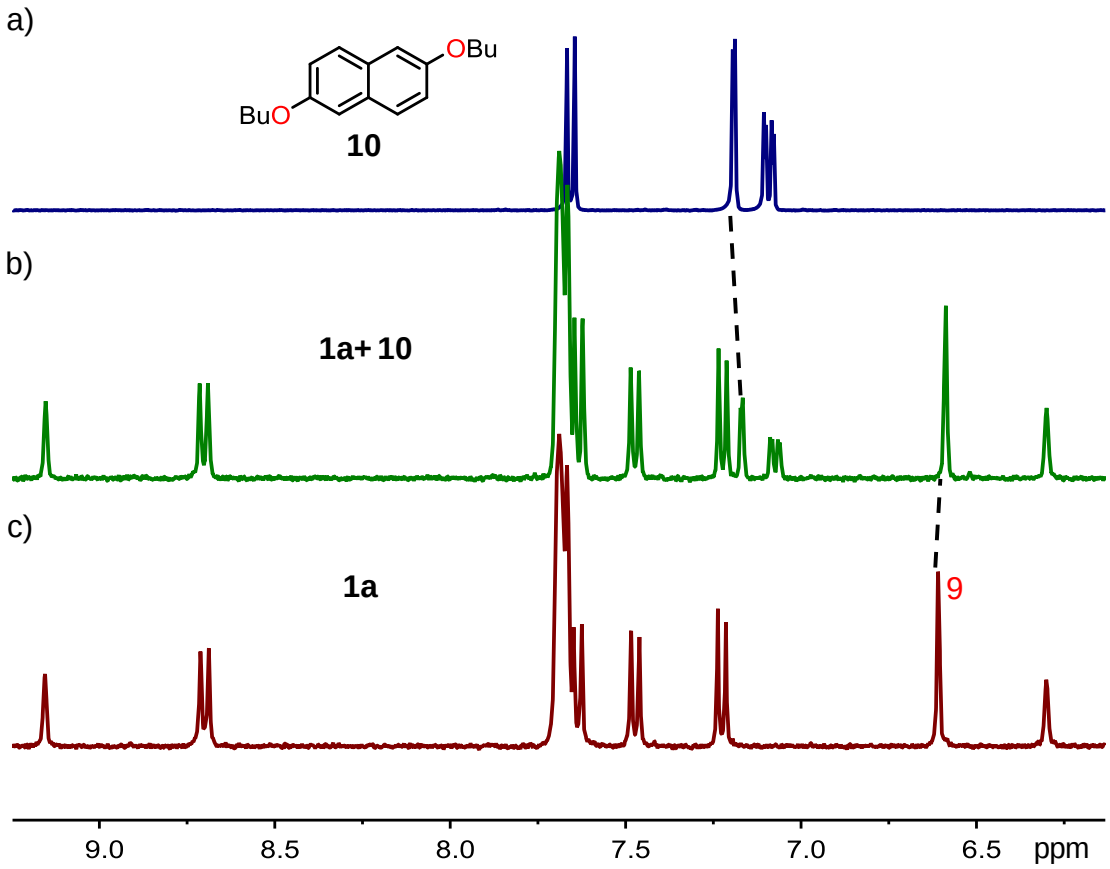

Fig. S32 ^{1}H NMR spectra (400 MHz, CD_3CN, 298 K) of (a) guest **10**, (c) **1a** and (b) its equimolar mixture. The proton of the guest experiences the upfield shift, the proton 9 of the host experiences the upfield shift, suggesting that the complexation between **1a** and guest **10**.

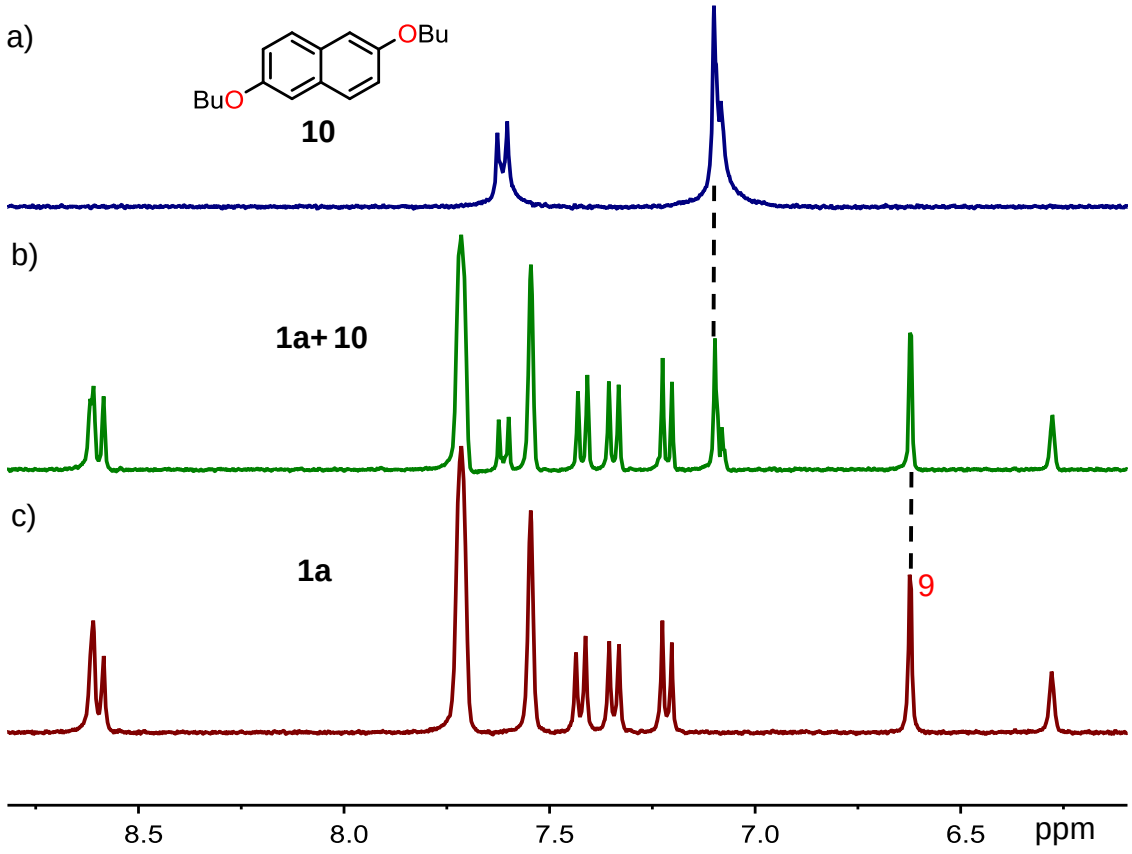

Fig. S33 ^{1}H NMR spectra (400 MHz, CD_2Cl_2, 298 K) of (a) guest **10**, (c) **1a** and (b) its equimolar mixture. The proton of the guest experiences the upfield shift, the proton 9 of the host experiences the upfield shift, suggesting that the complexation between **1a** and guest **10**.

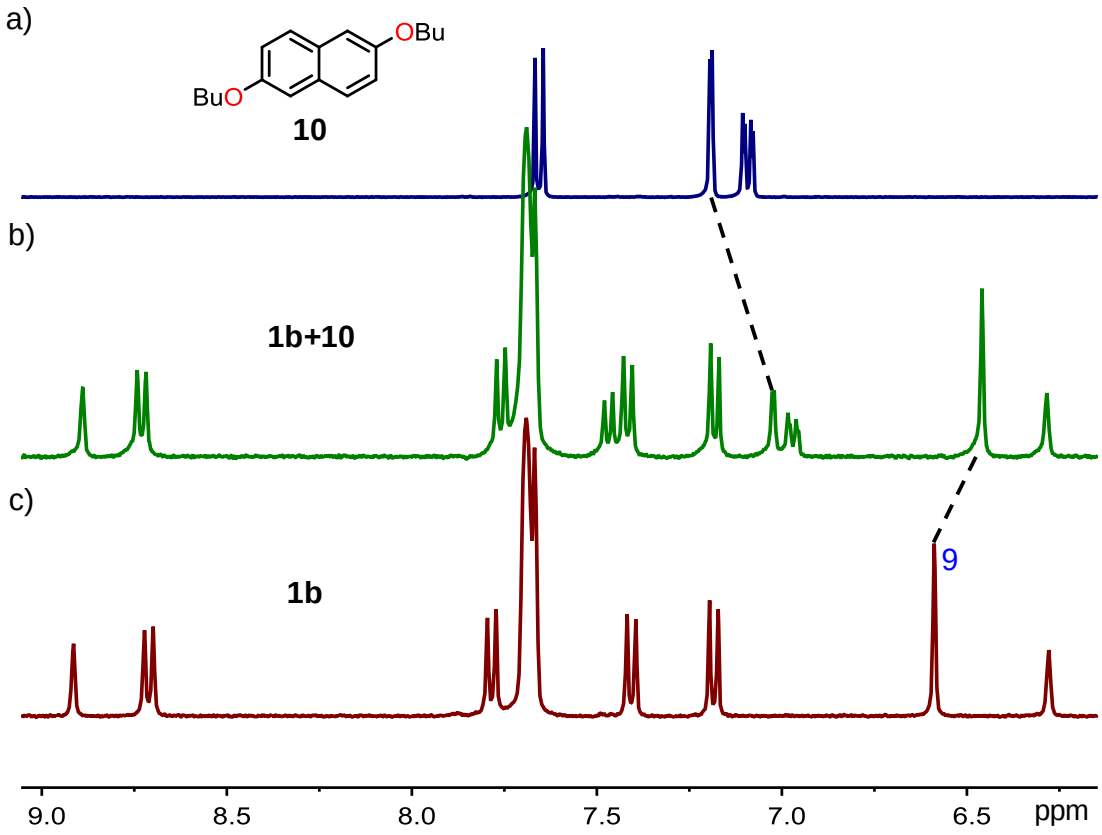

Fig. S34 ^{1}H NMR spectra (400 MHz, CD_3CN, 298 K) of (a) guest **10**, (c) **1b** and (b) its equimolar mixture. The proton of the guest experiences the upfield shift, the proton 9 of the host experiences the upfield shift, suggesting that the complexation between **1b** and guest **10**.

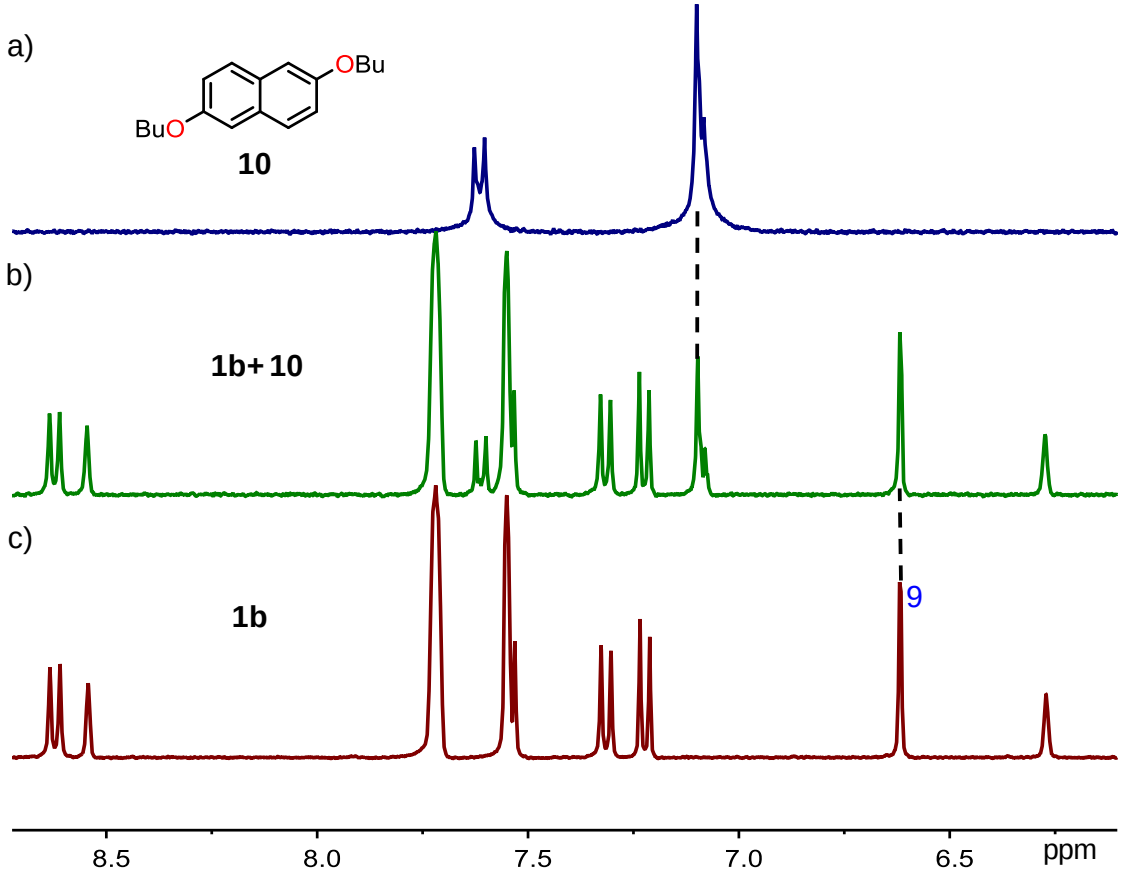

Fig. S35 ^{1}H NMR spectra (400 MHz, CD_2Cl_2, 298 K) of (a) guest **10**, (c) **1b** and (b) its equimolar mixture. The proton of the guest experiences the upfield shift, the proton 9 of the host experiences the upfield shift, suggesting that the complexation between **1b** and guest **10**.

5. Binding Constants Determined by NMR Titration.

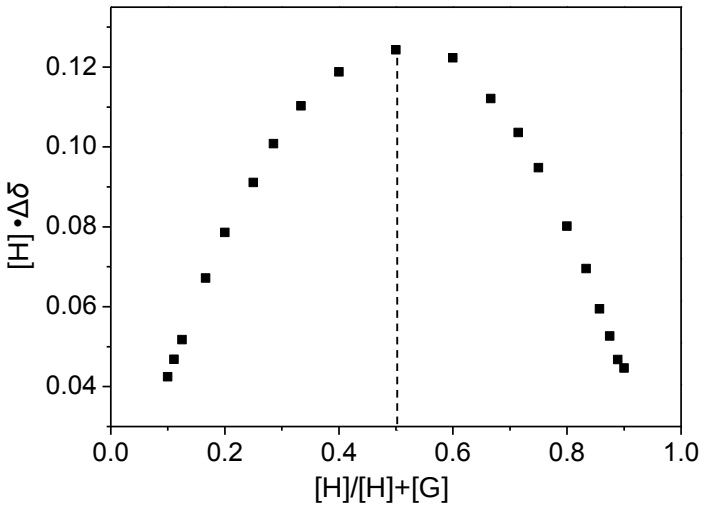

Fig. S36 Job's plot obtained by plotting the chemical shift change ($\Delta\delta$) of the Host's proton (10) in ^{1}H NMR spectra by varying the ratio of the host and the guest against the mole fraction of **1b**. The total concentration of the host and the guest is fixed: [Host] + [Guest] = 2.0 mM. This experiment supports the 1:1 binding stoichiometry between **9** and **1b** in CD_3CN.

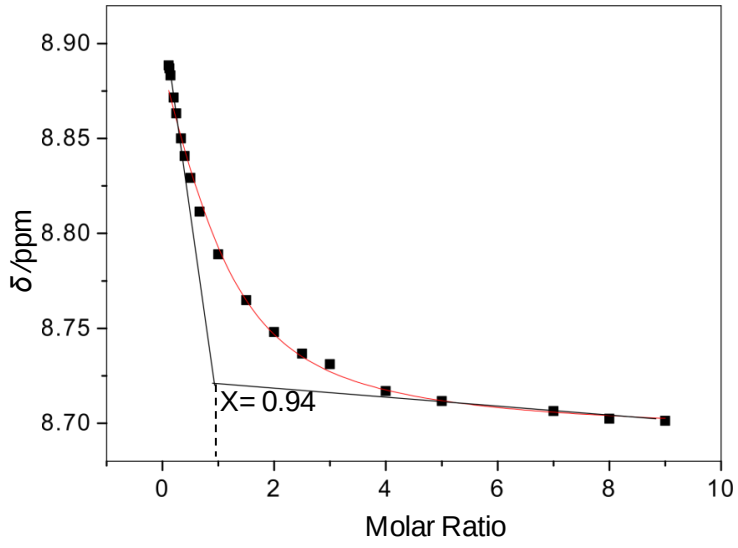

Fig. S37 Molar ratio plot of **1b** titrated by **9**. These experiments support the 1:1 binding stoichiometry between **9** and **1b** in CD_3CN.

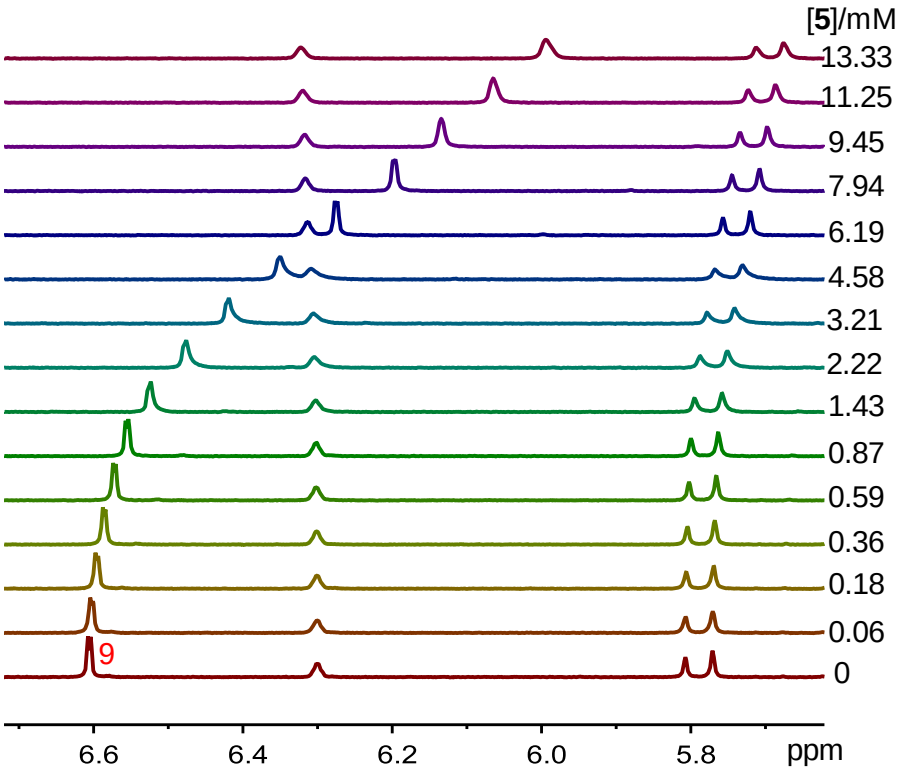

Fig. S38 Partial ^{1}H NMR spectra (400 MHz, CD_3CN, 298 K) of **1a** (0.5 mM) titrated by the **5** (0~13.33 mM).

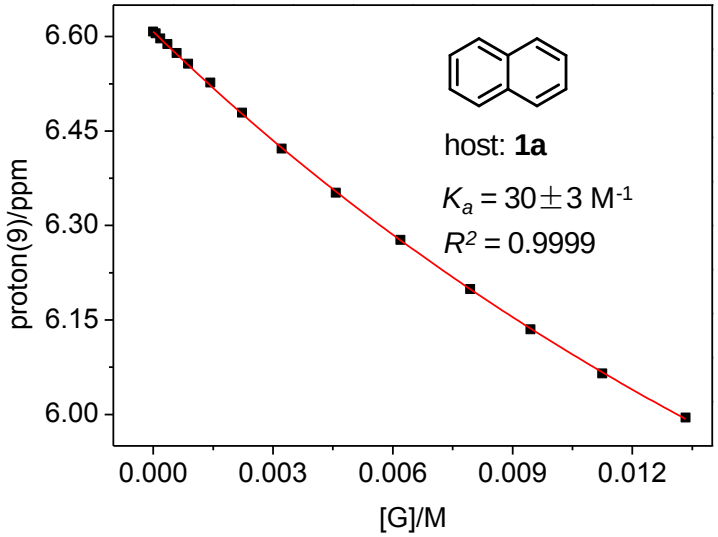

Fig. S39 Non-linear curve-fitting for the complexation between **1a** and **5** in CD_3CN at 298 K.

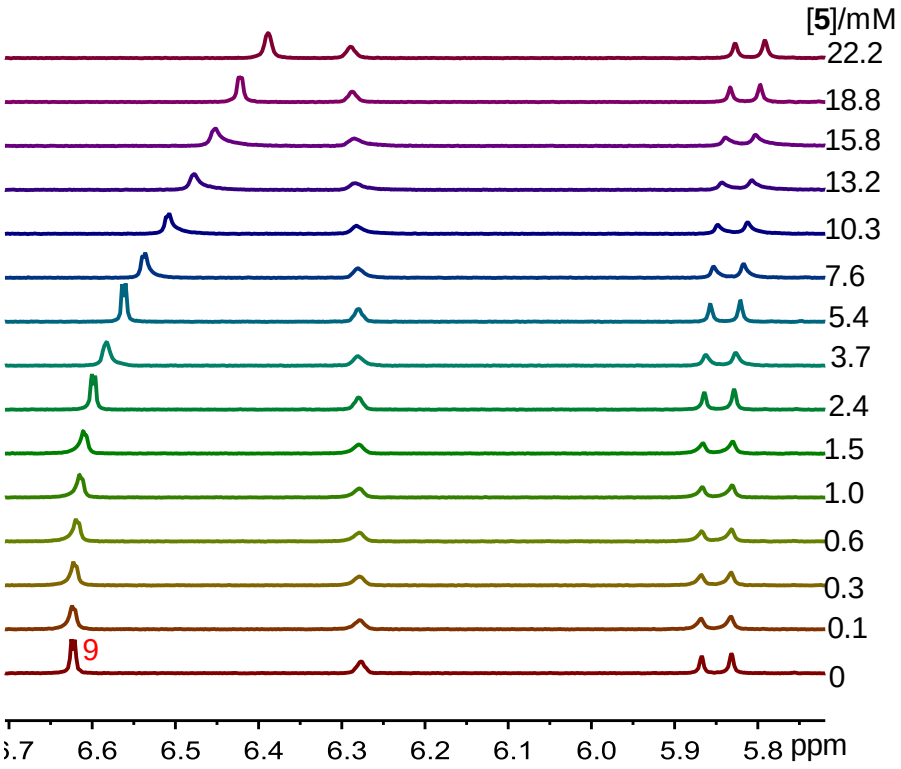

Fig. S40 Partial ^{1}H NMR spectra (400 MHz, CD_2Cl_2, 298 K) of **1a** (0.5 mM) titrated by **5** (0~22.22 mM).

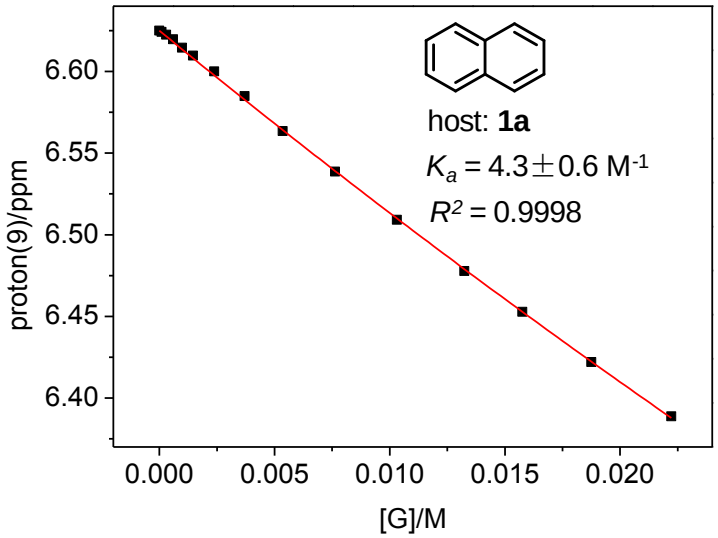

Fig. S41 Non-linear curve-fitting for the complexation between **1a** and **5** in CD_2Cl_2 at 298 K.

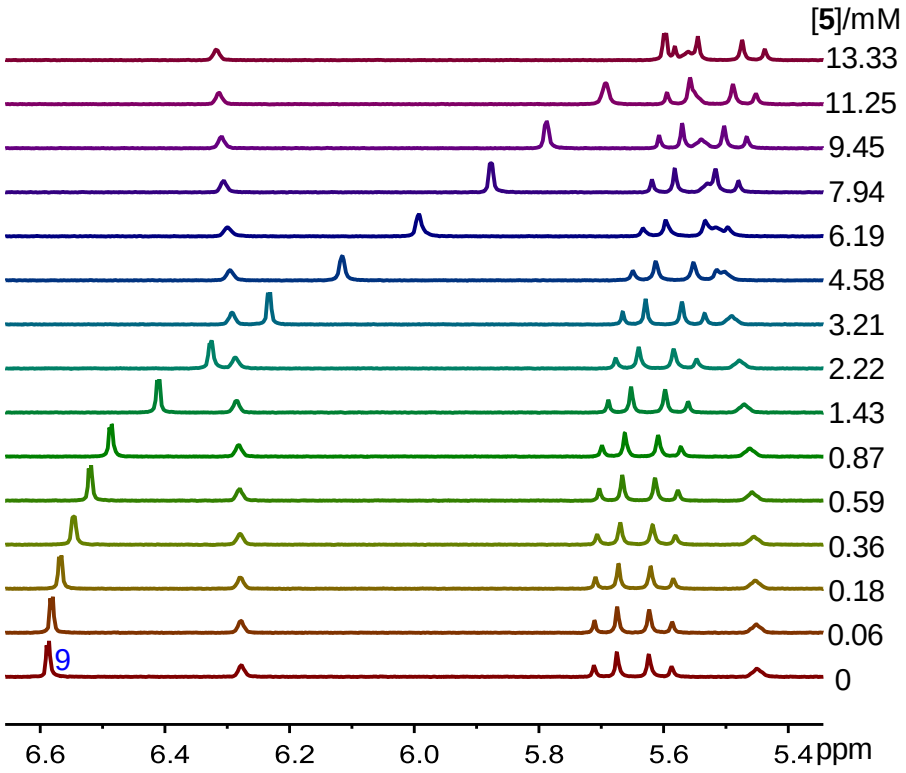

Fig. S42 Partial ^{1}H NMR spectra (400 MHz, CD_3CN, 298 K) of **1b** (0.5 mM) titrated by **5** (0~13.33 mM).

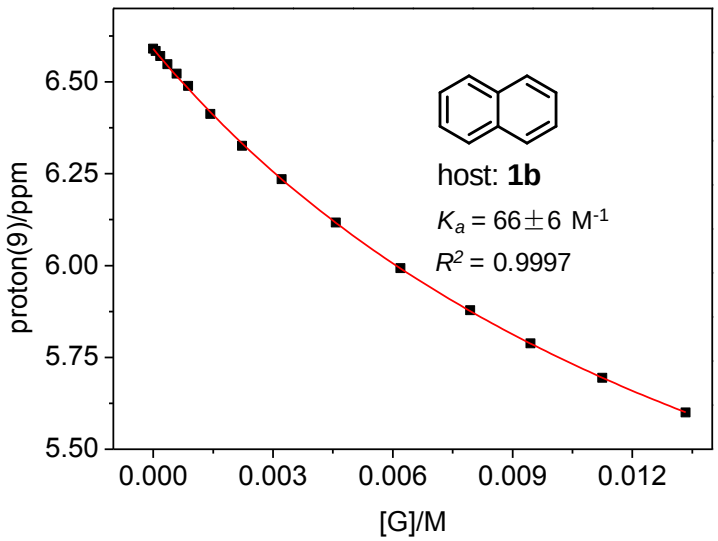

Fig. S43 Non-linear curve-fitting for the complexation between **1b** and **5** in CD_3CN at 298 K.

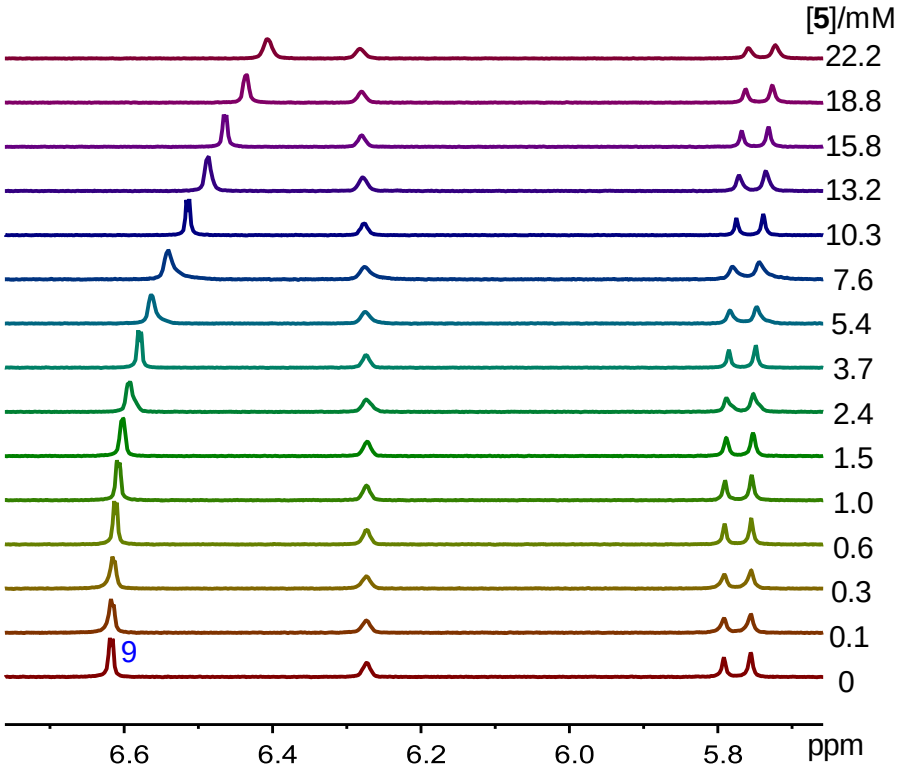

Fig. S44 Partial ^{1}H NMR spectra (400 MHz, CD_2Cl_2, 298 K) of **1b** (0.5 mM) titrated by **5** (0~22.22 mM).

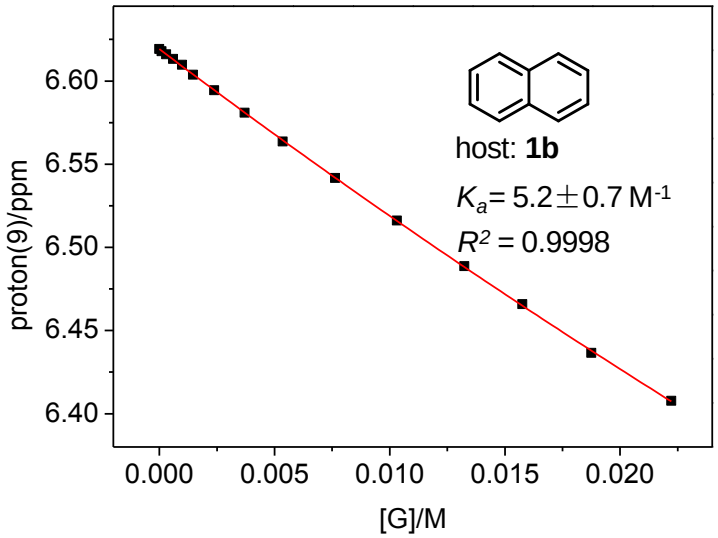

Fig. S45 Non-linear curve-fitting for the complexation between **1b** and **5** in CD_2Cl_2 at 298 K.

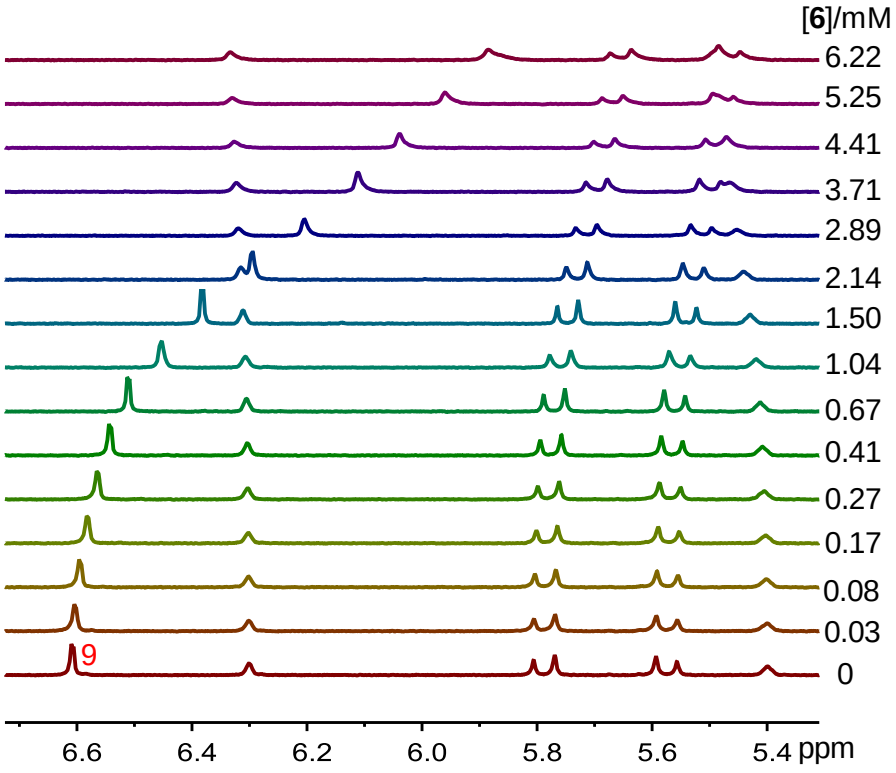

Fig. S46 Partial ^{1}H NMR spectra (400 MHz, $CDCN_3$, 298 K) of **1a** (0.5 mM) titrated by **6** (0~6.22 mM).

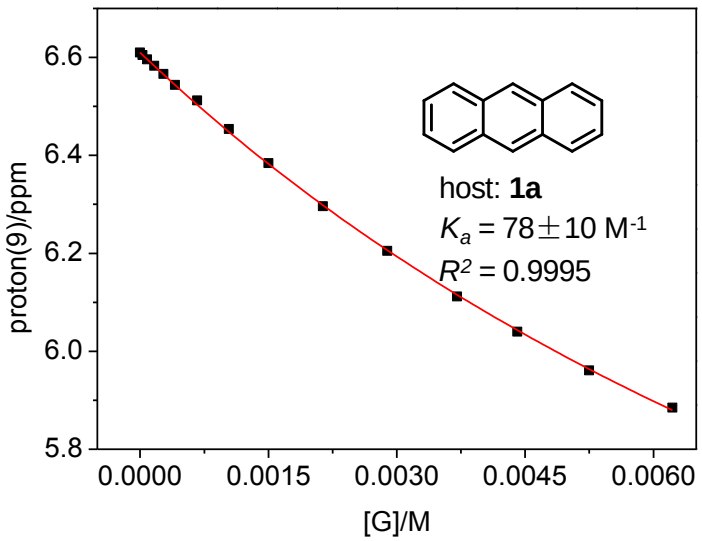

Fig. S47 Non-linear curve-fitting for the complexation between **1a** and **6** in $CDCN_3$ at 298 K.

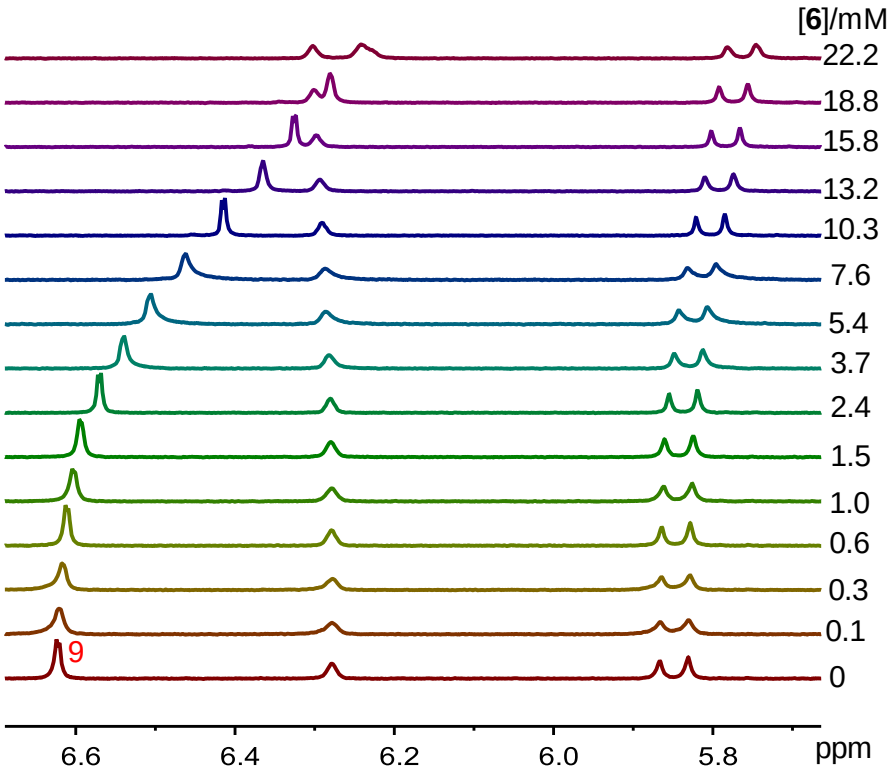

Fig. S48 Partial ^{1}H NMR spectra (400 MHz, CD_2Cl_2, 298 K) of **1a** (0.5 mM) titrated by **6** (0~22.2 mM).

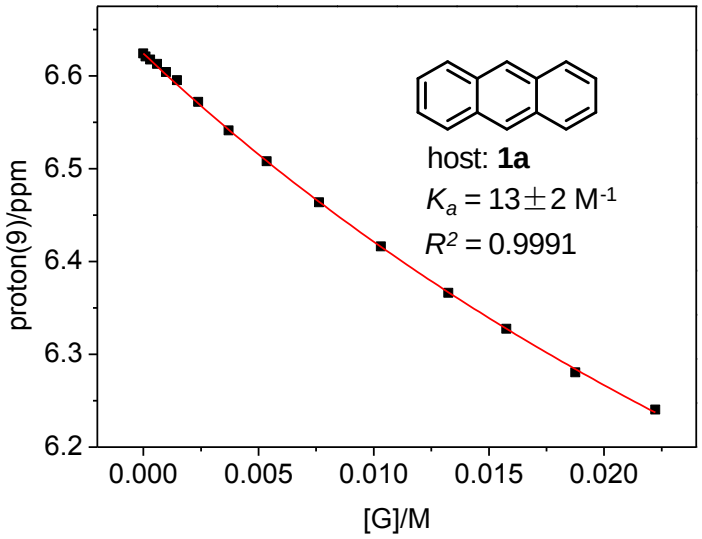

Fig. S49 Non-linear curve-fitting for the complexation between **1a** and **6** in CD_2Cl_2 at 298 K.

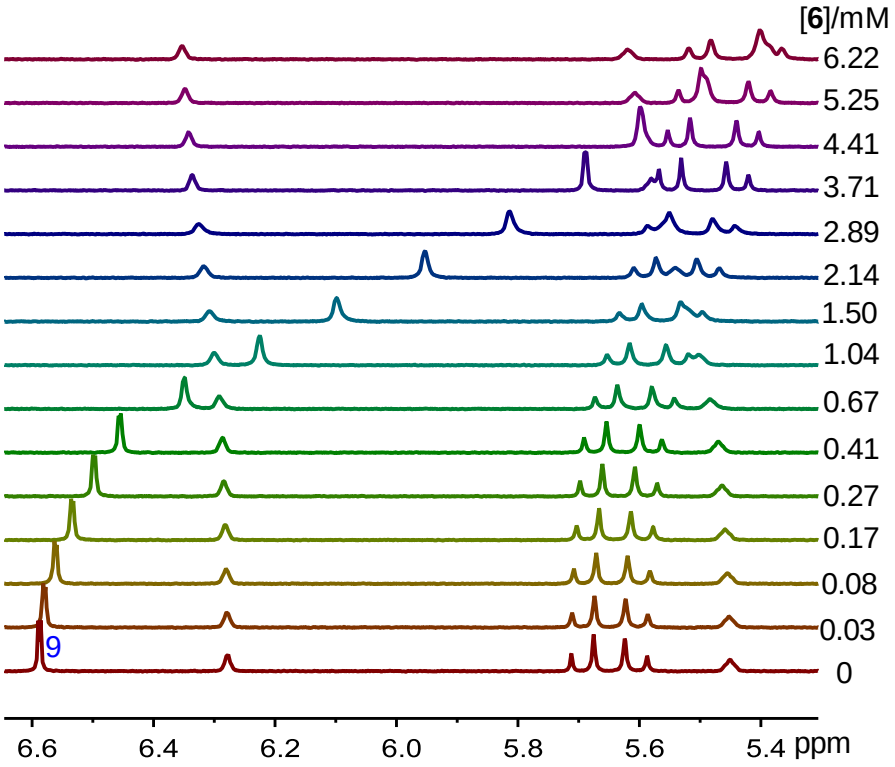

Fig. S50 Partial ^{1}H NMR spectra (400 MHz, $CDCN_3$, 298 K) of **1b** (0.5 mM) titrated by **6** (0~6.22 mM).

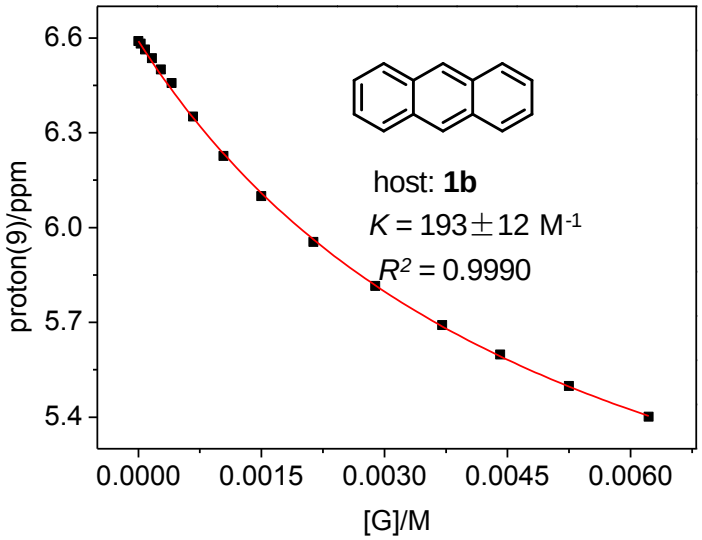

Fig. S51 Non-linear curve-fitting for the complexation between **1b** and **6** in $CDCN_3$ at 298 K.

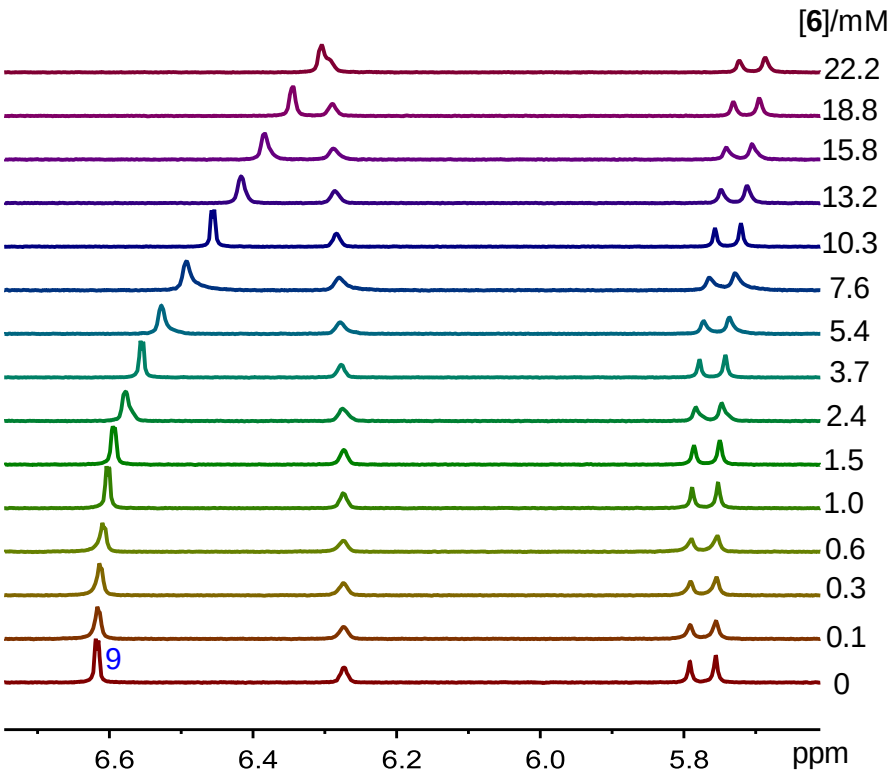

Fig. S52 Partial ^{1}H NMR spectra (400 MHz, CD_2Cl_2, 298 K) of **1b** (0.5 mM) titrated by **6** (0~22.2 mM).

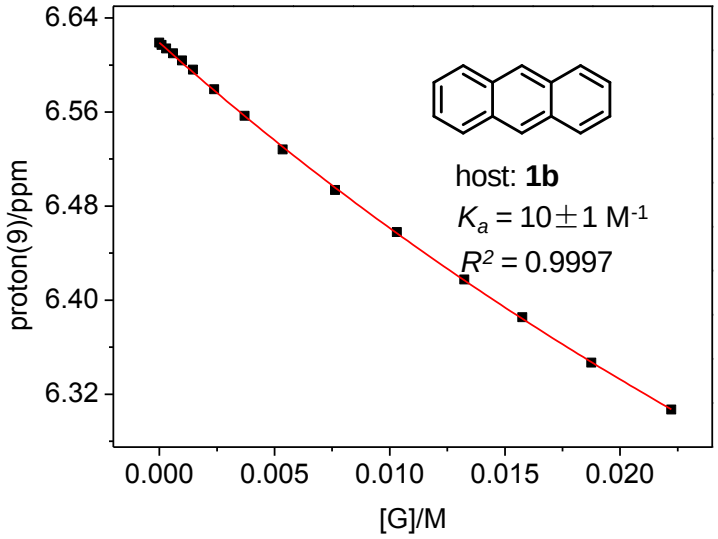

Fig. S53 Non-linear curve-fitting for the complexation between **1b** and **6** in CD_2Cl_2 at 298 K.

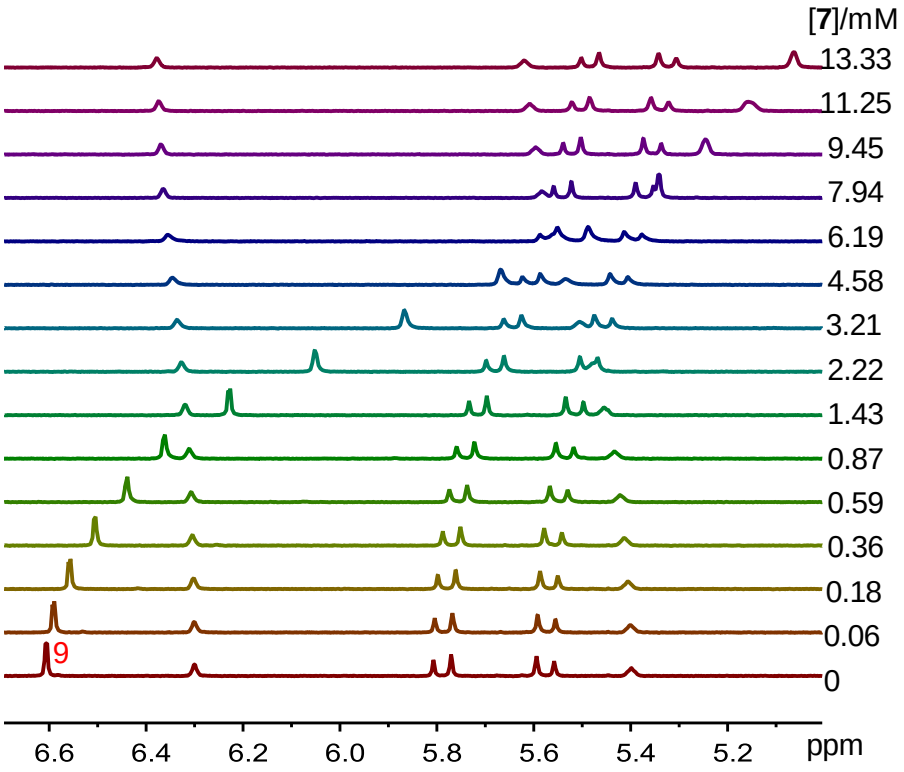

Fig. S54 Partial ^{1}H NMR spectra (400 MHz, CD_3CN, 298 K) of **1a** (0.5 mM) titrated by **7** (0~13.3 mM).

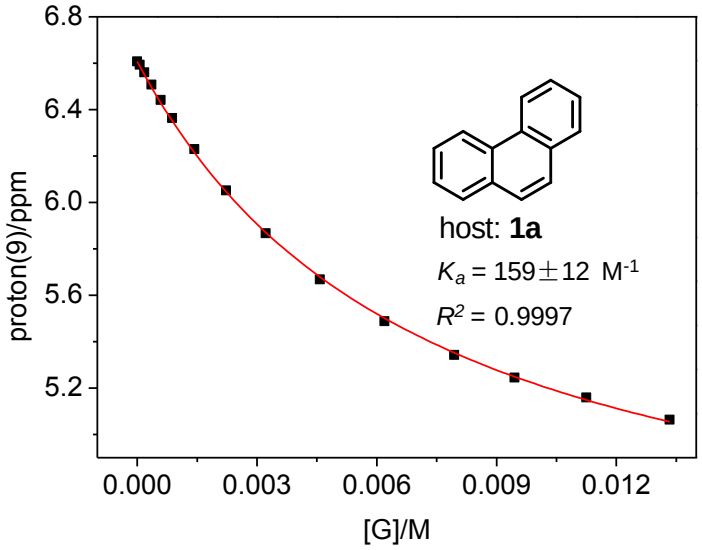

Fig. S55 Non-linear curve-fitting for the complexation between **1a** and **7** in CD_3CN at 298 K.

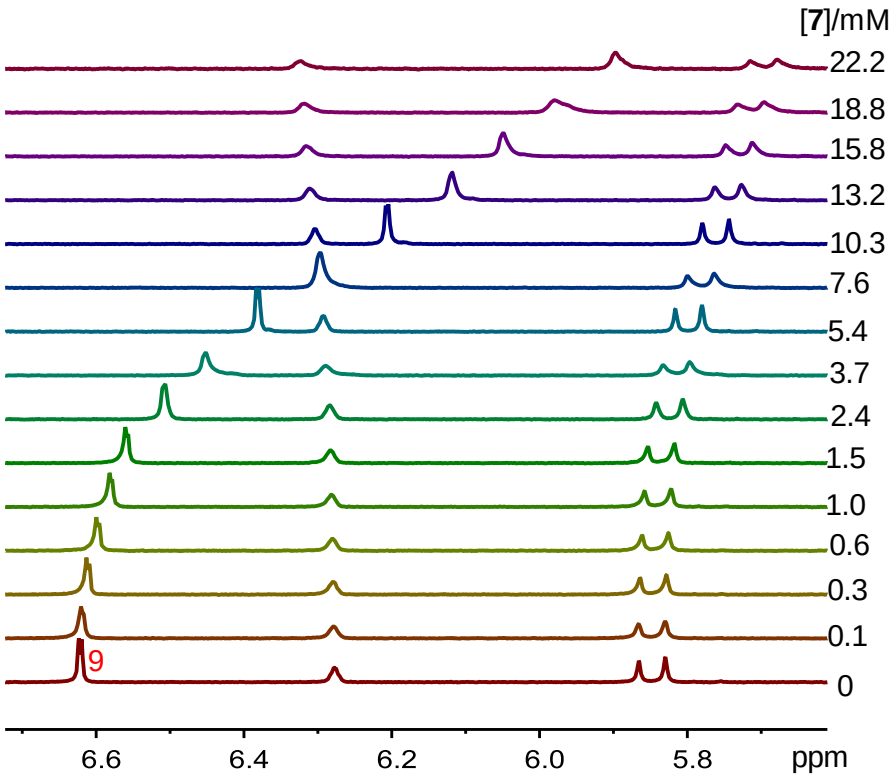

Fig. S56 Partial ^{1}H NMR spectra (400 MHz, CD_2Cl_2, 298 K) of **1a** (0.5 mM) titrated by **7** (0~22.2 mM).

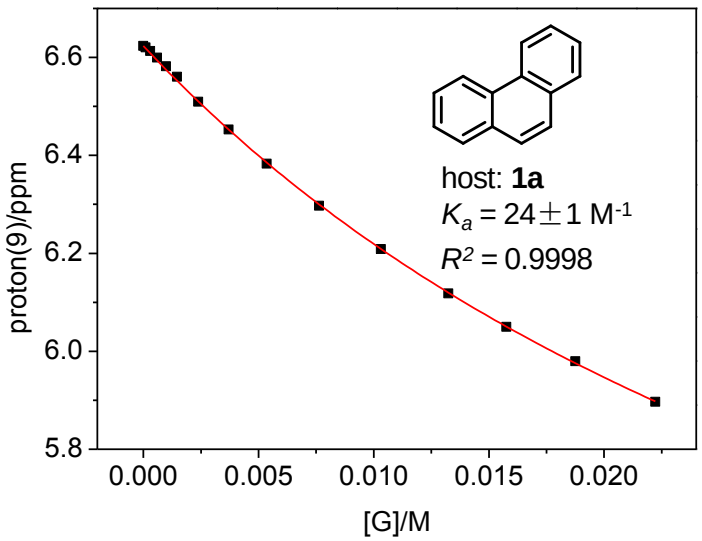

Fig. S57 Non-linear curve-fitting for the complexation between **1a** and **7** in CD_2Cl_2 at 298 K.

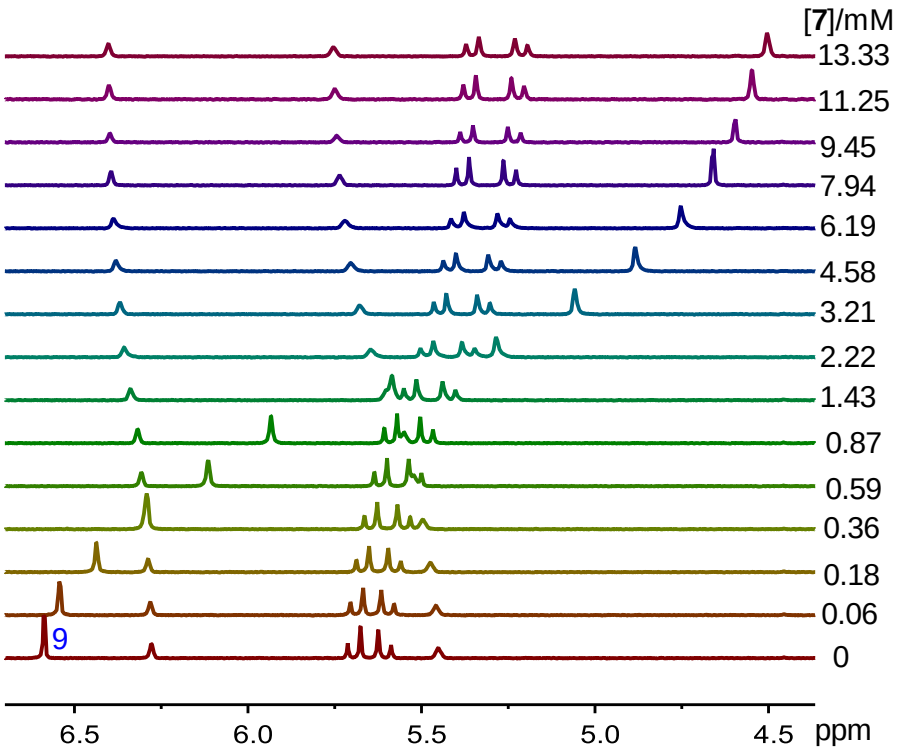

Fig. S58 Partial ^{1}H NMR spectra (400 MHz, CD_3CN, 298 K) of **1b** (0.5 mM) titrated by **7** (0~13.33 mM).

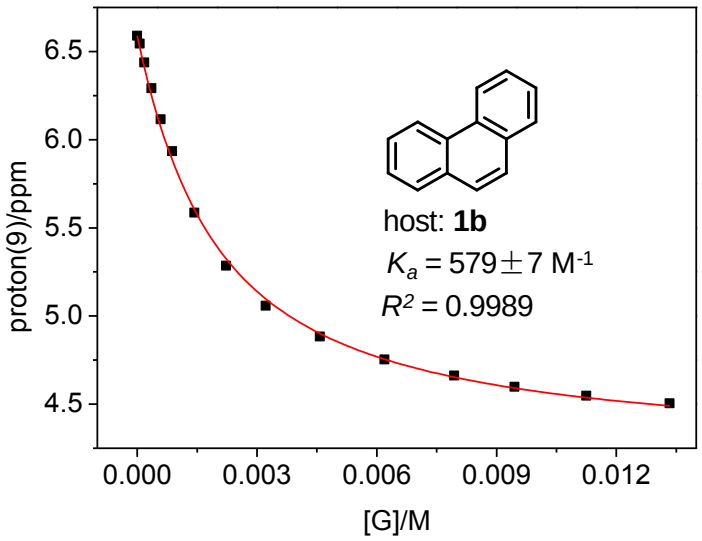

Fig. S59 Non-linear curve-fitting for the complexation between **1b** and **7** in CD_3CN at 298 K.

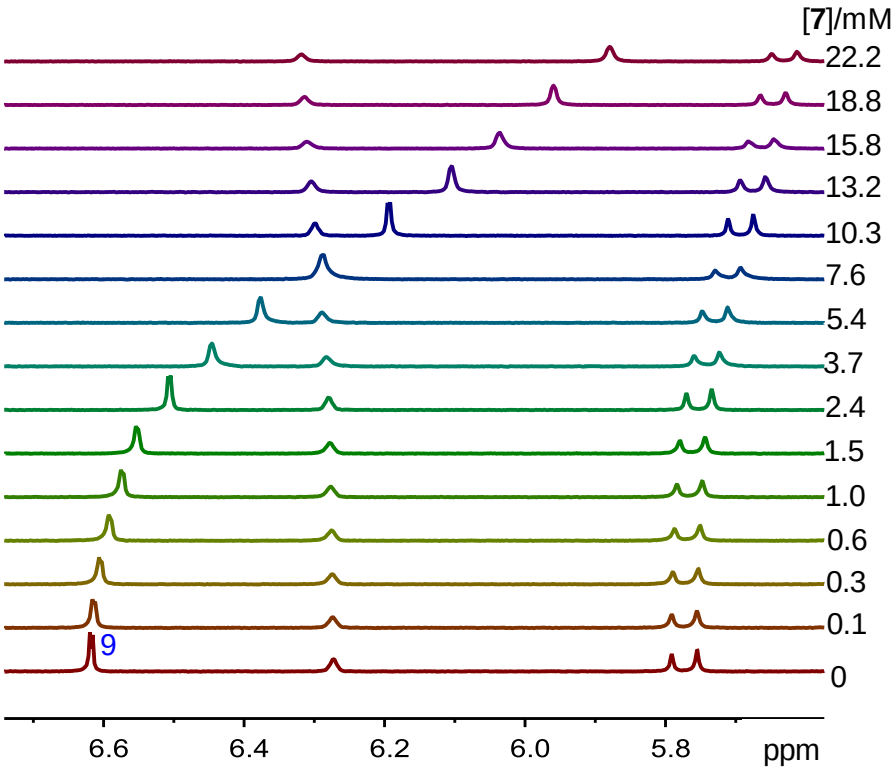

Fig. S60 Partial ^{1}H NMR spectra (400 MHz, CD_2Cl_2, 298 K) of **1b** (0.5 mM) titrated by **7** (0~22.2 mM).

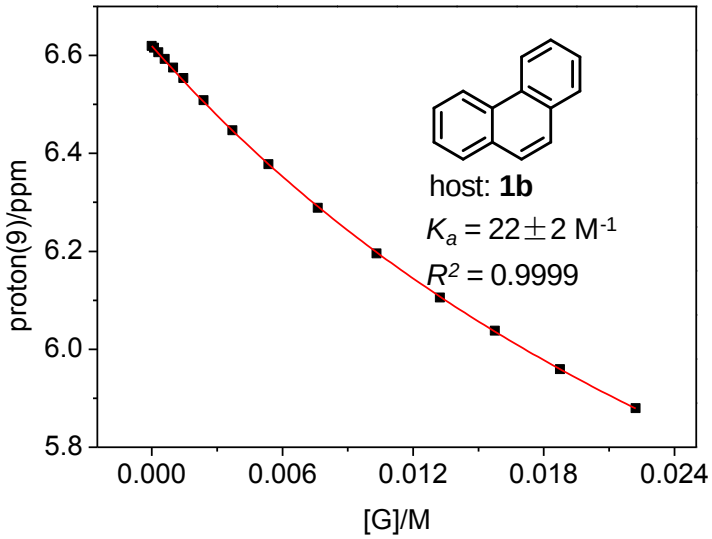

Fig. S61 Non-linear curve-fitting for the complexation between **1b** and **7** in CD_2Cl_2 at 298 K.

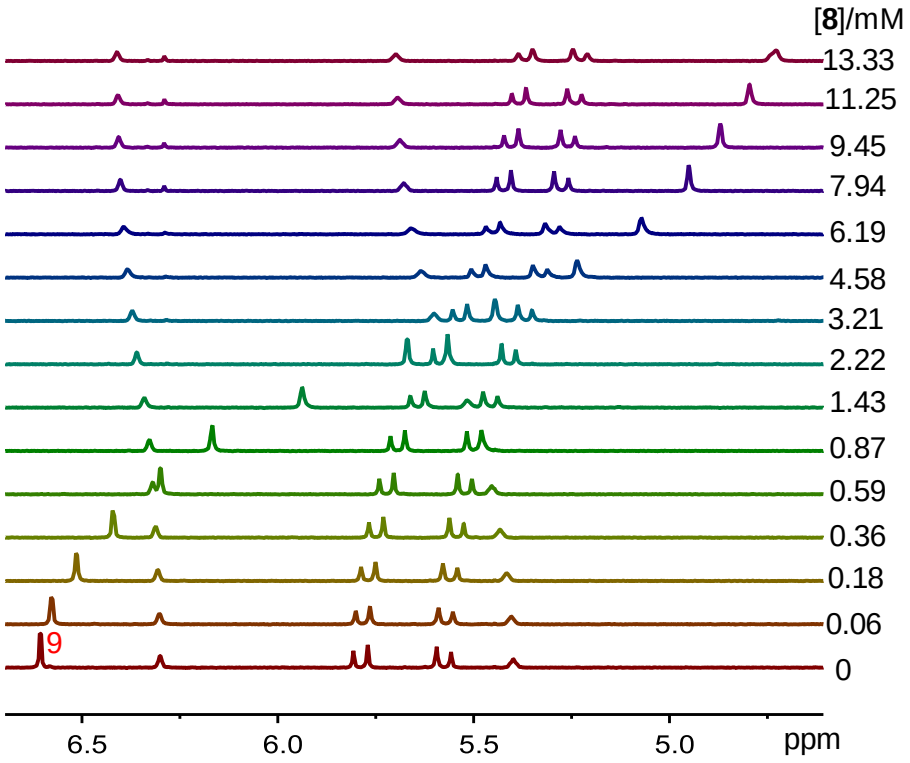

Fig. S62 Partial ^{1}H NMR spectra (400 MHz, CD_3CN, 298 K) of **1a** (0.5 mM) titrated by **8** (0~13.33 mM).

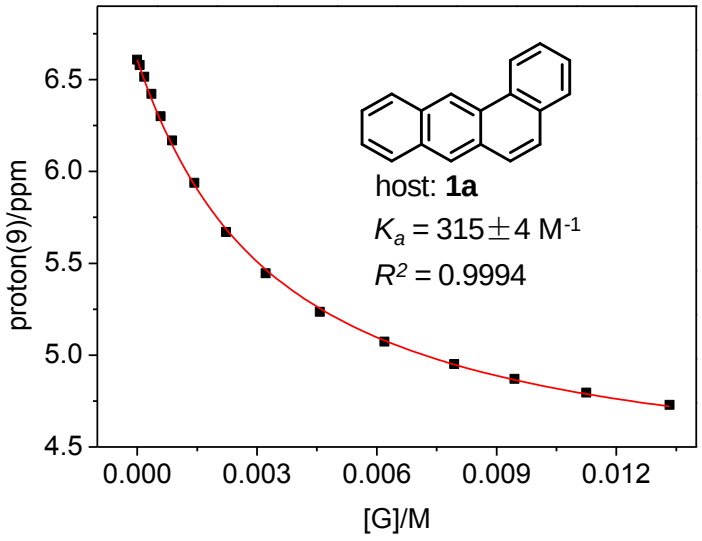

Fig. S63 Non-linear curve-fitting for the complexation between **1a** and **8** in CD_3CN at 298 K.

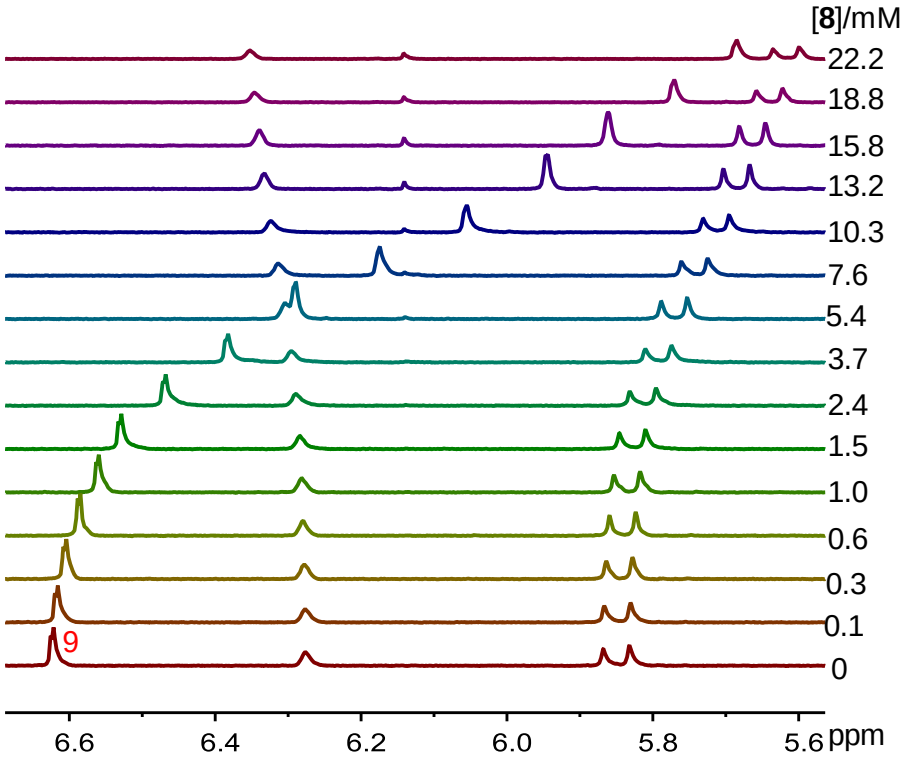

Fig. S64 Partial ^{1}H NMR spectra (400 MHz, CD_2Cl_2, 298 K) of **1a** (0.5 mM) titrated by **8** (0~22.2 mM).

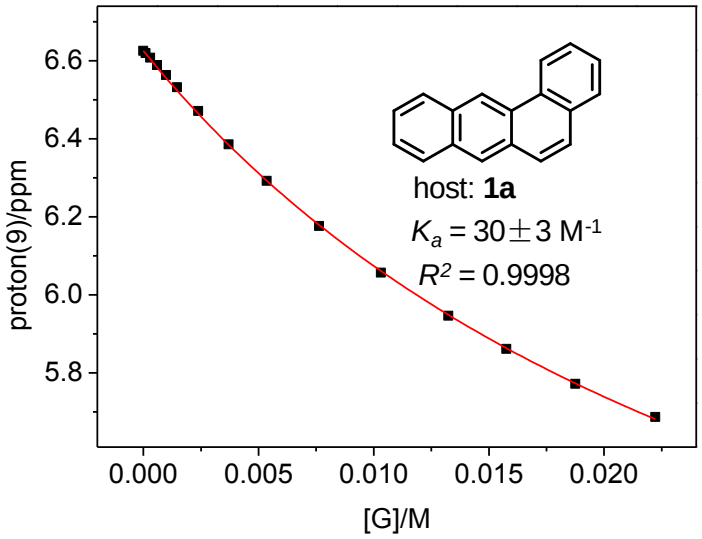

Fig. S65 Non-linear curve-fitting for the complexation between **1a** and **8** in CD_2Cl_2 at 298 K.

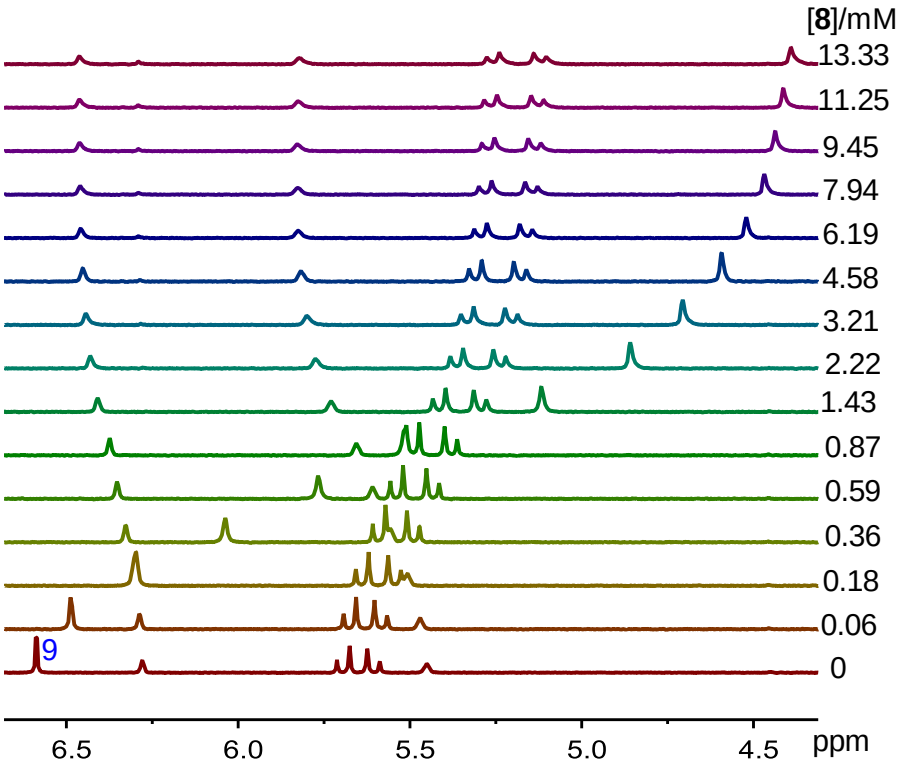

Fig. S66 Partial ^{1}H NMR spectra (400 MHz, CD_3CN, 298 K) of **1b** (0.5 mM) titrated by **8** (0~13.33 mM).

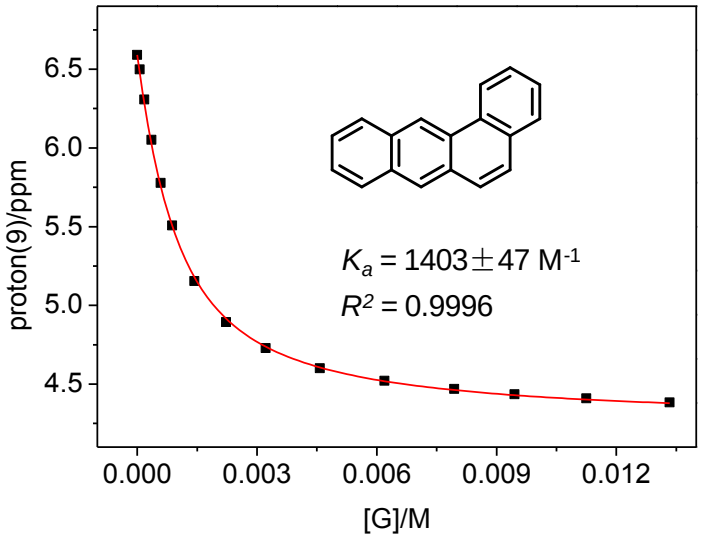

Fig. S67 Non-linear curve-fitting for the complexation between **1b** and **8** in CD_3CN at 298 K.

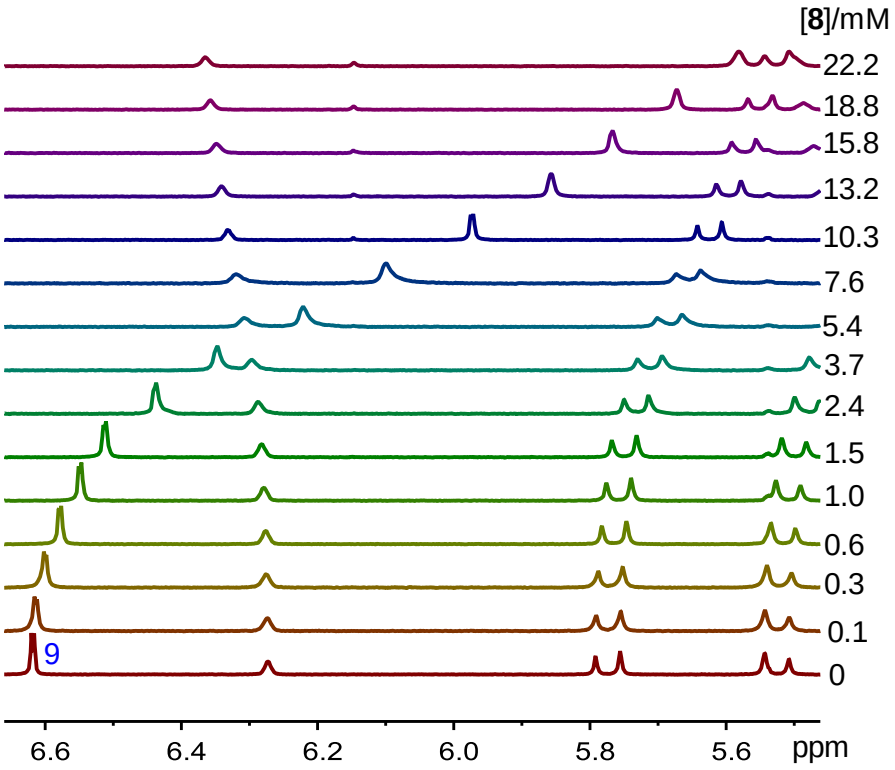

Fig. S68 Partial ^{1}H NMR spectra (400 MHz, CD_2Cl_2, 298 K) of **1b** (0.5 mM) titrated by **8** (0~22.2 mM).

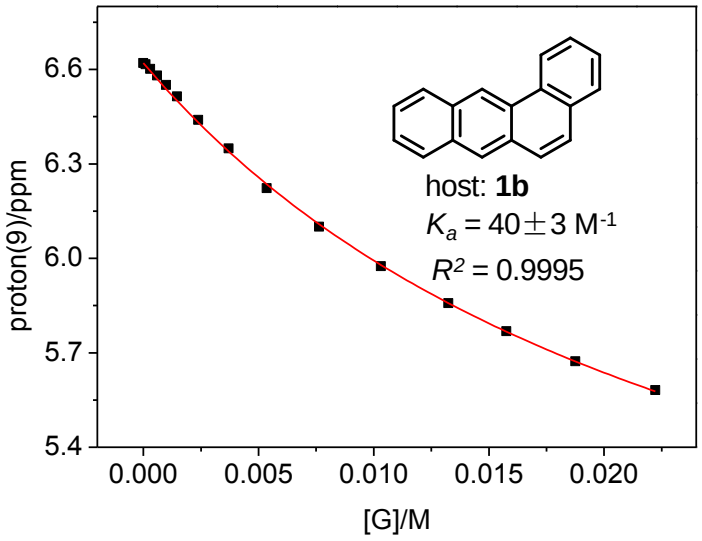

Fig. S69 Non-linear curve-fitting for the complexation between **1b** and **8** in CD_2Cl_2 at 298 K.

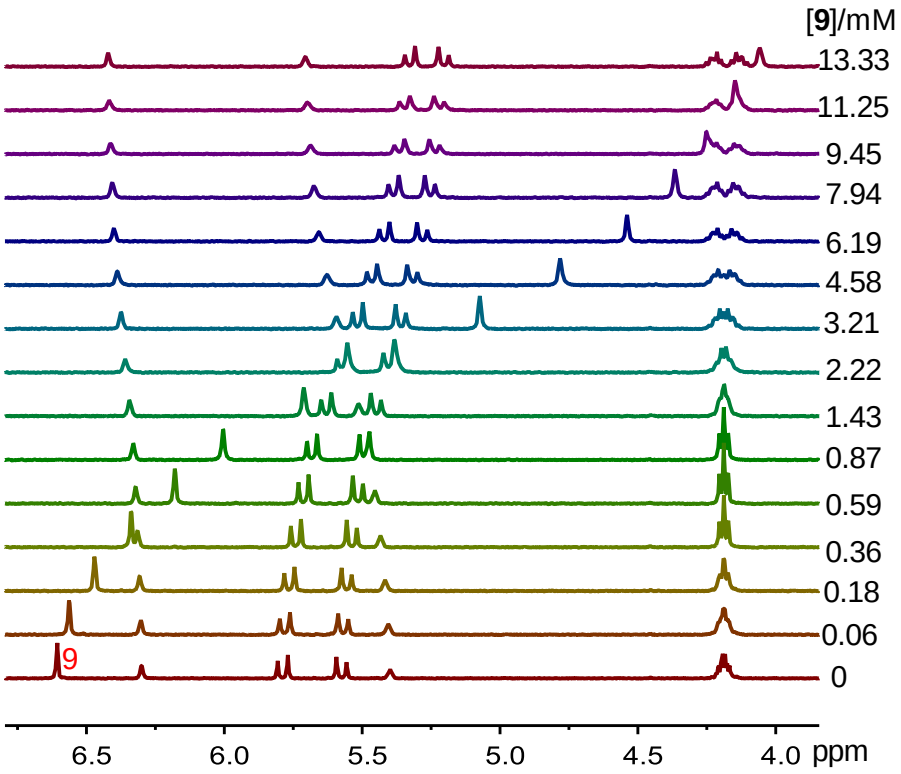

Fig. S70 Partial ^{1}H NMR spectra (400 MHz, CD_3CN, 298 K) of **1a** (0.5 mM) titrated by **9** (0~13.33 mM).

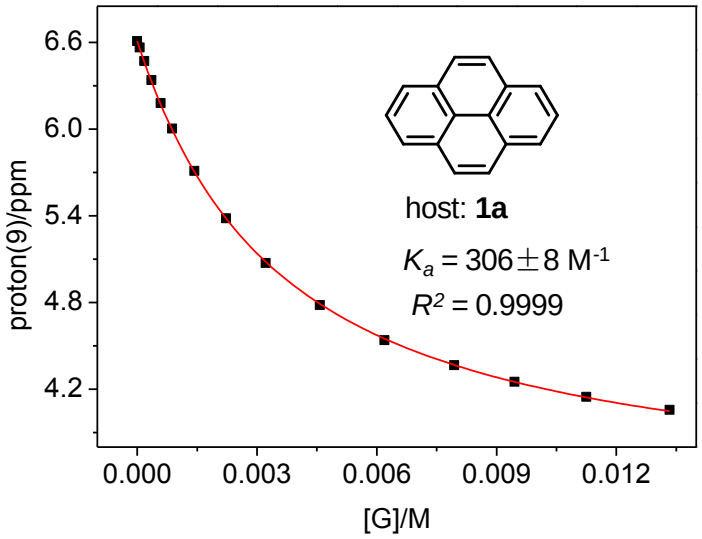

Fig. S71 Non-linear curve-fitting for the complexation between **1a** and **9** in CD_3CN at 298 K.

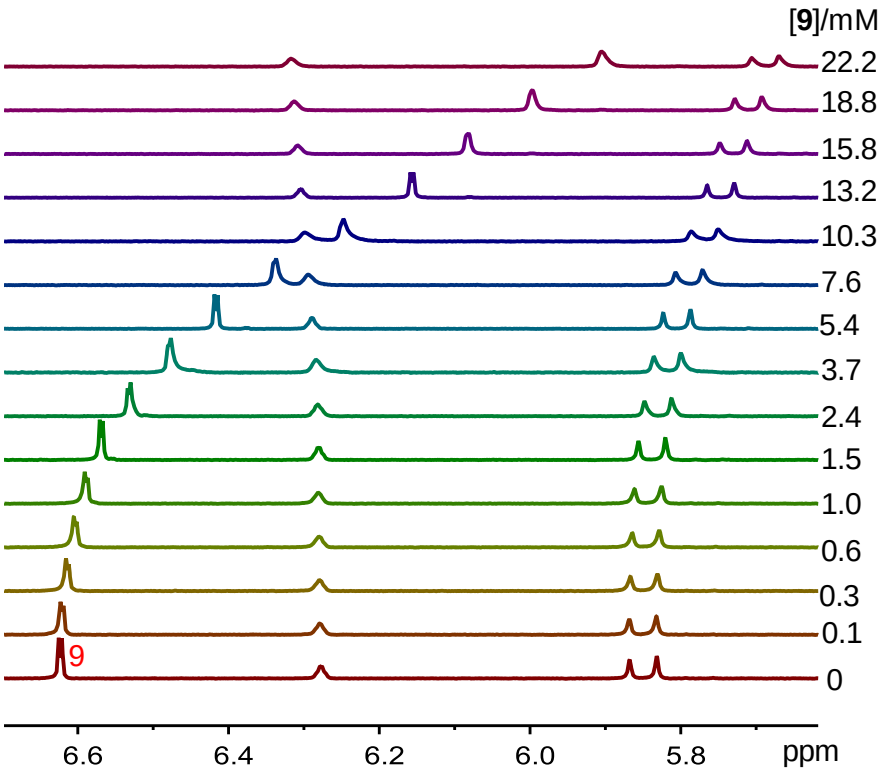

Fig. S72 Partial ^{1}H NMR spectra (400 MHz, CD_2Cl_2, 298 K) of **1a** (0.5 mM) titrated by **9** (0~22.2 mM).

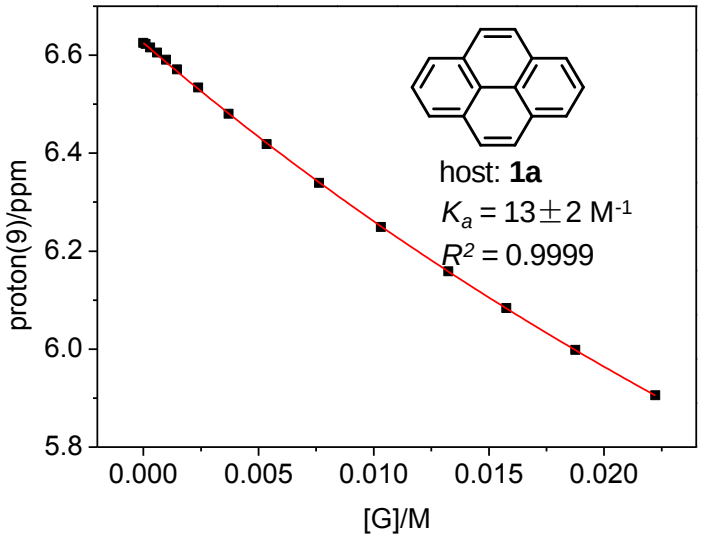

Fig. S73 Non-linear curve-fitting for the complexation between **1a** and **9** in CD_2Cl_2 at 298 K.

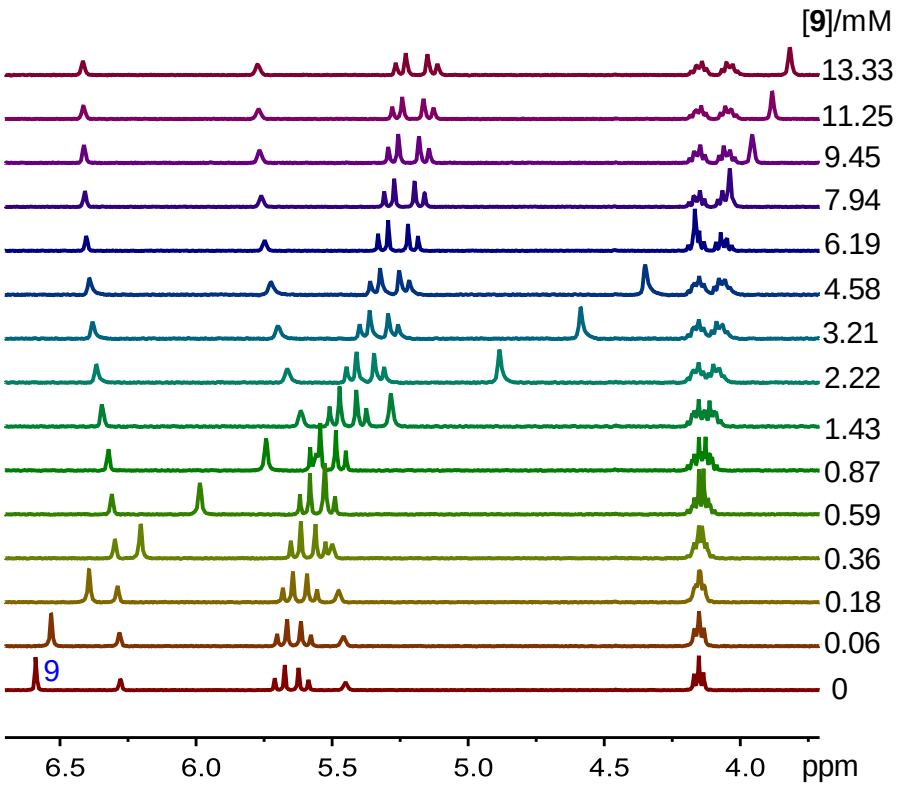

Fig. S74 Partial ^{1}H NMR spectra (400 MHz, CD_3CN, 298 K) of **1b** (0.5 mM) titrated by **9** (0~13.33 mM).

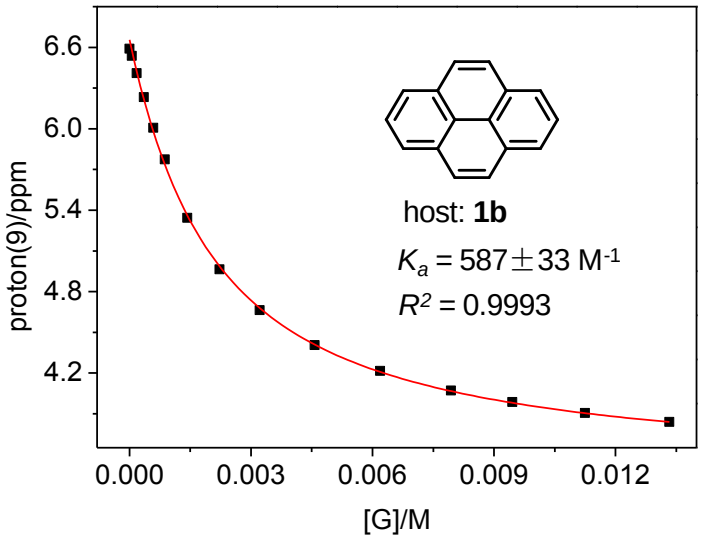

Fig. S75 Non-linear curve-fitting for the complexation between **1b** and **9** in CD_3CN at 298 K.

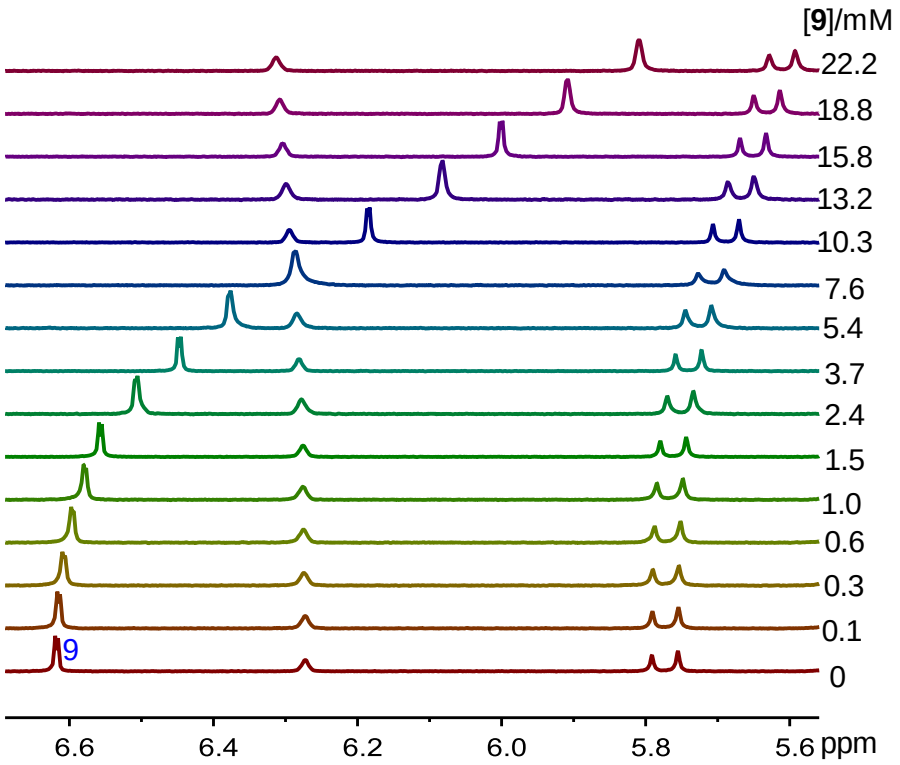

Fig. S76 Partial ^{1}H NMR spectra (400 MHz, CD_2Cl_2, 298 K) of **1b** (0.5 mM) titrated by **9** (0~22.2 mM).

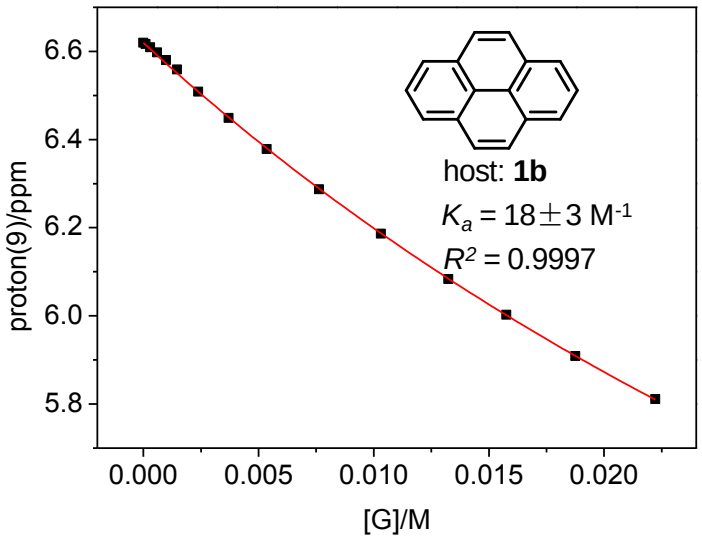

Fig. S77 Non-linear curve-fitting for the complexation between **1b** and **9** in CD_2Cl_2 at 298 K.

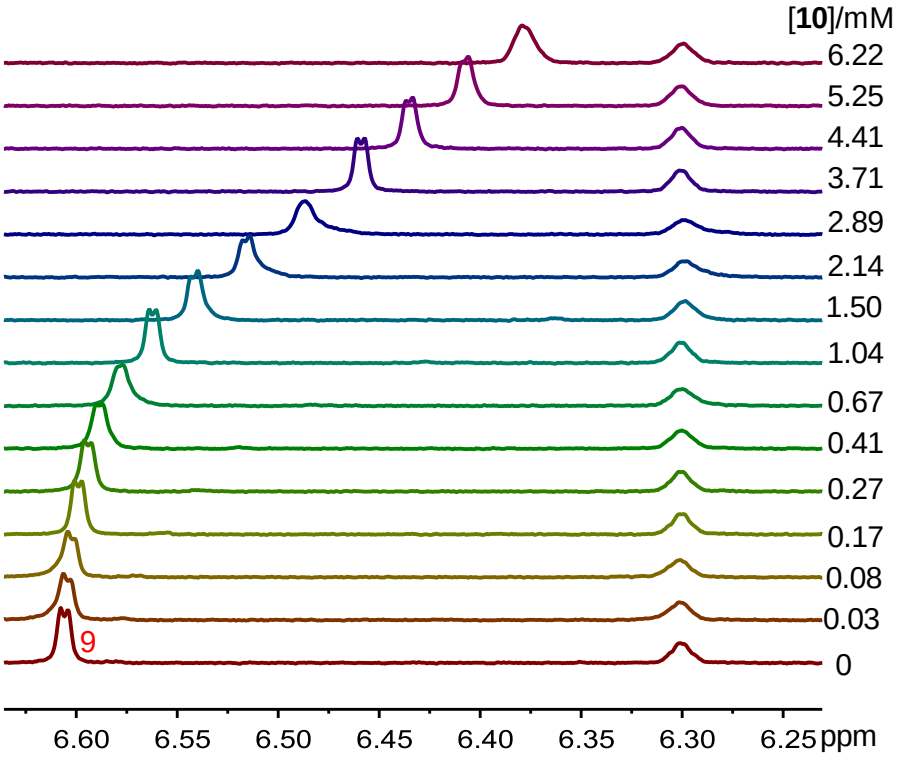

Fig. S78 Partial ^{1}H NMR spectra (400 MHz, CD_3CN, 298 K) of **1a** (0.4 mM) titrated by **10** (0~6.22 mM).

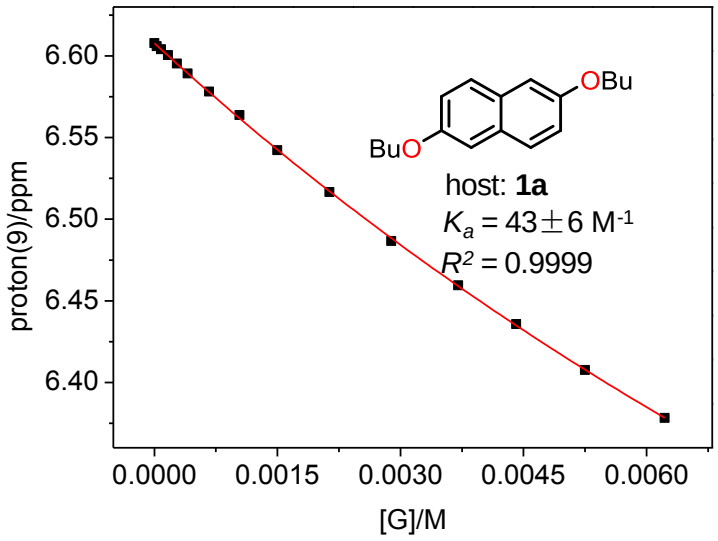

Fig. S79 Non-linear curve-fitting for the complexation between **1a** and **10** in CD_3CN at 298 K.

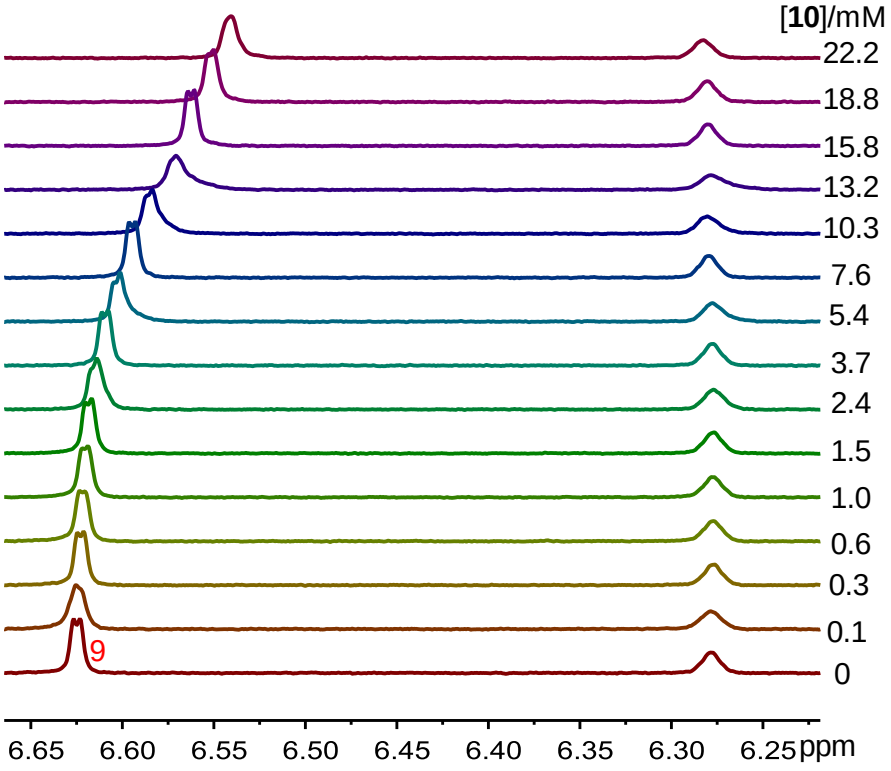

Fig. S80 Partial ^{1}H NMR spectra (400 MHz, CD_2Cl_2, 298 K) of **1a** (0.5 mM) titrated by **10** (0~22.2 mM).

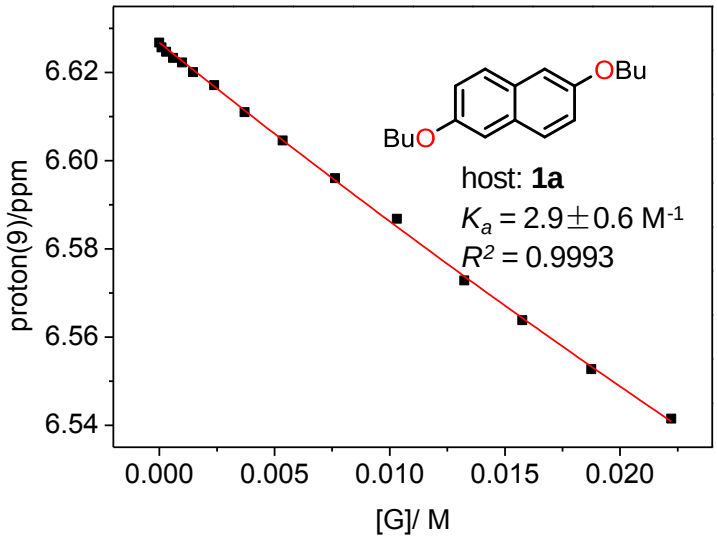

Fig. S81 Non-linear curve-fitting for the complexation between **1a** and **10** in CD_2Cl_2 at 298 K.

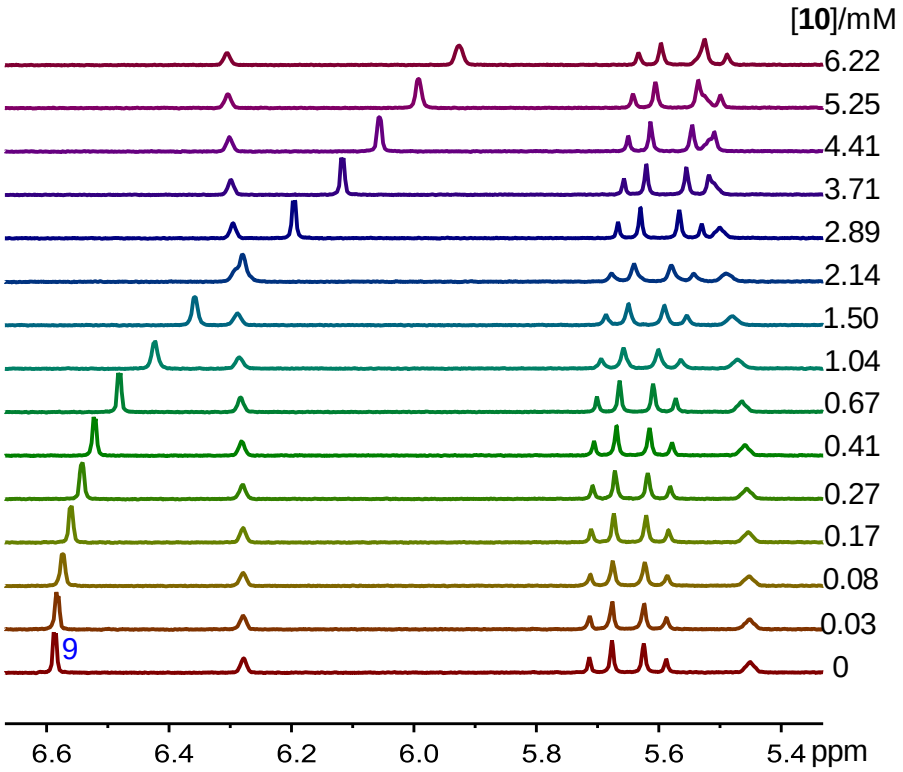

Fig. S82 Partial ^{1}H NMR spectra (400 MHz, CD_3CN, 298 K) of **1b** (0.4 mM) titrated by **10** (0~6.22 mM).

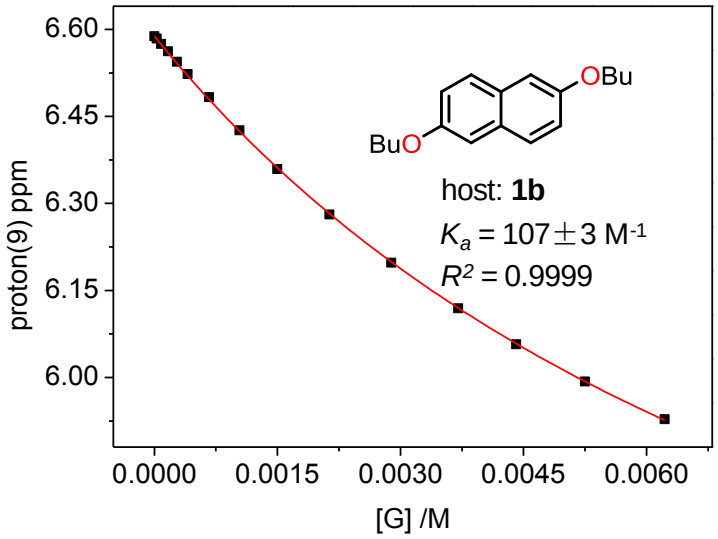

Fig. S83 Non-linear curve-fitting for the complexation between **1b** and **10** in CD_3CN at 298 K.

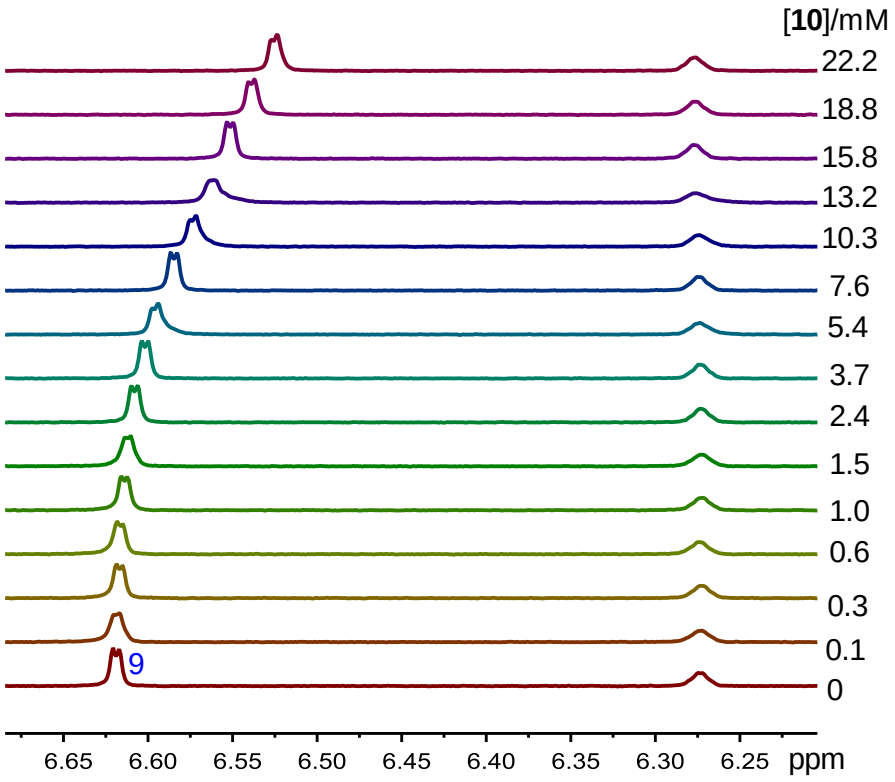

Fig. S84 Partial ^{1}H NMR spectra (400 MHz, CD_2Cl_2, 298 K) of **1b** (0.5 mM) titrated by **10** (0~22.2 mM).

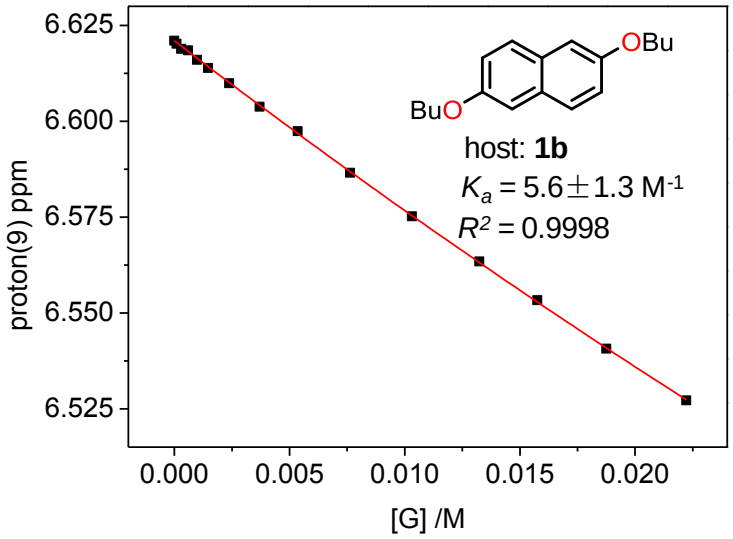

Fig. S85 Non-linear curve-fitting for the complexation between **1b** and **10** in CD_2Cl_2 at 298 K.

6. ^{1}H NMR Spectra of 1b titrated by Bu_4NBArF

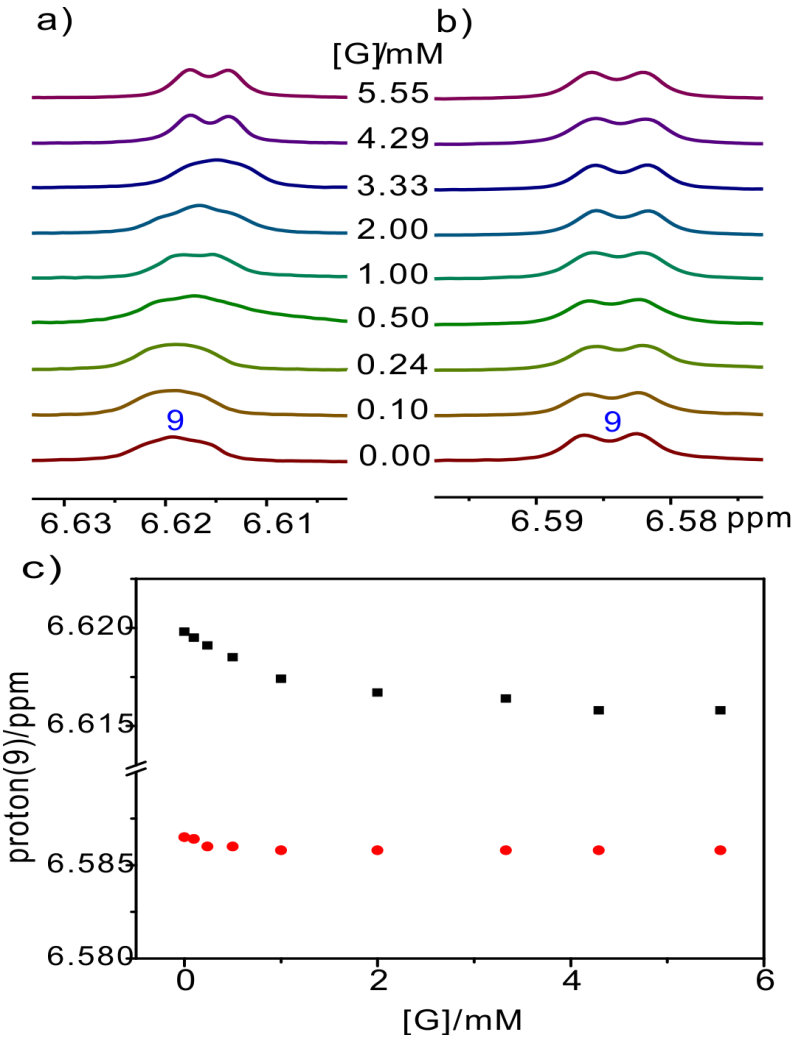

Fig. S86 ^{1}H NMR spectra (400 MHz, 298 K) of **1b** (0.5 mM) titrated by Bu_4NBArF; (a) in CD_2Cl_2 and (b) in CD_3CN; (c) chemical shift changes of proton 9 of **1b** with increasing concentrations of Bu_4NBArF (black square, CD_2Cl_2; red circle, CD_3CN)**.**

7. Control Experiments.

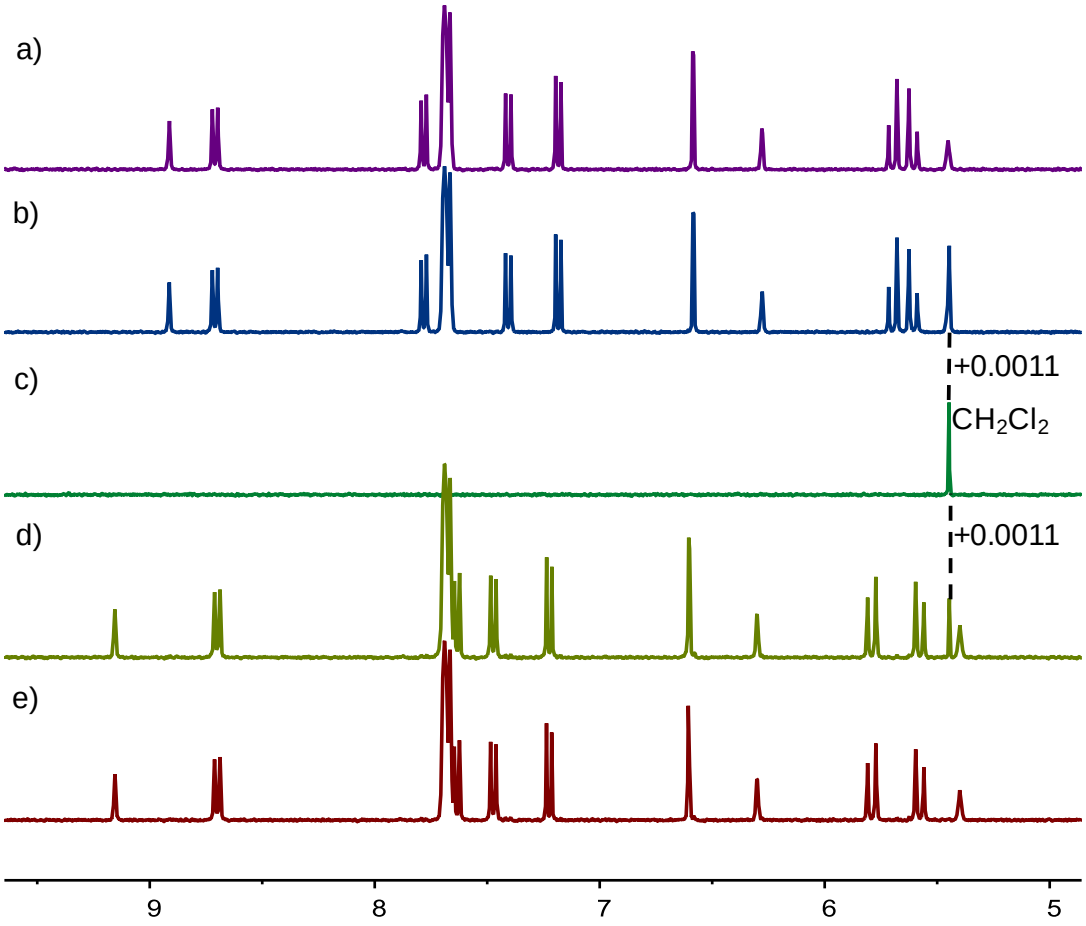

Fig. S87 Partial ^{1}H NMR spectra (400 MHz, CD_3CN, 0.5 mM, 298 K) of a) **1b**, b) the equimolar mixture of **1b** and CH_2Cl_2, c) CH_2Cl_2, d) the equimolar mixture of **1a** and CH_2Cl_2, and e) **1a**. In the presence of **1a**/**1b**, the signals of CH_2Cl_2 undergo slight upfield shift, suggesting that CH_2Cl_2 is a guest and should be encapsulated in the cavity of **1a**/**1b**. Consequently, a solvent molecule may sit in the cavity in CD_2Cl_2, and the incoming aromatic hydrocarbon guest has to compete with the solvent molecule. This is also in line with the single crystal structure obtained from CH_2Cl_2, in which a CH_2Cl_2 molecule is encapsulated in the cavity. This may be another reason why the binding affinity is smaller in CD_2Cl_2.

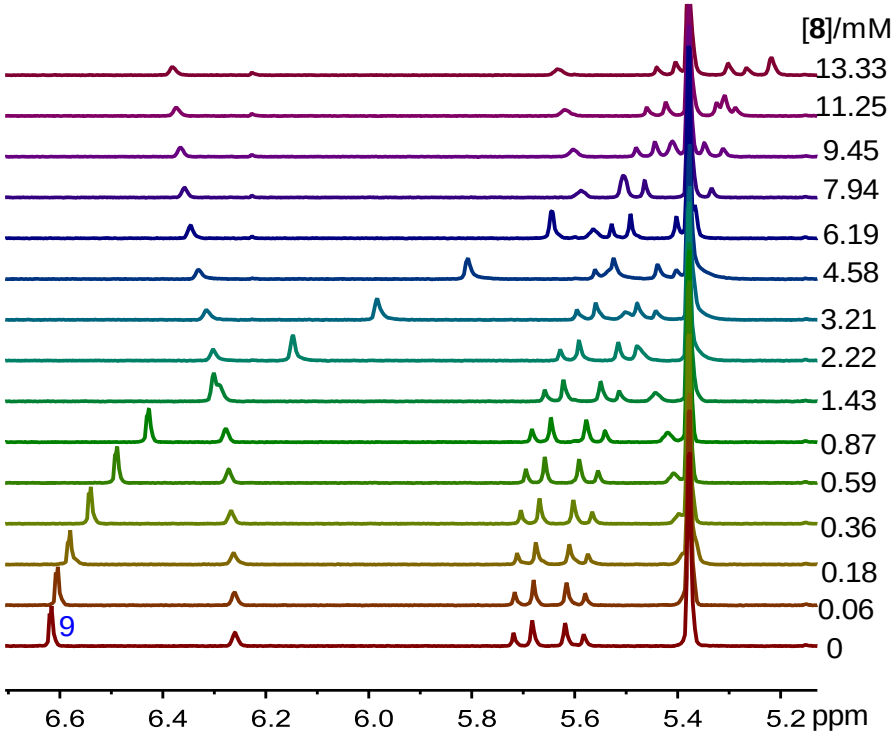

Fig. S88 Partial ^{1}H NMR spectra (400 MHz, CD_3CN:CD_2Cl_2 =1:1, 298 K) of **1b** (0.4 mM) titrated by **8** (0~13.33 mM).

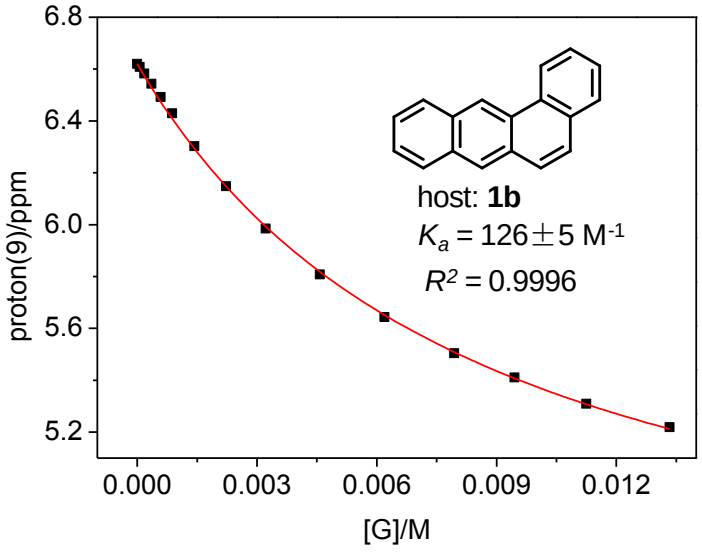

Fig. S89 Non-linear curve-fitting for the complexation between **1b** and **8** in CD_3CN:CD_2Cl_2 =1:1 at 298 K.

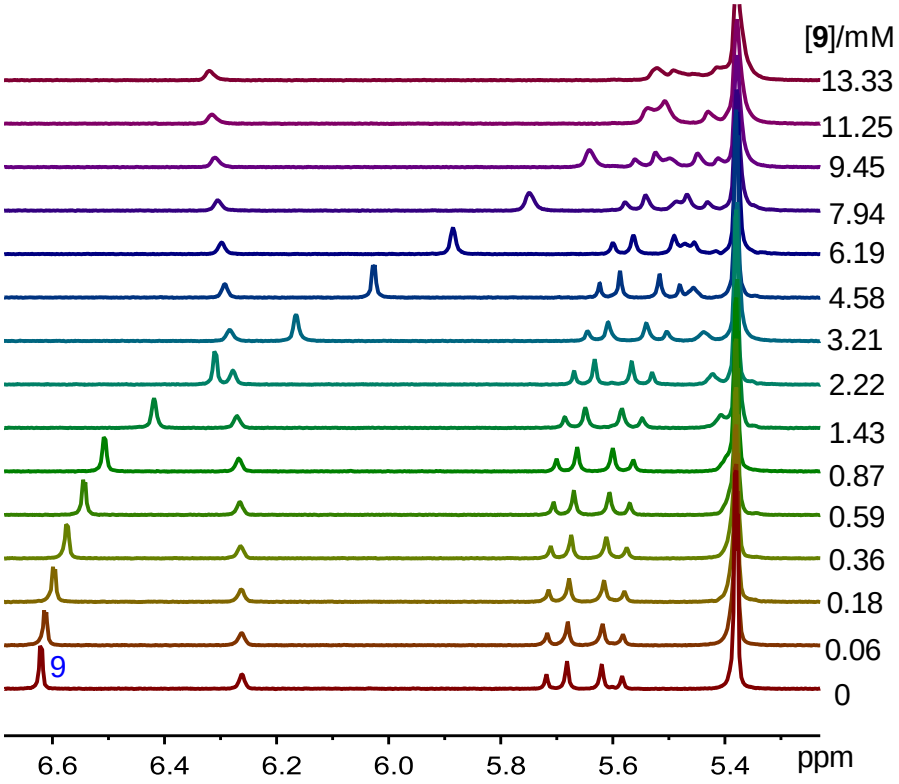

Fig. S90 Partial ^{1}H NMR spectra (400 MHz, CD_3CN:CD_2Cl_2 =1:1 298 K) of **1b** (0.5 mM) titrated by **9** (0~13.33 mM).

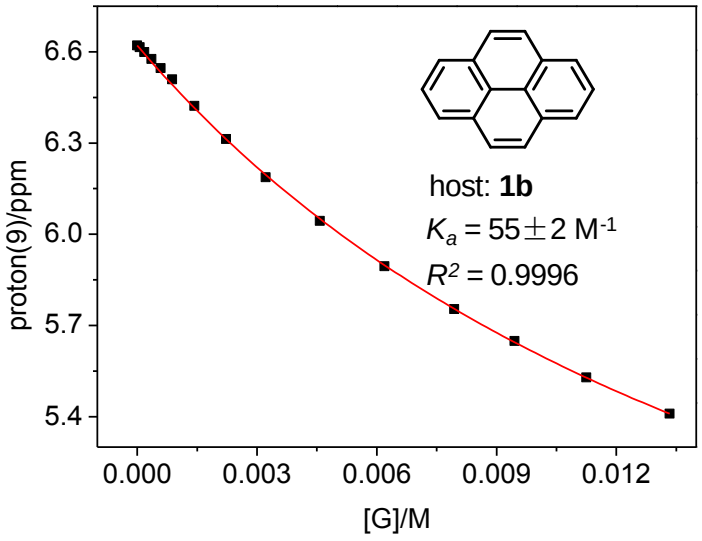

Fig. S91 Non-linear curve-fitting for the complexation between **1b** and **9** in CD_3CN:CD_2Cl_2 =1:1 at 298 K.

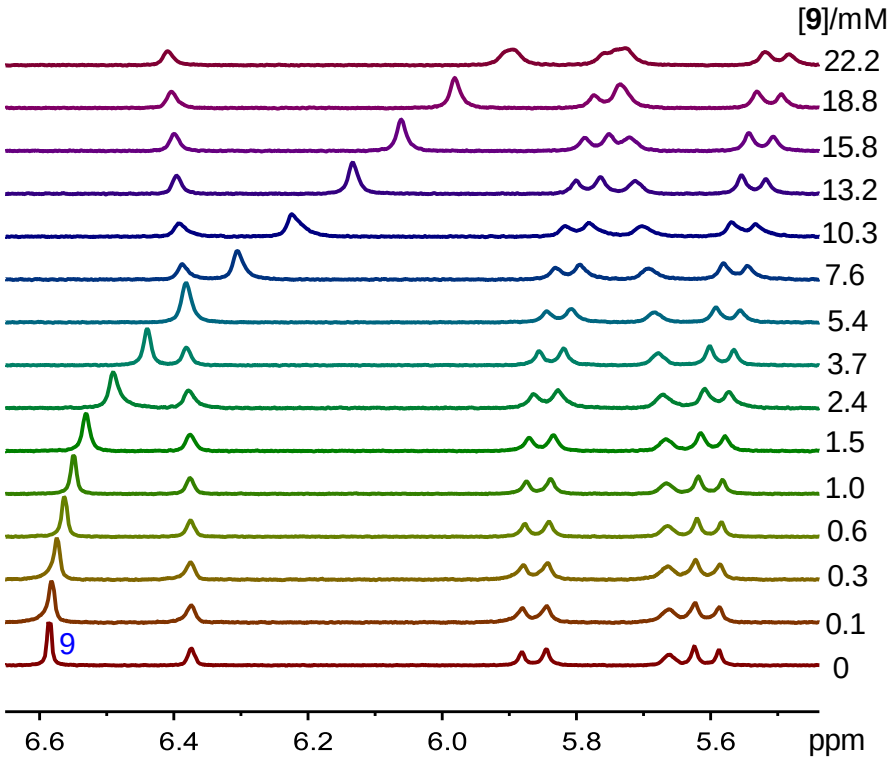

Fig. S92 Partial ^{1}H NMR spectra (400 MHz, DMSO-d_6, 298 K) of **1b** (0.5 mM) titrated by **9** (0~22.2 mM).

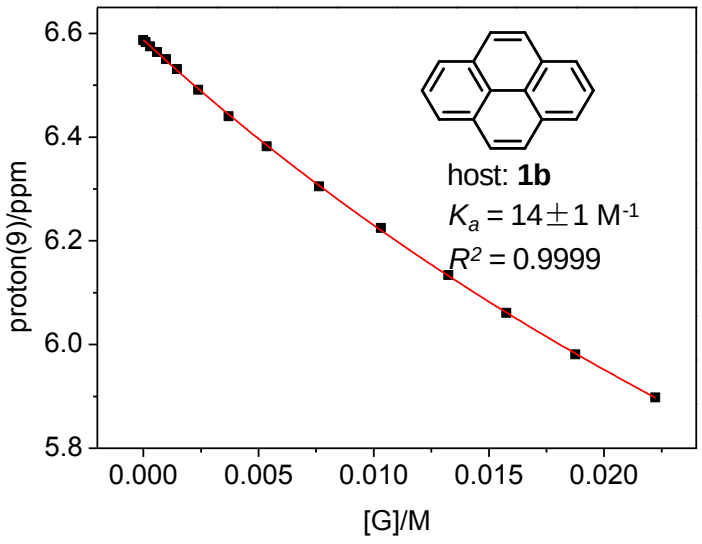

Fig. S93 Non-linear curve-fitting for the complexation between **1b** and **9** in DMSO-d_6 at 298 K.

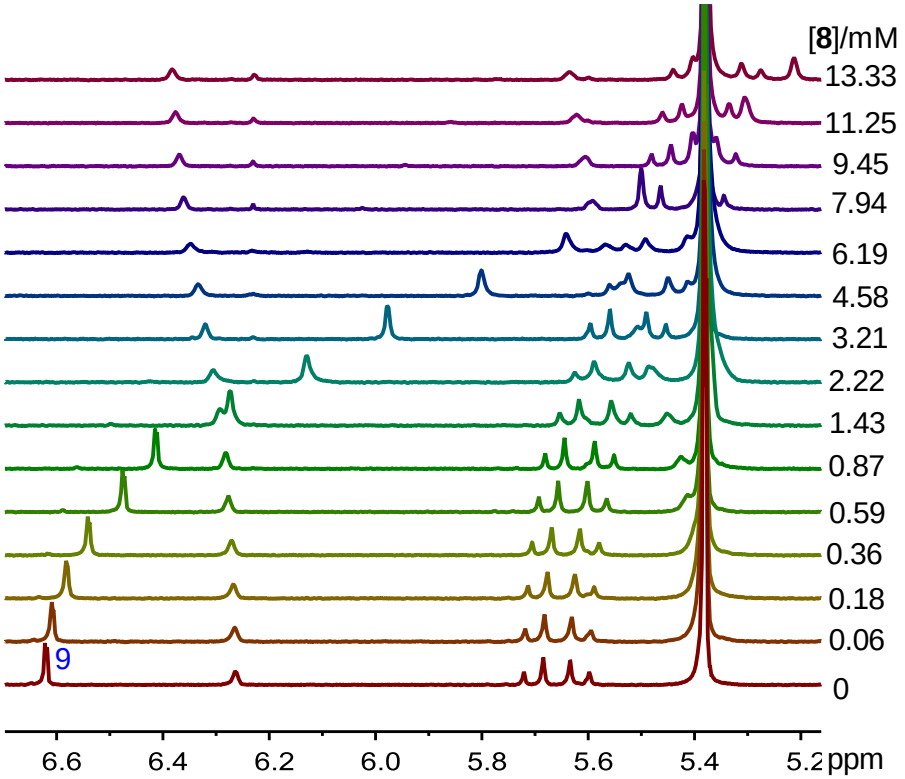

Fig. S94 Partial ^{1}H NMR spectra (400 MHz, CD_3CN:CD_2Cl_2 =1:1, 298 K) of **2b** (0.4 mM) titrated by **8** (0~13.33 mM).

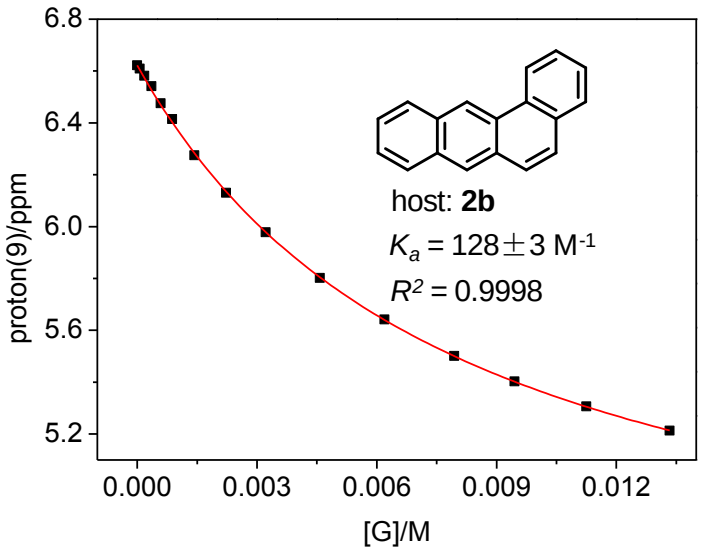

Fig. S95 Non-linear curve-fitting for the complexation between **2b** and **8** in CD_3CN:CD_2Cl_2 =1:1 at 298 K.

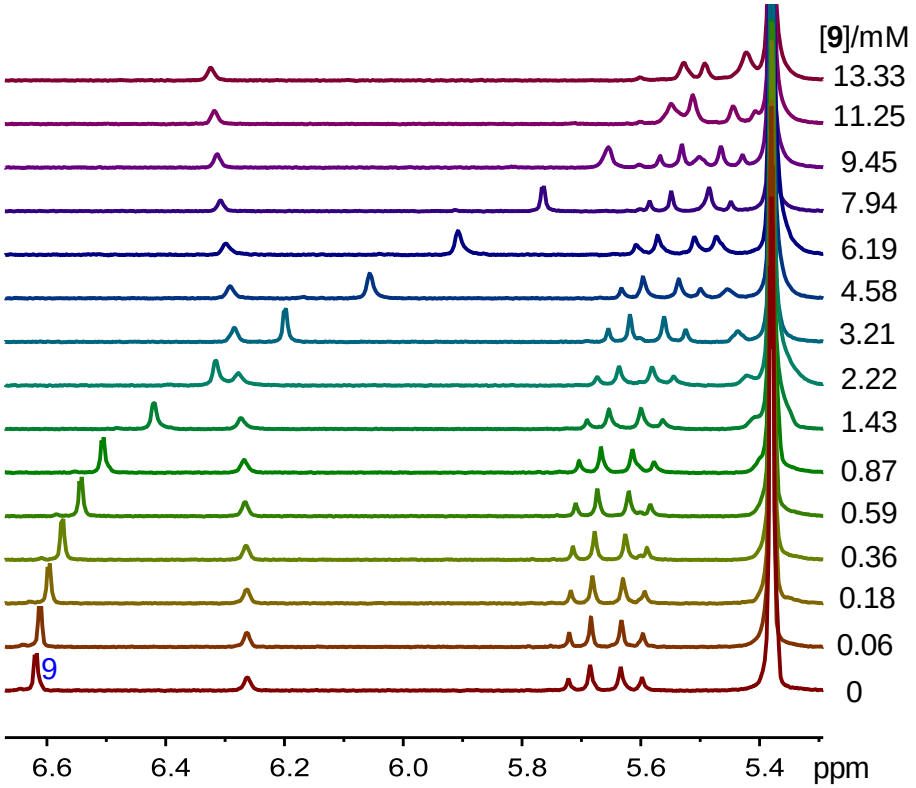

Fig. S96 Partial ^{1}H NMR spectra (400 MHz, CD_3CN:CD_2Cl_2=1:1 298 K) of **2b** (0.4 mM) titrated by **9** (0~13.33 mM).

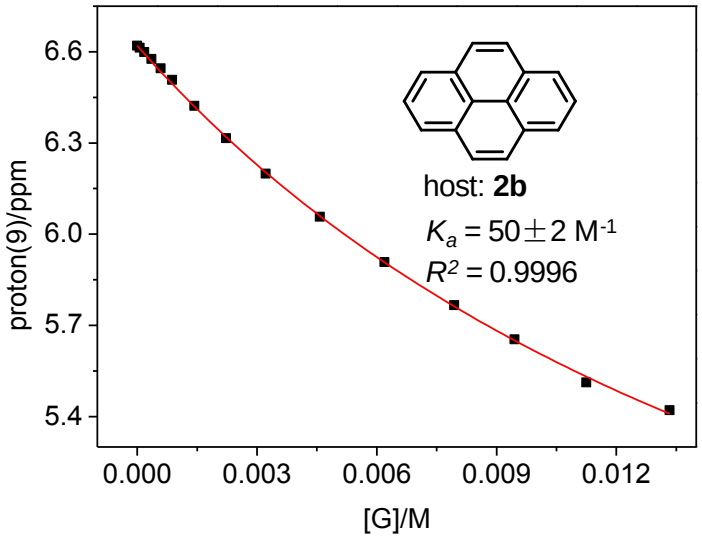

Fig. S97 Non-linear curve-fitting for the complexation between **2b** and **9** in CD_3CN:CD_2Cl_2 =1:1 at 298 K.

8. X-Ray Single Crystallography

Crystals were obtained by slow evaporation of dichloromethane or diethyl ether solutions of **1b**. Crystal data was collected on a Bruker D8 VENTURE with Cu Kα radiation (λ = 1.54178 Å) at 173(2) K. The structures were solved by the direct method and different Fourier syntheses. All calculations were performed by full-matrix least-squares methods on F^2 by using the SHELX-97 program[5,6], all non-hydrogen atoms were refined with anisotropic thermal parameters and the hydrogen atoms were fixed at calculated positions and refined by a riding mode. SQUEEZE routine implemented on PLATON was used to remove electron densities corresponding to disordered solvent molecules in Crystal data.

Crystal Data: **1b** obtained from dichloromethane-d_2: CCDC: 1945708. $C_{137}H_{98}B_2Cl_2D_2F_{48}N_4O_8$ (M=2936.74 g/mol): triclinic, space group P-1 (no. 2), a= 13.9528(5) Å, b= 15.9387(5) Å, c= 16.2647(6) Å, α= 75.310(2)°, β= 84.666(2)°, γ= 67.739(2)°, V= 3238.1(2) Å^3,Z= 1, T= 100.04 K, μ(CuKα)= 1.605 mm^{-1}, $Dcalc$= 1.506 g/cm^3, 45782 reflections measured (5.618° ≤ 2Θ ≤ 120.414°), 9579 unique (R_{int}= 0.0457, R_{sigma}= 0.0355) which were used in all calculations. The final R_1 was 0.0572 (I > 2σ(I)) and wR_2 was 0.1814 (all data).

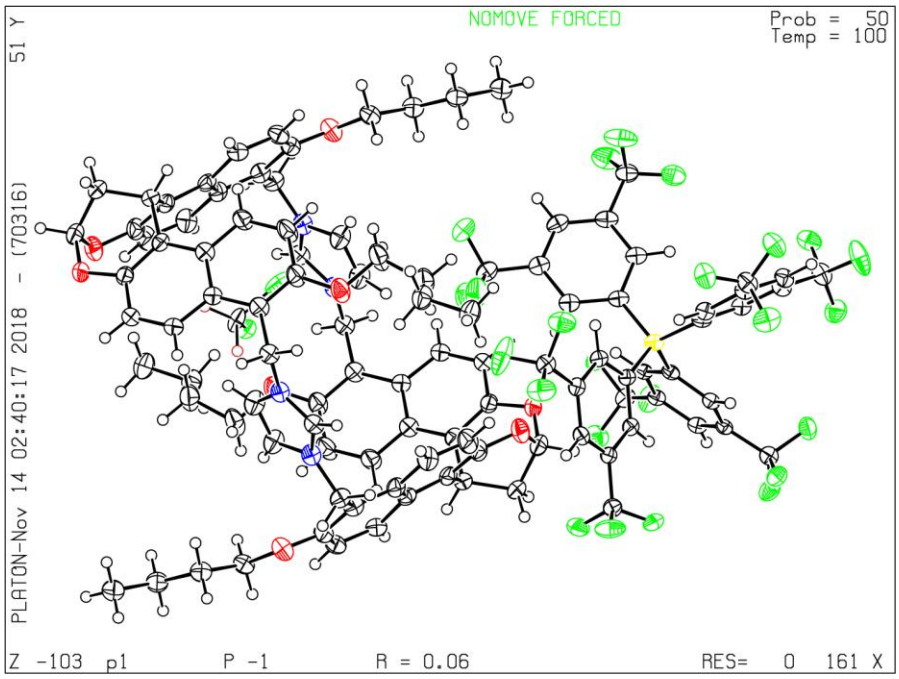

Crystal Data: **1b** obtained from diethyl ether: CCDC: 1945707. $C_{136}H_{98}B_2F_{48}N_4O_8$ (*M*=2849.80 g/mol): triclinic, space group P-1 (no. 2), *a*= 13.9780(5) Å, *b*= 15.6198(6) Å, *c*= 16.4650(6) Å, *α*= 75.3050(10)°, *β*= 85.4450(10)°, *γ*= 68.590(2)°, *V*= 3237.0(2) Å^3, *Z*= 1, *T*= 100.04 K, μ(CuKα)= 1.217 mm^{-1}, *Dcalc*= 1.462 g/cm^3, 42286 reflections measured (5.55° ≤ 2Θ ≤ 120.408°), 9575 unique (R_{int}= 0.0350, R_{sigma}= 0.0304) which were used in all calculations. The final R_1 was 0.0381 (I > 2σ(I)) and wR_2 was 0.1000 (all data).

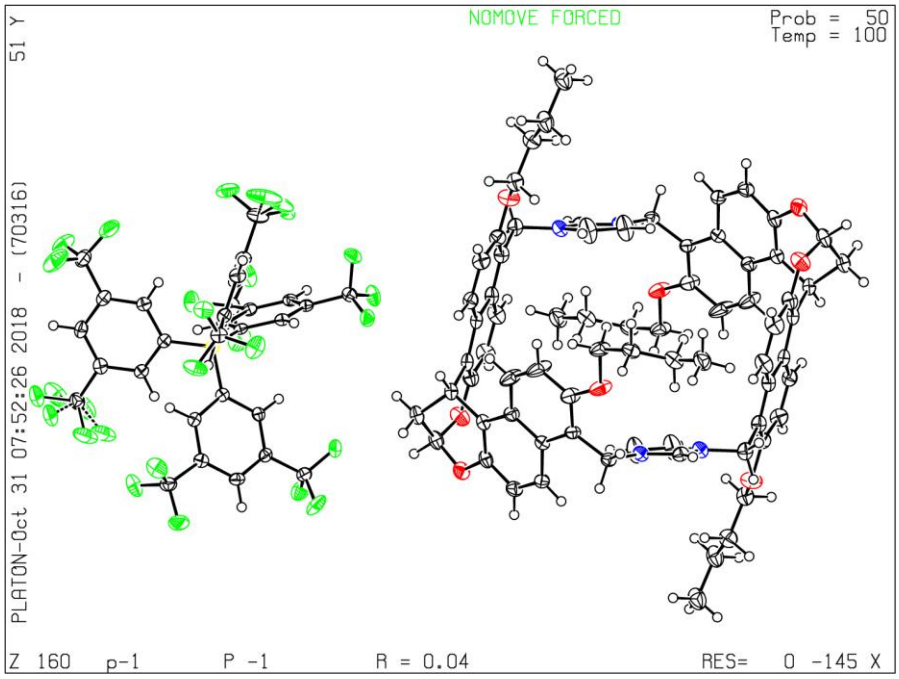

9. References

1 Y.-L. Ma, H. Ke, A. Valkonen, K. Rissanen and W. Jiang, *Angew. Chem. Int. Ed*., 2018, **57**, 709;

2 M. J. Frisch., G. W. Trucks, H. B. Schlegel, G. E. Scuseria, M. A. Robb, J. R. Cheeseman, G. Scalmani, V. Barone, B. Mennucci, G. A. Petersson, H. Nakatsuji, M. Caricato, X. Li, H. P. Hratchian, A. F. Izmaylov, J. Bloino, G. Zheng, J. L. Sonnenberg, M. Hada, M. Ehara, K. Toyota, R. Fukuda, J. Hasegawa, M. Ishida, T. Nakajima, Y. Honda, O. Kitao, H. Nakai, T. Vreven, J. A. Montgomery Jr., J. E. Peralta, F. Ogliaro, M. J. Bearpark, J. Heyd, E. N. Brothers, K. N. Kudin, V. N. Staroverov, R. Kobayashi, J. Normand, K. Raghavachari, A. P. Rendell, J. C. Burant, S. S. Iyengar, J. Tomasi, M. Cossi, N. Rega, N. J. Millam, M. Klene, J. E. Knox, J. B. Cross, V. Bakken, C. Adamo, J. Jaramillo, R. Gomperts, R. E. Stratmann, O. Yazyev, A. J. Austin, R. Cammi, C. Pomelli, J. W. Ochterski, R. L. Martin, K. Morokuma, V. G. Zakrzewski, G. A. Voth, P. Salvador, J. J. Dannenberg, S. Dapprich, A. D. Daniels, Ö. Farkas, J. B. Foresman, J. V. Ortiz, J. Cioslowski and D. J. Fox, *Gaussian 09*, Gaussian, Inc.: Wallingford, CT, USA, 2013.

3 R. C. Clark and J. S. Reid, *Acta Cryst*., 1995, **51**, 887.

4 G. M. Sheldrick, *Acta Cryst*., 2008, **64**, 112–122.

5 (a) J.-D. Chai, and M. Head-Gordon, *Phys. Chem. Chem. Phys*., 2008, **10**, 6615-6620. (b) K. I. Assaf, and W. M. Nau, *Supramol. Chem*., 2014, **26**, 657.

6 (a) A. V. Marenich, C. J. Cramer and D. G. Truhlar, *J. Phys. Chem. B*., 2009, **113**, 6378–6396. (b) J. C. Kromann, C. Steinmann and J. H. Jensen, *J. Chem. Phys*. 2018, **149**, 104102.